2013

The use of kinetic isotope effects in studies of hydrogen transfers

Daniel Harris Roston
University of Iowa

THE USE OF KINETIC ISOTOPE EFFECTS IN STUDIES OF HYDROGEN TRANSFERS

by

Daniel Harris Roston

A thesis submitted in partial fulfillment
of the requirements for the Doctor of
Philosophy degree in Chemistry
in the Graduate College of
The University of Iowa

December 2013

Thesis Supervisor: Professor Amnon Kohen

Graduate College
The University of Iowa
Iowa City, Iowa

CERTIFICATE OF APPROVAL

_____

PH.D. THESIS

_____

This is to certify that the Ph.D. thesis of

Daniel Harris Roston

has been approved by the Examining Committee
for the thesis requirement for the Doctor of Philosophy
degree in Chemistry at the December 2013 graduation.

Thesis Committee: _____
Amnon Kohen, Thesis Supervisor

_____
Christopher M. Cheatum

_____
Daniel M. Quinn

_____
Leonard R. MacGillivray

_____
Adrian H. Elcock

To Max z”l and Marie

We should have shotguns for this…

Quentin Tarantino
Pulp Fiction

ACKNOWLEDGMENTS

First and foremost, I wish to thank my thesis adviser: Amnon Kohen has been an excellent teacher and mentor whose dedicated supervision challenged and encouraged me while allowing me enough freedom to explore the world of chemistry for myself. The rest of my thesis committee provided additional support to my research and development as a chemist, and I especially thank Chris Cheatum for the many hours I spent in his office learning how to think as a real physical chemist. I thank Dan Major for providing a stimulating environment to teach me the ways of computational chemistry. I thank Bryce Plapp for many useful conversations about alcohol dehydrogenase, as well as general enzymology. And I thank Yun Lu for helping me to think about something besides enzymes.

They say it takes a village to raise a child; well, it takes a lab to produce a PhD. I will always be grateful to the members of the Kohen group, past and present, whose guidance and solidarity in navigating the lab and the world of chemistry have stimulated my productivity and creativity. It's hard to single out any specific members of the Kohen group, but I especially thank Zhen Wang, who constantly provided me with exciting intellectual challenges.

And of course there are many people, without whose support, I never would have made it to Iowa in the first place. Robin Kinnel's unrivalled teaching led me to fall in love with chemistry and his infinitely wise mentoring and unwavering support kept me going when I could have given up. Then there are family and friends: they know who they are and what they did, which is good, because they're too many to list and their help is not articulable.

ABSTRACT

The present dissertation seeks to deepen our understanding of hydrogen transfers and especially C-H bond activations in enzymes. Hydrogen transfers are ubiquitous in chemistry and biology and a thorough understanding of how they occur and what factors influence them will facilitate developments in biomimetic catalysis, rational drug design, and other fields. A particular difficulty with H-transfers is the importance of nuclear quantum effects to the reaction, particularly tunneling. The overall scope of the work here aims to examine how experimental kinetic isotope effects (KIEs) can be interpreted with a particular type of tunneling model, referred to as Marcus-like models, to yield a semi-quantitative picture of the physical mechanisms of H-transfers. Previous work had used this kind of model to qualitatively interpret experimental data using a combination of intuition and generalized theories. The work here examines these theories in quantitative detail, testing and calibrating our intuition in the context of several experimental systems. The first chapter of research (ch. II) focusses on the temperature dependence of primary KIEs and how these experiments can be quantitatively interpreted as a probe for certain kinds of enzyme or solvent dynamics. The subsequent chapters (ch. III-VI) focus on the use of secondary KIEs to determine the detailed structures of tunneling ready states (TRSs) and how the dynamics of H-tunneling affect those structures. These chapters focus primarily on the TRS of the enzyme alcohol dehydrogenase, but by examining an uncatalyzed analogue to that reaction (ch. VI), the work gains some insight about similarities and differences between catalyzed and uncatalyzed reactions. In summary, the work uncovers some principles of *catalysis*, not just the mechanism of a catalyzed reaction. The mechanism of C-H activation presented here provides an elegant solution to problems that have been vexing to accommodate within traditional models. This work constitutes some initial steps in making Marcus-like models quantitatively useful as a supplement or even replacement for traditional models of reactivity.

TABLE OF CONTENTS

LIST OF TABLES

Table

LIST OF FIGURES

Figure

LIST OF SCHEMES

Scheme

CHAPTER I

INTRODUCTION: ISOTOPE EFFECTS AS A PROBE FOR ENZYME CATALYZED HYDROGEN-TRANSFER REACTIONS

This chapter is composed of excerpts reprinted from Roston, D.; Islam, Z.; Kohen, A. 2013. *Molecules*, 18, 5543-5567, with permission from MDPI.

Abstract

Kinetic Isotope effects (KIEs) have long served as a probe for the mechanisms of both enzymatic and solution reactions. Here, we discuss various models for the physical sources of KIEs, how experimentalists can use those models to interpret their data, and how the focus of traditional models has grown to a model that includes motion of the enzyme and quantum mechanical nuclear tunneling. We then present a case study, alcohol dehydrogenase, and discuss how KIEs have shed light on the C-H bond cleavage that enzyme catalyzes. We will show how the combination of both experimental and computational studies has changed our notion of how enzymes exert their catalytic powers.

Introduction

One of the most powerful tools in the chemist's arsenal for studying reaction mechanisms and transition state structures is to measure kinetic isotope effects (KIEs). KIEs have become a pivotal source of information on enzymatic reactions, and a number of recent reviews have described the successes of KIEs in enzymology, from determining molecular mechanisms and transition state structures that are useful for drug design,[1] to answering questions on the roles of nuclear quantum tunneling,[2,3] electrostatics,[4] and dynamic motions[5-8] in enzyme catalyzed reactions.

Despite these many achievements, the enzymology community is still in need of a comprehensive model of catalysis. A current intense debate, for example, over the

possible role of non-statistical dynamics in enzyme catalysis,[9-17] shows little sign of abating. The present review seeks to provide an updated description of the achievements of KIEs in progressing toward a more comprehensive theory, as well as to highlight the remaining questions that KIEs may be suited to answer in the future. We will begin with a thorough theoretical background on the physical sources of KIEs and general schemes for measuring and interpreting them in the context of the complex kinetic cascades of enzymatic reactions. We will then proceed to describe how KIEs have illuminated a model reaction: alcohol dehydrogenase (ADH). This case study provides detailed examples of the many practical uses of KIEs for answering questions on the nature of enzymatic hydrogen transfers.

Theory of KIEs

Semi-classical models of KIEs

Models that ignore nuclear quantum effects typically (although not always[18]) predict no isotope effects, because the isotopes do not affect the electronic potential surface for the reaction under study. Semi-classical models refer to those models that ignore contributions of quantum mechanical tunneling, i.e., only consider quantum mechanical effects on vibrational zero point energy. We will discuss tunneling in detail later, but for historical perspective and because of semi-classical models' usefulness to heavy atom KIEs, we will describe those models first. Such models are rooted in transition state theory (TST), which assumes a dynamic equilibrium between the transition state (TS) and the ground state (GS). The rate constant (k) described by TST is

$$k = \kappa \frac{k_B \mathrm{T}}{\mathrm{h}} \mathrm{K}^{\ddagger} \qquad [1.1]$$

Here, $\mathrm{K}^{\ddagger}$ is the equilibrium constant between the TS and GS, κ is the transmission coefficient (which can be smaller than unity due to friction[19] or recrossing,[20] or be larger than unity due to tunneling as discussed below), T is the absolute temperature, h is

Planck's constant and k_B is Boltzmann's constant. The equilibrium constant, $K^{‡}$ can be expressed in terms of partition functions as follows:

$$k = \kappa \frac{k_B T}{h} \frac{Q^{‡}}{Q} e^{-\Delta \in / k_B T} \quad [1.2]$$

Here, Q and $Q^{‡}$ are the total partition functions of the GS and TS respectively and $\Delta \in$ is the energy difference between the TS and GS. A KIE is the ratio of rate constants for a reaction involving a light isotope (k_L) and a heavy isotope (k_H). Taking this ratio using the TST rate constants of Eq. (2) yields the Bigeleisen equation:[21,22]

$$KIE = \frac{k_L}{k_H} = \left(\frac{\kappa_L}{\kappa_H}\right) \times MMI \times EXC \times ZPE \quad [1.3]$$

Here, κ_L/κ_H is the ratio of transmission coefficients, which semiclassically (no tunneling) is close to unity. MMI, the "Mass Moment of Inertia" term, refers to the isotope effect on translation and rotation. In the vast majority of reactions, isotope effects on translation and rotation are very small because isotopic substitution does not significantly perturb the system's overall mass or moment of inertia, so the MMI term is usually smaller than one but close to unity.[23] EXC refers to the isotopic variations on excited vibrational levels. This term is bit larger than one but close to unity, since excited vibrational states have very small populations even at relatively high temperatures. The product of these two terms (MMI and EXC) is very close to unity and is usually negligible for hydrogen KIEs, but may make a more significant contribution to heavy atom KIEs because the relative contributions from other effects is smaller. ZPE is the contribution arising from the isotopic difference in vibrational zero-point energies, and is the primary contributor to KIEs in semiclassical models. Heavier isotopes have lower vibrational ZPEs at both the GS and TS, requiring different amounts of thermal activation to reach the TS. Thus, Eq. (1.3) can be approximated as follows:

$$KIE = \frac{k_L}{k_H} = e^{(\Delta\Delta G^{‡}_{H-L})/RT} \quad [1.4]$$

Here, $(\Delta\Delta G^{‡}_{H-L})$ is the difference in the free energy of activation between isotopologues.

Primary Kinetic Isotope Effects

A primary (1˚) KIE is a KIE where the isotopically labeled atom is directly involved in bond cleavage or formation. For most organic and biological reactions, the reaction coordinate can be thought of as a stretching vibrational mode at the GS becoming a translational mode at the TS. Thus, the GS-ZPE of the stretching mode is lost and only the much lower frequencies of vibrations orthogonal to the reaction coordinate are present at the TS (Figure 1.1), so a first-order approximation of the source of KIEs is just the difference in GS-ZPE between the two isotopes:

$$\text{KIE} \approx \exp\left(\frac{\Delta\text{ZPE}}{\text{RT}}\right) \qquad [1.5]$$

This approximation provides a semi-classical upper limit on KIEs, which, for C-H (GS frequency of 3000 cm^{-1}) cleavage at 25 ˚C is 6.9 and 15.8 for $k_{\text{H}}/k_{\text{D}}$ and $k_{\text{H}}/k_{\text{T}}$, respectively.[23]

However, the vibrational frequencies orthogonal to the reaction coordinate can deflate the primary KIEs from the maximum predicted values (Figure 1.1). Smaller KIEs can also be observed if the primary motion along the reaction coordinate is a bending mode, which has lower GS-ZPE, if recrossing is significant, in cases of exothermic or endothermic reactions. A typical use of 1˚ KIEs is to determine the symmetry and structure of the TS. The above approximation is most valid for a linear symmetric and dissociated TS. Thus, the size of the primary KIE reaches a maximum in that case. An associated TS, or reactant-like (very early, for exothermic reaction) or product-like (very late, for endothermic reaction) TS reduces the primary KIE from the semi-classical upper limit as the assumption of completely losing ZPE in the TS is less valid in these cases.[24]

Secondary KIEs

Secondary (2°) KIEs refer to KIEs resulting from isotopic substitution of an atom not directly involved in bond cleavage or formation. These KIEs result from changes in the vibrational frequencies of modes orthogonal to the reaction coordinate (Fig. 1.1b). In

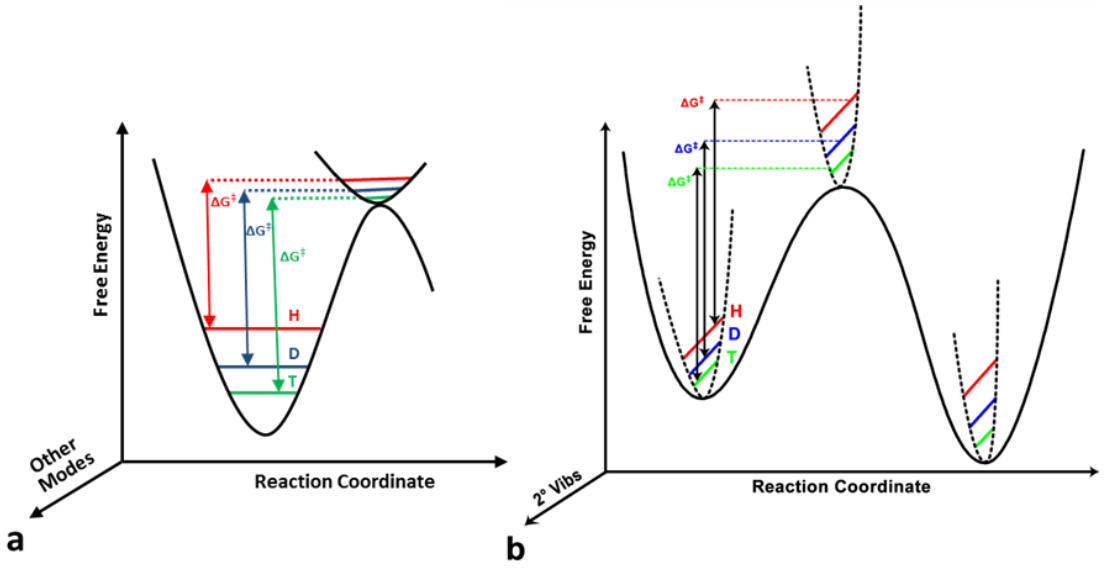

Figure 1.1 Semi-classical model of KIEs. (a) 1° KIEs arises from the difference in ZPE between the reactants at the GS and the TS. In this schematic, the reaction coordinate is a C-H stretch that becomes a translation in the TS, so the ZPE of that mode is lost. Isotopically sensitive vibrations orthogonal to the reaction coordinate are generally present at the TS, as well as the GS (although orthogonal GS modes are omitted here for clarity). (b) Semi-classical model of 2° KIEs for a reaction where the isotopically sensitive vibrational mode increases in frequency at the TS, yielding an inverse 2° KIE, and the ZPE in this case increases even more in the product, yielding an inverse equilibrium isotope effect (EIE). Figure (b) Reproduced with permission from ref 8.

this situation, the ZPE of the isotopically labeled atom is not completely lost at the TS; in fact, in many cases the ZPE of that atom *increases*. The magnitude of 2° KIEs, therefore, is generally smaller than primary KIEs. 2° KIEs are referred to as "normal" if the lighter isotopes react faster than heavier isotopes ($k_L/k_H > 1$), and "inverse" when heavier isotopes react faster than lighter isotopes ($k_L/k_H < 1$). An inverse KIE indicates that the ZPE of the isotopically sensitive modes increases in going from reactants to TS.

2° KIEs can be further divided into α- and β-2° KIEs, depending on whether isotopic substitution is made at the α- or β-position relative to the bond being cleaved or formed. α-2° KIEs (isotopic substitution of an atom directly bonded to an atom involved in bond cleavage/formation) typically report on the extent to which the central atom

changed its hybridization in going from GS to TS. β-2° KIEs, on the other hand, refer to isotopic substitution at a position two bonds away from a reacting atom, and report on the extent of charge formation at the TS, since different isotopes allow for differing levels of hyperconjugation.[25] In semiclassical theory, the direction (normal or inverse) and magnitude of 2° KIEs for many types of reactions are related to equilibrium isotope effects (EIEs). The EIE is the isotope effect on an equilibrium constant:

$$\mathrm{EIE} = \frac{K_L}{K_H} \qquad [1.6]$$

Here, K_L and K_H are the equilibrium constants for the light and heavy reactions, respectively. In contrast to 2° KIEs, the magnitude and direction of EIEs depend on the ZPE of the isotopically labeled vibrations at the reactant and product ground states. If the ZPE changes monotonically (i.e. either increasing or decreasing throughout the reaction), then the 2˚ KIE will fall between the EIE and unity. For example, if the hybridization of the central carbon changes from sp^3 in the reactant to sp^2 in the product, the α-2° EIE for a hydrogen bonded to that carbon will be greater than unity as the H gains bending freedom in going from sp^3 to sp^2. Thus, the difference in ZPE (ΔZPE) between reactant and product favor depletion of the heavy isotope in product. Comparisons of 2° KIEs with EIEs have traditionally been used to determine the position of the TS. 2° KIEs very close to unity indicate a very early TS, whereas a very late TS results in 2° KIEs close to the EIE. However, there are a few reports of cases where 2° KIEs fell outside of the aforementioned range (unity to EIE) and this has indicated non-classical behavior like tunneling (see below on ADH).[26-29] Note that for certain types of reactions, the ZPE does not change monotonically. For example, in an S_N2 reaction, the central carbon is penta-coordinate at the TS, so α-hydrogens have very little vibrational freedom and the ZPE is thus higher at the TS than in either the reactants or products. In this case, the EIE is likely to be close to unity, so a small KIE can indicate either an early or a late TS, whereas a large KIE indicates a symmetric TS.

Swain-Schaad Relationships

The Swain-Schaad relationship is the proportionality between different hydrogen KIEs (e.g. between k_H/k_D and k_H/k_T or k_D/k_T). A relatively simple derivation[30] based on the assumptions of the Bigeleisen equation and harmonic vibrational modes, shows that hydrogen KIEs are related to one another by simple exponential relationships:

$$\frac{k_H}{k_T} = \left(\frac{k_D}{k_T}\right)^{3.3} \quad [1.7]$$

Where the exponent only depends on the reduced masses of the different isotopes, which for Eq. (1.7) is:

$$\text{EXP} = \frac{\ln(k_H/k_T)}{\ln(k_D/k_T)} = \frac{(1/\sqrt{\mu_H})-(1/\sqrt{\mu_T})}{(1/\sqrt{\mu_D})-(1/\sqrt{\mu_T})} \quad [1.8]$$

where μ_i is the reduced mass of the C_i bond under study (where i is H, D, or T). In these equations, the exponent is referred to as the Swain-Schaad exponent (SSE).

Breakdown of the Semi-classical Model: Quantum Tunneling

Since the 70s, a variety of experiments have shown that not all data can be explained by semi-classical models, particularly in reactions involving the transfer of hydrogen (H^+, H^-, or $H\cdot$). One of the first indications of a breakdown of the semi-classical model was the discovery by Cleland and co-workers that 2˚ KIEs in ADH[26] and formate dehydrogenase[29] fell outside of the semi-classical limits of the EIE to unity. The researchers proposed quantum mechanical tunneling and 1˚ -2˚ coupled motion (Figure 1.2). Tunneling is the phenomenon where a particle's probability density spreads through a potential energy barrier without ever obtaining the energy necessary to surmount that barrier. Since a particle's ability to tunnel depends on mass, KIEs are an excellent probe for tunneling effects. Further evidence for tunneling came from the breakdown of the Swain-Schaad relationship in so-called "mixed labeling" experiments, which measure the 2˚ H/T KIE with H at the 1˚ position, and the 2˚ D/T KIE with D at the 1˚ position.[31-33]

Another experimental finding that could not be explained semiclassically are 1˚ KIEs with magnitudes drastically inflated from the semi-classical limits[34] or with temperature dependence outside the semiclassical predicted range.[7,8,23,33-36]

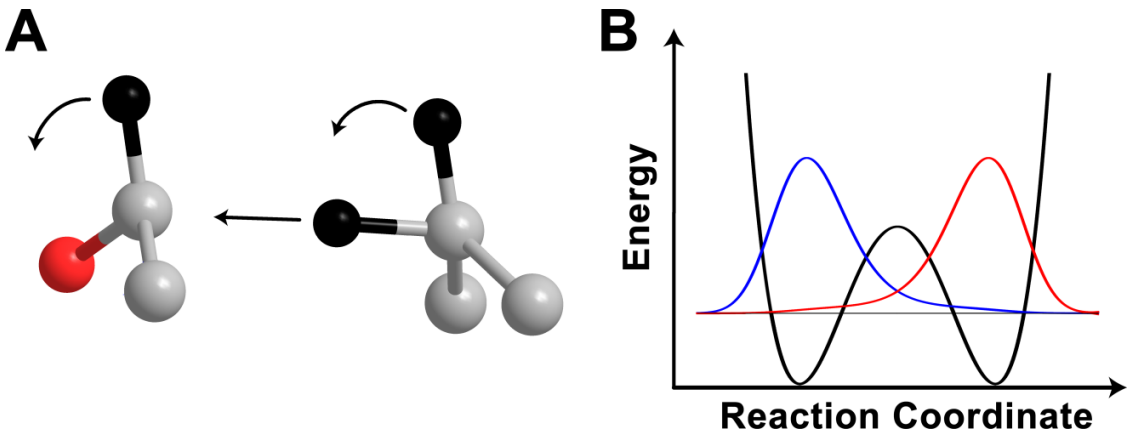

Figure 1.2 The model of tunneling and coupled motion. (a) The reaction coordinate involves motion of both the 1˚ and 2˚ atoms, which tunnel through the reaction barrier. (b) The efficiency of tunneling is proportional to the overlap between donor (blue) and acceptor (red) wavefunctions. Reproduced with permission from ref 8.

In the semi-classical model, KIEs originate from the difference in activation energy of the isotopologues (ΔE_a) and the KIEs can be modeled with the Arrhenius equation, which for KIEs is identical to the or Eyring equation

$$\frac{k_L}{k_H} = \frac{A_L}{A_H} \exp\left(\frac{\Delta E_a}{RT}\right) \qquad [1.9]$$

where A_L/A_H is the isotope effect on the Arrhenius pre-exponential factor, which is expected to be close to unity (*e.g.* $0.5 < A_H/A_D < 1.47$).[37] In some cases, the observed isotope effect on the pre-exponential factor is greater than unity, corresponding to smaller than expected temperature dependence of KIEs, whereas other reactions exhibit an isotope effect on the pre-exponential factor that is smaller than unity, corresponding to

larger than expected temperature dependence. Several attempts to account for these deviations from semi-classical behavior have arisen over the years.

Models of Tunneling

Some formalisms add a tunneling correction term to the TST rate constant, giving rate constants of the form

$$k = Q_{\mathrm{T}} k_{\mathrm{TST}} \qquad [1.10]$$

where k_{TST} is the TST rate constant and Q_T is a correction for tunneling effects. For example, the Bell correction[38] used a parabolic reaction barrier and was able to account for some rate and KIE behavior as illustrated in Fig. 1.3. In the high temperature limit (region I in Fig. 1.3), reactions mostly take place by thermal activation which leads to temperature-dependent rates and KIEs, reflecting the differences in activation energy between two isotopologues (light in blue and heavy in red), and the corresponding A_L/A_H is close to unity, as predicted by semi-classical models.[37] In the low temperature limit, very little thermal energy is available for activation; therefore, reactions take place exclusively by tunneling, leading to temperature independent rates and KIEs (Fig 1.3, region III) and A_L/A_H much higher than unity. Between these two extremes lies the moderate tunneling region (II) where the lighter isotope mostly tunnels, but the heavier isotope reacts mostly by thermal activation. This results in a very steep temperature dependence of KIEs and A_L/A_H much smaller than unity due to a temperature dependent rate for the heavy isotope, but temperature independent rate for the light isotope.

Such tunneling correction models can reproduce temperature-dependent or temperature independent KIEs,[40] but cannot yield temperature-dependent rates with temperature-independent KIEs, which is precisely what numerous experiments have reported for various systems.[7,8,33,36,39,41] We note that several high level simulations[42-46] have used sophisticated tunneling corrections to TST, along with other corrections, to reproduce the temperature dependence of experimental rates and KIEs, but such

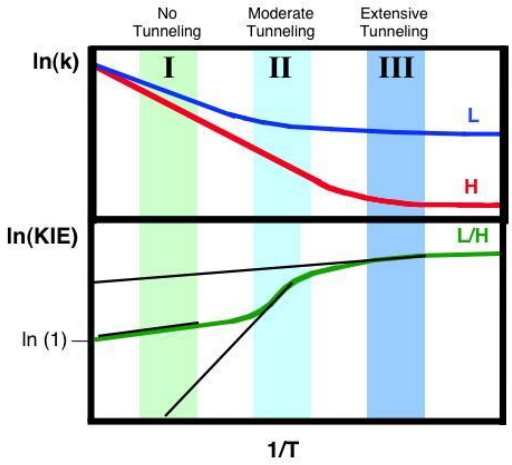

Figure 1.3 Arrhenius plot of rates (top panel) and KIEs (bottom panel, green line) of light (L, in blue) and heavy (H, in red) isotopes. In region I tunneling is negligible so AL/AH is close to unity. Region II is the moderate tunneling region where only the lighter isotope tunnels and the corresponding AL/AH is much smaller than unity. Both isotopes tunnel in region III, making the AL/AH much higher than unity. Reproduced with permission from ref. 39.

corrections are outside the scope of this review.

To rationalize findings that could not fit the above models, researchers have adapted Marcus Theory of electron tunneling [47] to the case of hydrogen tunneling (Figure 1.4). Full tunneling models of this type are referred to as Marcus-like models, but have also been called by a variety of other names such as environmentally coupled tunneling, vibrationally enhanced tunneling, tunneling promoting vibrations and others.[5-9,36,48-50] The underlying feature of Marcus-like models is the separation of light atom motion (i.e. hydrogen tunneling) from heavy atom motion, which includes both the protein environment as well as the surrounding solvent. According to these models, rates are governed by three major processes: 1) heavy atom motion that brings the system to a tunneling ready state (TRS), where the reactant and product potential surfaces are degenerate and tunneling can occur, 2) fluctuations of the tunneling barrier, modulated by

heavy atom motion, and 3) the actual process of hydrogen tunneling through the barrier. A general functional form for the rate constant in such models is[5,48,51-53]

$$k = \frac{|V|^2}{\hbar}\sqrt{\frac{\pi}{\lambda k_B T}}e^{-\frac{(\Delta G^\circ+\lambda)^2}{4k_B T\lambda}}\int_0^\infty F(m,DAD)e^{-E(DAD)/k_B T}\,dDAD \qquad [1.11]$$

In this equation, the factors in front of the integral give the rate of reaching a TRS based on the electronic coupling between reactant and product (V, the degree of adiabacity of the reaction), the reorganization energy (λ), and the driving force of the reaction (ΔG˚). The integral measures the probability of hydrogen transfer once the system reaches a TRS. The first factor inside the integral determines the probability of tunneling as a function of mass (m) and the donor-acceptor distance (DAD). The last integrated exponential is a Boltzmann factor, giving the probability of being at any given DAD.

Since the rate of reaching a TRS (the factors outside the integral) is governed by heavy atom motion, it essentially isotopically insensitive, though it governs some of the temperature dependence of the reaction rate. The Boltzmann and tunneling factors, however, make the integral isotopically sensitive and potentially sensitive to temperature, depending on the free energy as a function of DAD, E(DAD) in Eq. 1.11. Thus, Marcus-like models can explain temperature-dependent or temperature-independent rates with temperature-dependent or temperature-independent KIEs. Please note that for DADs shorter than the vertical line in panel C, the ZPE is above the barrier, thus the reaction is practically over-the-barrier.

Interpreting KIEs with this kind of model suggests that the temperature dependence of KIEs is a function of the temperature dependence of the distribution of DADs. That is, temperature independent KIEs result from a very narrow distribution of DADs at the TRS that does not change with temperature. Temperature dependent KIEs, on the other hand, result from a loose active site where the TRS can attain a wide range of DADs at thermal equilibrium, and the distribution of DADs is thus temperature sensitive. In fact, we recently proposed a numerical model[51] suggesting that the systems

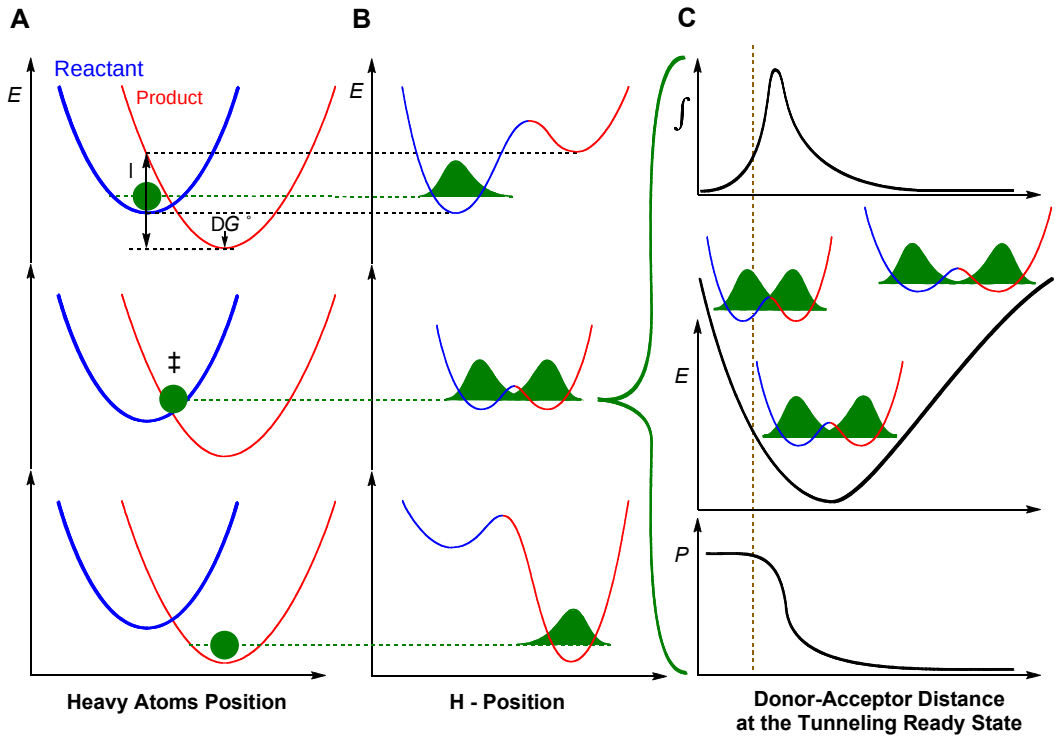

Figure 1.4 Marcus-Like models of hydrogen tunneling—a visualization of Eq. (1.11). Three slices of the potential energy surface (PES) along components of the collective reaction coordinate showing the effect of heavy-atom motions on the zero point energy in the reactant (blue) and product (red) potential well. Panel A presents the heavy atom coordinate (also known as the Marcus parabolas), and Panel B shows the H-atom position, which is orthogonal to the heavy atom coordinate. In the top panels the hydrogen is localized in the reactant well, and the zero point energy of the product state is higher than that of the reactant state. Heavy atom reorganization brings the system to the tunneling ready state (TRS, middle panels A and B), where the zero point energy in the reactant and product wells are degenerate and the hydrogen can tunnel between the wells. Further heavy atom reorganization breaks the transient degeneracy and traps the hydrogen in the product state (bottom panels). The rate of reaching the TRS depends on the reorganization energy (λ) and driving force ($\Delta G°$), which are indicated in the top panel, and further discussed under Eq. (1.11). Panel C shows the effect of DAD sampling on the wavefunction overlap at the TRS (middle panel). Transmission probability (P) is a function of the overlap integral of the hydrogen wavefunctions in the reactant (blue) and product (red) wells (bottom panel C). The top panel C presents the contribution to H-transfer at each DAD as a function of the P and the population at each DAD (i.e., the integrated terms in Eq. 1.11). The vertical dashed line represents the DAD under which the ZPE is greater than the barrier height. At such distances, the process of a wavefunction spreading from reactant well to product well is no longer "tunneling", but one can still use the particle's transmission probability analogously to the tunneling probability at longer DADs.

with the most steeply temperature dependent KIEs may actually result from multiple distinct populations in equilibrium with one another along the DAD coordinate. We will further discuss the utility of interpreting KIEs with Marcus-like models in the following case study on the enzyme ADH.

Alcohol Dehydrogenase

Alcohol dehydrogenase (ADH) has served as one of the classic models for enzymology and specifically, the many uses of isotope effects to study the physical mechanism of hydride transfers.[8,54-56] ADH catalyzes the oxidation of an alcohol to an aldehyde using a nicotinamide cofactor (Scheme 1.1). Some of the benefits of using ADH as a model are that one can study both the forward (alcohol to aldehyde) and reverse reactions using relatively similar conditions, and that for a number of ADHs (e.g. from either yeast or from bacillus stearothermophilus) the hydride transfer step is fully exposed (i.e., kinetic complexity does not interfere with experimental results). Pioneering studies on the hydride transfer in yeast ADH (yADH) by Klinman and coworkers compared isotope effects with linear free energy relationships (Hammett substituent effects) using benzyl alcohols and aldehydes.[57-59] While the 1˚ KIEs were not particularly noteworthy, the 2˚ KIEs and the substituent effects showed a fascinating contradiction. The α-2˚ KIEs on the oxidation of benzyl alcohol were close to the EIE (1.35), while those on the reduction of benzaldehyde were close to unity, clearly suggesting an aldehyde-like TS.[59] The substituent effects, however, told the complete opposite story. By measuring rates using benzyl alcohols and benzaldehydes with para-substituents possessing a range of electronic effects, Klinman examined the electronic structure of the TS and found that it was more alcohol-like than aldehyde like.[57,58] This blatant contradiction between KIEs and linear free energy relationships was, in retrospect, the first indication that something non-classical was occurring in the reaction, but the idea of tunneling had yet to enter the consciousness of the enzymology community.

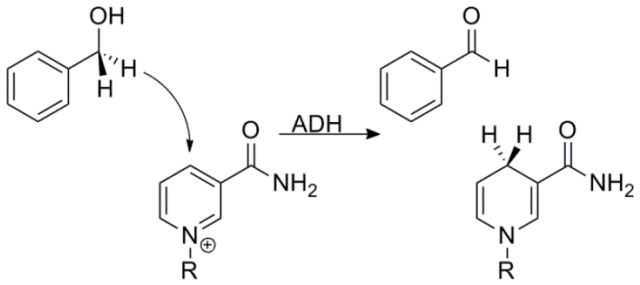

Scheme 1.1 The reaction catalyzed by ADH (R = adenine diphosphate ribosyl-) with BnOH as alternative substrate.

Shortly after the publication of those studies, Cleland and coworkers[26,60] measured α-2˚ KIEs on the nicotinamide cofactor in ADH and found that they were significantly inflated. In fact, despite the fact that the relevant EIE was inverse, as expected for a change from sp^2 to sp^3 (reduction of NAD^+ to NADH), the KIE was significantly greater than unity. The authors interpreted this surprising result as an indication of 1˚-2˚ coupled motion (Figure 1.2). A theoretical model[61] solidified that interpretation, with the additional component of quantum tunneling of the coupled atoms. The theoretical calculations further suggested that a breakdown of the "rule of the geometric mean" (RGM) could be a strong indicator of tunneling and coupled motion. The RGM is one of the results of the assumptions of the Bigeleisen model of KIEs and states that isotope effects should be independent of one another—there are no isotope effects on isotope effects.[62] Quickly after the predictions of the theoretical model appeared, Cleland and coworkers tested the RGM in the enzyme formate dehydrogenase (FDH), finding that it did not hold, thus supplying very solid evidence for the phenomenon of tunneling and 1˚-2˚ coupled motion.[29]

Additional calculations soon provided another important prediction of the model of tunneling and coupled motion. If a reaction involved tunneling and coupled motion, the study asserted, then observed SSEs should deviate significantly from the value predicted by semi-classical theory.[63] Klinman's group ended up testing this prediction in

yADH using what has come to be known as a mixed labeling experiment.[31] In this kind of experiment, the 2˚ H/T KIE is measured with H at the 1˚ position, while the 2˚ D/T KIE is measured with D at the 1˚ position. These experiments provided a mixed-labeling SSE (mSSE):

$$mSSE = \frac{\ln(k_{\mathrm{H}}^{\mathrm{H}}/k_{\mathrm{T}}^{\mathrm{H}})}{\ln(k_{\mathrm{D}}^{\mathrm{D}}/k_{\mathrm{T}}^{\mathrm{D}})} \quad [1.12]$$

where k_j^i indicates the rate with isotope i at the 1˚ position and isotope j at the 2˚ position. Semi-classical models typically predict that mSSE=SSE=3.3, although some calculations have suggested that even without tunneling the SSE can be somewhat larger than that.[27,64] No semi-classical models, however, can explain the experimental value in yADH, which was over 10, clearly supporting the theory of tunneling and coupled motion.[31]

After confirming that inflated mSSEs—and thus tunneling and coupled motion—also occur in horse liver ADH (hlADH) when mutation causes the hydride transfer to be rate-limiting,[32] Klinman's group began to explore the possible role of enzyme structure and dynamics in modulating the tunneling process. A study of a series of active site mutants of hlADH found that based on the measured mSSE for each mutant, the degree of tunneling depends on the hydrogen transfer distance apparent in crystal structures of the mutants.[65] This result suggested that enzymes may have evolved to hold the DAD to a short enough distance for hydrogen tunneling.

Additional information on the mechanisms by which enzymes modulate tunneling came from a study of the temperature dependence of KIEs in a thermophilic ADH from *bacillus stearothermophilus* (bsADH).[33] These experiments found that within this enzyme's physiological temperature range (30-65 ˚C), the 1˚ KIEs were nearly independent of temperature and the mSSEs were inflated. Below 30˚ C, however, the 1˚ KIEs showed a temperature dependence and the mSSEs were within error of the semi-classical value. The temperature independent 1˚ KIEs, along with the inflated mSSEs, in the physiological temperature range suggested that in that range, the enzyme adopted a

conformation that was well-suited for tunneling, but below the physiological temperature range, a sort of phase transition left the enzyme in a conformation that was not suitable for tunneling.

Since that time, the temperature dependence of 1˚ KIEs has become an important tool for understanding how enzymes modulate the reaction barrier for, but the interpretation of experimental results—both the temperature dependence of KIEs and the inflated mSSEs—has changed with the growing acceptance of Marcus-like models for H-transfers. These models assume that tunneling is a major contributor to the reactive flux for all isotopes and in all temperature ranges accessible to enzymes. As discussed above, Marcus-like models provide a mechanism for a reaction to exhibit both temperature independent and temperature dependent KIEs, depending on the population distribution along the DAD coordinate. We recently applied a numerical fitting of the Marcus-like model[51] to the 1˚ KIE data from wt bsADH, as well as those from a series of mutants.[55] The fittings showed that the wt in its physiological temperature range had a very narrow distribution along the DAD coordinate (at a relatively short DAD) and that this distribution did not change significantly with temperature, thus leading to temperature independent KIEs. At low temperatures, though, the enzyme adopts a conformation such that the distribution along the DAD coordinate is greatly perturbed and the system appears to undergo reaction by two distinct pathways. One lower energy population tunnels inefficiently from a long DAD, while the other reacts by heavy atom motion shortening the DAD so much that the hydride is practically over the barrier. The population with the short DAD is somewhat higher in energy, so increasing temperature increases the population at that DAD, leading to smaller KIEs at higher temperatures. We found qualitatively similar results when applying the fitting procedure to a series of active site mutants, although the mutations tended to flip the temperature ranges where KIEs were temperature independent with those where they were temperature dependent.

One of the most surprising and counterintuitive conclusions based on this model was that at high temperatures, reactions with temperature dependent KIEs must occur from a shorter DAD than similar reactions with temperature independent KIEs. Within the mathematical form of Marcus-like models (eq. 1.11), the only way to achieve a small KIE is to achieve a short DAD. Thus, if at a given temperature some reaction (reaction A) has a smaller KIE than another reaction (reaction B), one can conclude that on average, reaction A occurs from a shorter DAD than reaction B at that temperature. This was a most surprising result because wt enzymes often exhibit temperature independent KIEs under physiological conditions, while active site mutants like those in the bsADH[55] and other systems[66,67] often show temperature dependent KIEs. Intuitive arguments had suggested that the role of active site hydrophobic residues was to maintain a short DAD and that mutations that made those residues smaller lengthened the DAD, leading to the observed temperature dependence of the KIEs. One study,[53] however, found direct evidence that decreasing the size of a hydrophobic active site residue (V106A morphinone reductase) *decreased* the DAD. Based on these findings, one can rationalize that, given the many complex interactions in an enzyme active site, decreasing the size of a side chain may not have the direct effects on DAD that intuition would predict.

Another important result of Marcus-like models is that D and T must tunnel from shorter DADs than H. Knowing this, and reassessing the many mSSE data from ADHs, Klinman proposed an explanation for the inflated mSSEs that modified the traditional model of tunneling and 1˚-2˚ coupled motion.[54] The H/T KIEs with H-transfer from all the different studies had relatively constant magnitude, near the EIE (1.35), but the D/T KIEs with D-transfer were all diminished from their expected values; the diminished D/T values, therefore, appeared to cause the varying levels of inflation in the mSSEs. The new proposal suggested that the D at the 1˚ position in those D/T measurements has to tunnel from a shorter DAD and the requirement of a shorter DAD sterically hindered the rehybridization of the donor carbon, thus lowering the KIE. We recently tested this

notion in the reverse reaction (benzaldehyde to benzyl alcohol) and found that indeed, the 2˚ H/T KIE is smaller when D is the transferred atom. Furthermore, we developed a computational model, based on the ideas of Marcus-like models and a shorter DAD for D-transfer, which explained the many different seemingly-incoherent data for yADH. In a relatively simple and intuitive model, we reproduced the 2˚ KIEs, the inflated mSSEs, and even the Hammett substituent effects, thus bringing together decades of confusing data on this enzyme into a single model.[68]

One of the most important open questions regarding ADH is why it is so unique in its display of inflated mSSEs. A number of systems, both enzymatic[69,70] and non-enzymatic,[28] display 2˚ KIEs outside of the range of the EIE to unity, but very few other systems[71] have exhibited inflated mSSEs, despite the ubiquity of tunneling. Another important area for exploration is the question of how conditions and mutations that enzymologists intuitively expect to lead to longer DADs seem to create situations where the DAD reaches smaller values.[51,53] Is this an artifact of a model that is poorly suited for the experimental data? Or is this a real physical phenomenon that should be investigated further? Both experimental and theoretical avenues of exploration are likely necessary to answer these problems.

Concluding Remarks

KIEs provide unique data on the chemical step in enzyme catalyzed reactions. An example (i.e., ADH) was brought above to demonstrate some of the uses of KIEs. Studies of ADH demonstrated how 2˚ KIEs can assess TS structure and how to interpret 2˚ KIEs within the framework of different models, as well as the use of the temperature dependence of 1˚ KIEs in the investigation of hydride transfers.

While KIE studies have helped tremendously to understand enzyme mechanisms, important questions remain over the interpretation of the temperature dependence of KIEs. Marcus-like models seem to provide a framework for modeling enzymatic

hydrogen transfers, and so far appear to be able to fit all published experimental findings (without invoking non-statistical dynamics coupled to the H-transfer). However quantitative attempts to fit experimental data to such models have yielded surprising results that some perceive as counter-intuitive.[34,51] Additional work is needed to test those models and find a comprehensive model with broad applications. Additional guidance from high level calculations may be particularly helpful in this regard. Some simulations,[44] for example, have used similar ideas to Marcus-like models to explain the varied temperature dependence of KIEs, but other computational studies[42,43,46] have relied on different approaches to reproduce the experimental data. A theory that best explains the experimental results might eventually be different for different enzymes, or represent a unified model for temperature dependence of KIEs in all systems (enzymatic and non-enzymatic). The experimental community will benefit from better understanding of what physical phenomenon the temperature dependence of KIEs is measuring. Determining how different enzyme environments give rise to different KIEs may assist rational drug design to take advantage of the unique mechanisms of enzyme catalysis, and for biomimetic catalysts to bridge the present gap in catalytic efficiency versus natural catalysts.[72,73]

CHAPTER II

HYDROGEN DONOR-ACCEPTOR FLUCTUATIONS FROM KINETIC ISOTOPE EFFECTS: A PHENOMENOLOGICAL MODEL

This chapter is reprinted from Roston, D; Cheatum, C.M.; Kohen, A. *Biochemistry*. 2012, 51, 6860-6870, with permission from ACS.

Abstract

Kinetic isotope effects (KIEs) and their temperature dependence can probe the structural and dynamic nature of enzyme-catalyzed proton or hydride transfers. The molecular interpretation of their temperature dependence requires expensive and specialized quantum mechanics/molecular mechanics (QM/MM) calculations to provide a quantitative molecular understanding. Currently available phenomenological models use a nonadiabatic assumption that is not appropriate for most hydride and proton-transfer reactions, while others require more parameters than the experimental data justify. Here we propose a phenomenological interpretation of KIEs based on a simple method to quantitatively link the size and temperature dependence of KIEs to a conformational distribution of the catalyzed reaction. This model assumes adiabatic hydrogen tunneling, and by fitting experimental KIE data, the model yields a population distribution for fluctuations of the distance between donor and acceptor atoms. Fits to data from a variety of proton and hydride transfers catalyzed by enzymes and their mutants, as well as nonenzymatic reactions, reveal that steeply temperature-dependent KIEs indicate the presence of at least two distinct conformational populations, each with different kinetic behaviors. We present the results of these calculations for several published cases and discuss how the predictions of the calculations might be experimentally tested. This analysis does not replace molecular QM/MM investigations, but it provides a fast and accessible way to quantitatively interpret KIEs in the context of a Marcus-like model.

Introduction

The detailed mechanisms of enzyme-catalyzed H-transfer reactions have tantalized researchers for many years, because of the important intellectual questions and medicinal applications associated with enzymes. It is now well accepted that both enzyme-catalyzed and nonenzymatic hydrogen transfers involve quantum mechanical tunneling, the phenomenon by which a particle passes through an energy barrier due to its wavelike properties. Because tunneling is highly mass dependent, kinetic isotope effects (KIEs) are excellent probes of these reactions. In recent years, the temperature dependence of KIEs has emerged as an important indication of the nature of tunneling and has suggested that fluctuations of the donor− acceptor distance (DAD) may be mechanistically important.[2-7,49,50,74] Here the DAD is defined as the distance between the two heavy atoms transferring the hydrogen.

Conventional transition state theory (TST) models chemical kinetics under a set of assumptions where the width of the barrier is unimportant; all that affects the rate is the height of the barrier. Some attempts to account for the effects of tunneling on KIEs rely on corrections to TST of the form

$$KIE = \frac{k_L}{k_H} = \frac{Q_L \cdot k_L^{TST}}{Q_H \cdot k_H^{TST}} \qquad [2.1]$$

where k^{TST} is the TST rate for the light (L) or heavy (H) isotope and Q is the correction for tunneling effects for each isotope. The tunneling correction is generally based on a parabolic barrier with some more sophisticated treatments available, but the barrier is assumed to be static.[75] Tunneling corrections can reproduce both temperature-dependent and temperature-independent KIEs, but such simple corrections to TST cannot reproduce small and temperature-independent KIEs where the rate is temperature-dependent (E_a>0). Certain enzymatic, as well as nonenzymatic, reactions, however, exhibit just that: large activation energies, but temperature-independent KIEs that are not inflated.[33,35,53,76-81] To account for this behavior, many researchers have adapted Marcus theory of electron

tunneling[47] to the situation of hydrogen tunneling (Figure 2.1). The Marcus-like models[3,49,56] (also known as full-tunneling models,[36] environmentally coupled tunneling,[7] and vibrationally enhanced tunneling[6]) suggest that heavy-atom motions bring the system to a tunneling-ready state (TRS), where the vibrational energy levels for the hydrogen in the reactant and product states are degenerate and tunneling can occur.[5,7,34,44,48-50,83-85] This type of model gives a rate constant (k) with the functional form

$$k = \frac{|V|^2}{\hbar}\sqrt{\frac{\pi}{\lambda k_B T}}\, e^{-\frac{(\Delta G^\circ+\lambda)^2}{4k_B T\lambda}} \int_0^\infty F(m, DAD)\, e^{E(DAD)/k_B T}\, dDAD \qquad [2.2]$$

In this equation the factors in front of the integral include the electronic coupling between the reactants and products (V) and the thermally averaged equilibrium probability of heavy-atom "reorganization" to reach the TRS, which depends on the reaction driving force (ΔG°), the reorganization energy (λ), and the absolute temperature (T); k_B is Boltzmann's constant. These factors are nearly completely insensitive to the mass of the transferred particle, so only the integral contributes to the isotope effects. The integral computes the probability of tunneling to form products once the system reaches the TRS. The first factor inside the integral gives the probability of tunneling as a function of the mass (m) of the transferred particle (H, D, or T) and the DAD. The second factor in the integral is a Boltzmann factor giving the probability of being at any given DAD. Thus, because the thermal reorganization to reach the TRS is isotopically insensitive, but tunneling at the TRS is isotopically sensitive, the model accounts for either temperature-dependent or temperature-independent rates with temperature-dependent or temperature-independent KIEs. Previous studies have reported all four possibilities for both enzymatic and non-enzymatic systems, requiring a flexible model that can accommodate all of these outcomes. We note that this kind of model assumes that all the motions of the system are in thermal equilibrium with the environment, in accordance with established theories.[2,10,48,50,74]

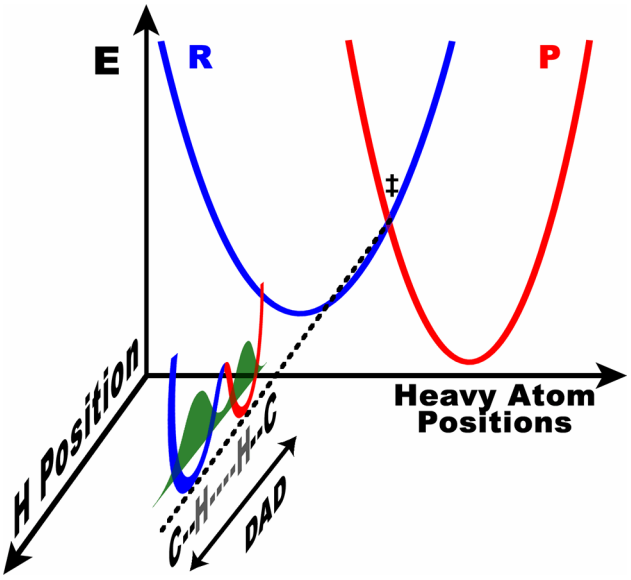

Figure 2.1 Marcus-like model of hydrogen tunneling. The heavy atoms reorganize to bring the reactant (blue) and product (red) potential surfaces to a point of transient degeneracy (‡, the TRS) where the hydrogenic wavefunction (green) can pass from the donor well to the acceptor well, which is called tunneling. The TRS actually represents a seam in multi-dimensional space, including all conformations where the reactant and product surfaces are degenerate. Figure 2.2 highlights how the fluctuation of the DAD along this seam dictates the probability of tunneling at the TRS.

Interestingly, several enzymes that exhibit temperature-independent KIEs have mutants for which KIEs are temperature-dependent. Qualitative arguments have rationalized that differences in thermal fluctuations of the DAD (the Boltzmann factor in the integral of eq. 2.2) can account for both behaviors (Figure 2.2).[7,49] In the case of temperature-dependent KIEs, thermal excitations that populate conformations with shorter DADs, where the heavy isotope can tunnel, will lower the KIE as temperature increases. In contrast, if the enzyme stabilizes a TRS with a very short DAD, where tunneling is efficient for both isotopes, then thermal activation will not alter the magnitude of the KIE.[1] Although this model appears to account for the wide range of

[1] Please note that enzymes only evolve for H-transfer (rather than D or T-transfers), and, although many WT enzymes exhibit temperature independent KIEs, this result does not necessarily indicate a faster reaction rate (ref. 77) or otherwise better evolved enzyme.

experimental observations, few attempts have tried to quantitatively link the size and temperature dependence of KIEs to the population distribution along the DAD coordinate,[34,53,86] and in most cases, detailed QM/MM simulations have been necessary to achieve a molecular understanding of the reaction.[42-44,87]

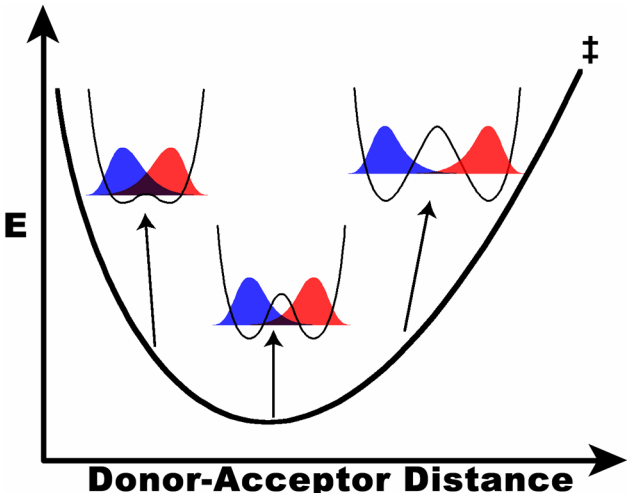

Figure 2.2 PES of the DAD coordinate along the seam where the reactant and product surfaces are degenerate (the TRS). Slices along the orthogonal tunneling coordinate are shown at three different DADs, demonstrating the change in overlap between reactant (blue) and product (red) wave functions. The wave function overlap at each distance is proportional to the tunneling probability at that distance and is isotopically sensitive. This model uses the temperature dependence of KIEs to determine the population distribution of DADs, which is dictated by this PES.

To assist experimentalists in quantitative analysis of data, we expand on previous efforts to connect the temperature dependence of KIEs to a simple physical model. The value of such a phenomenological model, like that of most statistical models, is that it captures the essential physics of the problem for initial assessment of the system under study without all of the molecular detail of an explicit simulation. Although cases where a detailed molecular interpretation is required to understand the chemistry motivate high-level simulations, e.g., QM/MM, they are not necessary in many situations where an

analysis using modified TST or Marcus-like models provides sufficient physical insight into the reaction dynamics (including assessment of whether molecular simulation is needed). We apply the proposed model to several different enzymes and their mutants, including dihydrofolate reductase (DHFR),[35,66,67,88-90] morphinone reductase (MR),[53] thymidylate synthase (TSase),[76,91] alcohol dehydrogenase (ADH),[33,55] formate dehydrogenase (FDH),[92] and pentaerythritol tetranitrate reductase (PETNR),[77] as well as two nonenzymatic sigmatropic rearrangements.[79,93] In contrast to some previous fitting models, we maintain that the experimental data correspond to a single-exponential relationship, and thus, any fitting model must be limited to two adjustable parameters. The question for the experimentalist trying to interpret data is what physical quantities those parameters represent. Fits to the Arrhenius equation and the parameters of that equation have limited physical meaning (i.e., ΔE_a and A_H/A_D) for these kinds of reactions. The method described here allows experimental enzymologists and organic chemists to obtain a quantitative interpretation of their results in terms of a distribution of DADs, but without requiring the expertise, time, and resources necessary to conduct costly QM/MM simulations.[2,4,6,42-45,87,94-97] Furthermore, these calculations result in a number of intriguing predictions that could be examined experimentally.

Methods

We conducted all geometry optimizations and potential-energy surface (PES) scans at the B3LYP/6-31+G* level with *Gaussian 03*.[98] We did all other calculations with *Mathematica 7*.[99]

The overall framework used here follows the model developed by Kuznetsov and Ulstrup (ref. 48, eq. 2.2), but with significant modifications relative to other attempts to implement this type of model.[34,53,86,100] Since the factors outside the integral of eq. 2.2 are essentially isotopically insensitive (i.e., affected by motions of many heavy atoms with

little or no contribution of the isotopically labeled atom), the following ratio of integrals contains the experimental 1˚ KIEs:

$$KIE = \frac{k_L}{k_H} = \frac{\int_{r1}^{r2} F(m_L,DAD)e^{E(DAD)/kT}dDAD}{\int_{r1}^{r2} F(m_H,DAD)e^{E(DAD)/kT}dDAD} \quad [2.3]$$

As mentioned above, the first factor in each integral represents the probability of tunneling as a function of the DAD and the mass of the transferred particle and the second factor is a Boltzmann factor, giving the probability of being at any given DAD. The integral is formally over all DADs, but in reality it is negligible outside of a small region within which the DAD is short enough to give a non-zero tunneling probability (DAD < r_2) but long enough that van der Waals repulsions between the donor and acceptor are small (DAD > r_1). Because upon calculation of KIEs many of the assumptions and expressions that are not isotopically sensitive drop from the equation, and because many experiments directly measure KIEs, without measuring individual rates,[56] this equation should have greater utility than individual rate equations.

The Tunneling Probability

Previous calculations of this type have based the tunneling probability on non-adiabatic models using harmonic[34,100] or Morse[53,86] potentials to describe the donor and acceptor wells. For many reactions, though, adiabatic coupling is very important.[101] Thus, we allow for strong coupling between the donor and acceptor wells, which is more relevant to hydride and proton transfers and gives markedly different results (see below). As with previous models, we assume that the probability of tunneling as a function of DAD does not differ among similar reactions. For computational simplicity, therefore, we base our calculations on the hypothetical symmetric transfer of H^- from reduced to oxidized nicotinamide moieties, in a manner similar to a model for symmetric H-transfer in solution.[102] The donor and acceptor moieties are analogous to the ubiquitous nicotinamide biological cofactor $NAD(P)^+$. A hydrogen truncates the nicotinamide rings

where they normally link to the ribosyl moiety of $NAD(P)^+$, so the system contains a total of 33 atoms (Figure 2.3) and an overall charge of +1. Heavy-atom geometries of the two nicotinamide moieties are optimized at a range of DADs from 2.6 Å to 3.5 Å with the C-H-C angle constrained at 180° and the hydrogen at the midpoint between the donor and acceptor C4 atoms. We previously found this approach sufficient for assessment of the structure of the TRS in yeast ADH.[68] At each DAD, we scanned the PES for linear hydrogen transfer with all other atoms frozen and fit these scans (least-squares) to symmetric quartic potentials (Figure 2.4).

When the system reaches the TRS, the hydrogen is localized in the donor well. Before the degeneracy of the TRS is broken, the donor wave function evolves so that some probability density ends up in the acceptor well (Figure 2.3). To calculate the time evolution of the probability density, we construct donor and acceptor wave functions for each isotope from linear combinations of the ground (φ_0) and first excited (φ_1) eigenstates of the potentials in Figure 2.4.

$$\Psi_{Donor} = \frac{1}{\sqrt{2}}\varphi_0 + \frac{1}{\sqrt{2}}\varphi_1 \quad [2.4]$$

$$\Psi_{Acceptor} = \frac{1}{\sqrt{2}}\varphi_0 - \frac{1}{\sqrt{2}}\varphi_1 \quad [2.5]$$

When the system reaches the TRS, the nonstationary donor wave function evolves in time by coherent oscillations between the donor and acceptor state with a period (τ) dependent on the tunneling splitting (ΔE_t),[103] where

$$\tau(m, DAD) = \frac{\hbar}{\Delta E_t} \quad [2.6]$$

and ΔE_t is the difference in energy between φ_0 and φ_1:

$$\Delta E_t = E(\varphi_1) - E(\varphi_0) \quad [2.7]$$

We calculate ΔE_t for each DAD for H, D, and T by numerical solution of the Schrödinger equation as described previously.[68] To get an expression for ΔE_t as a function of DAD, we fit (least-log-squares) the calculated values to a sum of two exponentials, which

correspond to the behaviors above and below the barrier, respectively (Figure 2.5). When the zero-point energy (ZPE) of the hydrogen is above the barrier, the process is not formally tunneling, but an advantage of this methodology is that the calculations smoothly transition between the region of tunneling[84] and the region of over-the-barrier events.[104]

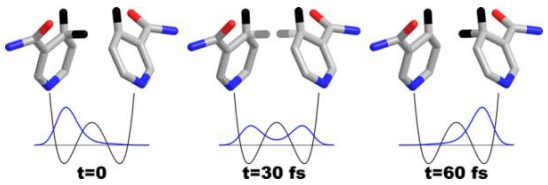

Figure 2.3 The time evolution of the ^{1}H-wavefunction tunneling between two NAD^{+} moieties frozen with a DAD of 3.2 Å. All the heavy atoms used in the calculations are shown, along with hydrogens of particular interest. When the system reaches the TRS (t=0) the hydrogen is effectively localized in the donor well, but its probability density evolves over time, as shown. The coherent oscillation of this wave packet dephases due to environmental perturbations yielding some finite probability of decaying to the acceptor state, resulting in net transfer. An exponential decay with time constant of 10 fs models the dephasing, which is consistent with more sophisticated calculations.[105-107]

The oscillations of the hydrogen wave function result in a probability density in the acceptor well (corresponding to net transfer) as a function of time (*t*) after reaching the TRS given by the expression

$$P(t, m, DAD) = -\frac{1}{2}\left(1 + \cos\left(\frac{2\pi}{\tau(m,DAD)}\, t\right)\right) \qquad [2.8]$$

After reaching the TRS, however, environmental perturbations lead to dephasing of the coherent wavefunction, such that the oscillations effectively cease after a short dephasing time. Calculating the rate of dephasing is not within the scope of the present model, but we can approximate the rate as an exponential decay with time constant of θ=10 fs.[105] This approximation is consistent with other treatments that calculated the

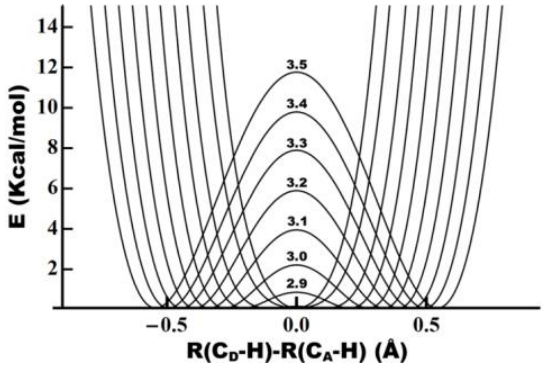

Figure 2.4 PESs for linear C-H→C transfer between two NAD^+ moieties with the heavy atoms frozen at a range of DADs (defined as the distance from C4 of the donor to C4 of the acceptor). Each surface is a symmetric quartic fit (least squares) to a scan of 15-25 points (depending on the DAD) calculated at the B3LYP/6-31+G* level. The DAD in Å is labeled above the barrier for each surface. From this figure it is clear that below 2.8 Å there is no barrier to H-transfer and calculations of ZPE indicate that the hydrogen is above the barrier at even longer distances, depending on the isotope (cf. Figure 2.5).

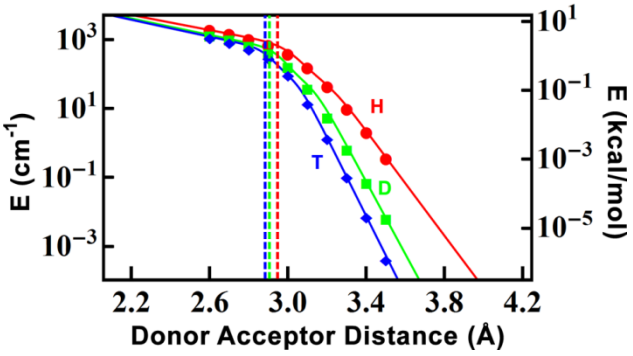

Figure 2.5 Tunnel splitting (ΔE_t) of the three isotopes of hydrogen as a function of DAD (eq. 2.7), calculated as the difference in energy of the first two eigenstates of the potentials in Figure 2.4. The vertical lines indicate the DAD at which each isotope's ZPE is greater than the height of the reaction barrier.

decay of the probability flux correlation function based on the spectral density of the environment,[106,107] a method first described for solution reactions[108] that has found much subsequent use in solution and enzymes.[83,109] Furthermore, the general behavior of the model is not sensitive to the value of θ within the range of 1-100 fs. Using this

exponential dephasing, the overall probability of tunneling as a function of DAD (Figure 2.6) is

$$F(m, DAD) = \frac{\int_0^\infty e^{\left(t/\theta\right)} * P(t,m,DAD)dt}{\int_0^\infty e^{\left(t/\theta\right)} dt} \quad [2.9]$$

We expect this term to be nearly invariant among different hydride transfers between carbon atoms, and at least to yield reasonable trends for other types of hydride and proton transfers. The utility of this function for several different reactions is explored below.

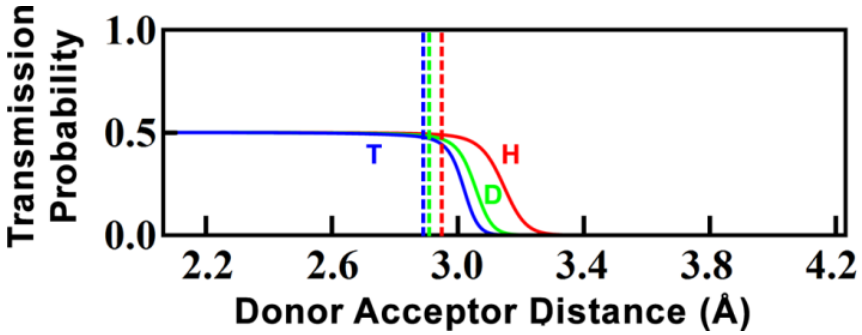

Figure 2.6 Transmission probability for each of the three isotopes of hydrogen as a function of DAD (eq. 2.9). The vertical lines indicate the DAD at which each isotope's ZPE is greater than the height of the reaction barrier.

The DAD Population Distribution

In eq 2.3, the Boltzmann factor within the integral represents the population distribution along the DAD coordinate. This term dictates the size and temperature dependence of the KIEs. We analyze experimental data that range from reactions with completely temperature-independent KIEs (within experimental error) to reactions with steeply temperature-dependent KIEs. Most surprisingly, we find that a model with a single population could not fit the steeply temperature-dependent KIEs. Thus, we present two models below: a single-population model for KIEs with little or no temperature dependence and a model with two populations that accounts for KIEs with all levels of

temperature dependence. We use these two forms of the Boltzmann factor in eq. 2.3 to fit the KIEs. Importantly, we use only two parameters to fit the data with either model. Since experiments measure the temperature dependence of KIEs across a narrow temperature range, and this dependence follows a single exponential relationship, at most two fitting parameters are justified.

Temperature Independent KIEs: One Population

Previous methods used a harmonic potential to approximate the PES that describes the DAD coordinate,[34,53,86,87,100] and where possible, we follow this standard. This gives a Gaussian population distribution of the form

$$e^{E(DAD)/k_BT} = e^{f(DAD-DAD_0)^2/k_BT} \quad [2.10]$$

where the average DAD (DAD_0) and the force constant (f) of the corresponding harmonic potential are adjustable fitting parameters when this factor is substituted into eq. 2.3. In formal terms, this distribution is normalized, but because the probability distribution of DADs is not mass-sensitive, the normalization constants for the two isotopes are equal and thus cancel one another. This type of distribution can fit KIEs with little to no temperature dependence, but even if we allow for physically unreasonable parameters, this distribution cannot lead to the small, steeply temperature-dependent KIEs observed in some reactions (Figure 2.9).

Temperature Dependent KIEs: Two Populations

It is not surprising that simple distributions like eq. 2.10 fail in some cases. For reactions where the donor and acceptor are not well constrained in reactive orientations, they are unlikely to have the same steep potential-energy gradient at long separations (when held by "soft" protein or solvent forces) as when closely approaching each other (under van der Waals radii), as implied by a harmonic potential. Our efforts to fit the temperature-dependent KIEs with more sophisticated functions lead to the conclusion

that at least two distinct populations are required to fit these experimental data in the context of a Marcus-like model.

After exploring a number of ways to describe the population distribution in systems with steeply temperature-dependent KIEs, we find that the simplest model that can fit the data is as follows: One population is centered at a short enough DAD (DAD_{short}) that all isotopes cross the dividing surface between reactant and product with similar probabilities (i.e. the KIE is unity for this population). We choose this population as the zero of free energy (G=0) for the sake of computational simplicity. A second, lower-energy population is centered at a longer DAD (DAD_{long}), where the overall tunneling probability is lower but the isotope effect is larger. In the present model, the precise DAD of the shorter population does not significantly affect the fit to the data, as long as the DAD is short enough that the ZPEs of all three isotopes are above the reaction barrier (cf. vertical lines in Figure 2.6). This population effectively corresponds to a semiclassical transition state.[42,110,111] We assume that the two conformational populations are in thermal equilibrium with one another and that the temperature-dependent change in the relative populations gives rise to the temperature dependence of the KIEs. Thus, the population distribution (the Boltzmann factor in eq. 2.3) has the form

$$e^{-E(DAD)/k_BT} = \delta(DAD - DAD_{short}) + e^{-\Delta G/k_BT}\delta\left(DAD - DAD_{long}\right) \quad [2.11]$$

where the two fitting parameters are DAD_{long} (the DAD of the population at longer distances) and ΔG (the difference in free energy between the two populations). Including a distribution about the average DADs of the two populations requires more parameters and does not yield a better fit, so we leave the populations as δ functions. As with eq. 2.10, this distribution function need not be normalized to calculate KIEs.

Fitting the KIEs

We fit (least-squares) experimental KIEs as a function of temperature to eq. 2.3, using both the single Gaussian distribution (eq. 2.10) and the two-population distribution

(eq. 2.11). Except in cases where one attempts to fit steeply temperature-dependent KIEs to a single population, the fits converge to 16-digit precision within a few seconds, using a Sony laptop with an Intel Core2Duo P8700 processor (2.53 GHz) and 8 GB of RAM. The *Mathematica* program for conducting this type of fitting is available free of charge on the web at http://chemmath.chem.uiowa.edu/webMathematica/kohen/marcuslikemodel.html.

Results and Discussion

We propose a simple phenomenological model that enables quantitative fitting of experimental KIEs and their temperature dependence, yielding up to two physically meaningful parameters that describe the distribution(s) of DADs. To do so, we have modeled the tunneling probability, assuming adiabatic coupling between the donor and acceptor wells. This approach expands the space of possible reactions that can be modeled beyond those in which strictly non-adiabatic tunneling is appropriate.[34,86] Several studies have provided in-depth analyses of the differences between adiabatic and nonadiabatic approaches in this type of vibronic model.[101,112] Here, we find that the coupling of the donor and acceptor increases the length of the C-H bond and substantially decreases the height of the barrier, yielding large regions of wave function overlap at DADs where nonadiabatic models predict negligible probabilities of tunneling (Figure 2.7). As a result, our adiabatic model demonstrates that tunneling occurs from DADs relatively close to the van der Waals distance of the two heavy atoms (3.4 Å for carbon). While several high level simulations suggest tunneling from DADs between 2.6 and 2.8 Å,[42,111] we have shown that there is no barrier to H-transfer at that distance (Figure 2.4) and that distance actually corresponds to the semiclassical transition state. Tunneling from longer DADs, however, is consistent with a model of the TRS of yeast ADH based on 2° KIEs[68] as well as high-level QM/MM simulations of DHFR.[44] A further advantage of the present method is that we need not assume that every reactive trajectory occurs by

tunneling. The transferred hydrogen in the current model behaves as a quantum particle, regardless of the electrostatic environment applied by the heavy atoms of the system. Whether above or below the barrier, the hydrogen is wave-like.[104] Thus, as shown in Figure 2.6, the transmission probability smoothly transitions between DADs where the ZPE is below the barrier to those where it exceeds the barrier height. Even for these over-the-barrier trajectories, though, the heavy-atom reorganization remains the primary motion leading to H-transfer[113,114] (i.e., "the reaction coordinate is the solvent coordinate"[104]). In this type of mechanism, all isotopes cross the dividing surface to products with similar probability once they are above the barrier. As discussed below, this result turns out to be of vital importance in describing steeply temperature-dependent KIEs.

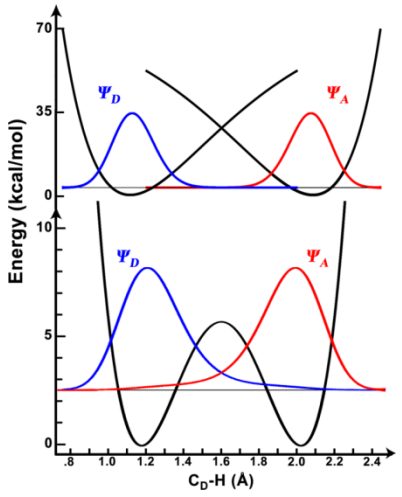

Figure 2.7 Comparison of the wave function overlap between donor (blue) and acceptor (red) states of ^{1}H for the nonadiabatic limit, using Morse potentials (top), and the adiabatic limit used in our calculations (bottom). In both examples the DAD is set at 3.2 Å. The Morse wave functions are the ground eigenstates of the Hamiltonian and the wave functions for the double-well potential were constructed as linear combinations of the ground and first excited eigenstates of the Hamiltonian.

Our approach also expands the range of temperature dependencies of KIEs that can be quantitatively interpreted by a full-tunneling model. The previous phenomenological methods, which used only single harmonic potentials to describe the DAD coordinate, cannot reproduce the steep temperature dependence of KIEs that has been observed in a number of systems (see the Supporting Information). By allowing for two populations along the DAD coordinate, this model fits a variety of KIEs that have been reported for biological hydride and proton transfers, as well as non-enzymatic H-transfers (see examples below). As discussed under Methods, the nature of the experimental data (KIEs over a narrow temperature range, which conform to a single exponential) allows for at most two meaningful fitting parameters.

Fitting the KIEs

The present method gives good fits to experimental KIEs exhibiting a wide range of temperature dependences (ΔE_a), resulting in physically meaningful population distributions along the DAD coordinate in a variety of reactions. The fitted parameters for each reaction are listed in Table 2.1. The experimental data are from measurements by a number of independent researchers who used an assortment of techniques, and all cases represent intrinsic KIEs that are not masked by kinetic complexity. To give a sense of the quality of the fits, we present the results for the enzyme DHFR and two series of mutants in Figure 2.8,[66,67,88] The model achieves similar accuracy for the other systems we examine (see details and figures in the Supporting Information): the nicotinamide-dependent C-H→C transfers in thermophilic ADH from *Bacillus stearothermophilus,* bsADH,[33,55] and FDH,[92] the C-H→N transfer between flavin and nicotinamide in two flavoenzymes, MR[53] and PETNR,[77] the hydride (C-H→C) and proton (C-H→O) transfers that are part of the kinetic cascade in TSase,[76,91] and two non-enzymatic [1,5]sigmatropic rearrangements.[79,93] Given the method of parameterizing the tunneling probability (Eq. 2.9), the details of the current model are most applicable to C-H→C transfers involving

Table 2.1: Experimental ΔE_a and resulting fitting parameters for the systems studied here.

Enzyme/ Reaction	Mutation/ conditions/ reactants	ΔE_a[a]	Fitting Parameters				ref
			1 Population		2 Populations		
			DAD_0[b]	f[c]	DAD_{long}[b]	ΔG[d]	
DHFR active site mutants	**WT**	-0.1±0.2	3.058	>250	3.057	>2.5	35
	I14V	0.30±0.07	3.082	200	3.064	2.3	67
	I14A	0.38±0.03	3.093	190	3.072	2.4	66
	I14G	3.31±0.07	NA	NA	3.307	3.8	67
DHFR distal mutants	**WT**	-0.1±0.2	3.058	>250	3.057	>2.5	35
	G121V	0.25±0.02	3.084	390	3.072	2.8	90
	M42W	0.55±0.03	3.119	80	3.072	1.9	89
	G121V-M42W	3.7±0.2	NA	NA	3.342	4.4	88
bsADH[f]	**WT > 30°**	0.1±0.2	3.094	>100	3.086	>2.0	33
	WT < 30°	0.7±0.2	NA	NA	3.158	1.1	33
	L176V > 30°	1.7±0.9	NA	NA	3.232	2.3	55
	L176V< 30°	2.3±0.5	NA	NA	3.282	3.1	55
	L176A > 30°	1.6±0.5	NA	NA	3.231	2.3	55
	L176A < 30°	0.8±0.6	NA	NA	3.158	1.3	55
	L176G > 30°	1.4±0.5	NA	NA	3.212	1.9	55
	L176G < 30°	1.0±0.7	NA	NA	3.177	1.4	55
	L176Δ > 30°	1.8±0.3	NA	NA	3.244	2.5	55
	L176Δ < 30°[g]	-0.4±0.3	3.095	>1000	3.094	>4.0	55
	V260A > 40°	1.8±0.7	NA	NA	3.239	2.4	55
	V260A < 40°	0.0±0.4	3.094	>100	3.091	>2.0	55
MR[f]	**W106A**	0.0±0.4	3.110	>150	3.110	>2.5	53
	WT	2.0±0.4	NA	NA	3.211	2.3	53
	V108L	2.1±0.4	NA	NA	3.235	2.6	53
PETNR[f]	**NADH**	0.1±0.2	3.120	>400	3.117	>3	77
	NADPH	1.4±0.1	NA	NA	3.175	1.9	77
TSase	**H^--transfer**	0.0±0.6	3.062	>100	3.061	>2	76
	H^+-transfer	8.3±0.3	NA	NA	3.612	9.5	91
FDH	**WT**	-0.03±0.04	3.057	>1000	3.056	>3	92
[1,5]sigmatropic rearrangement[f]	**Pentadiene**[h]	1.4	3.553	16	3.145	2.3	93
	Quinolizine	-0.01±0.02	3.101	>2000	3.100	>5	79

Table 2.1 continued

[a]H/T KIEs except where noted. All energies are in kilocalories per mol. In some cases raw data were not published so we used approximations of the actual data points and errors based on visual inspection of published figures (on log scales) in the fittings. Thus, the ΔE_a shown here may differ from previously published values, but corresponds to the data points used in the modeling.

[b]In angstroms. Errors are <5% of reported value.

[c]In kilocalories per mole per square angstrom. Only a lower bound is given for systems within error of ΔE_a=0; the lower bound is the value such that the calculated ΔE_a (in the middle of the observed temperature range, using the best fit value for DAD_0) is equal to the upper error of the observed ΔE_a ($\Delta E_a + \sigma$). Errors for other systems are <15% of reported value.

[d]Only a lower bound is given for systems within error of ΔE_a=0; errors for other systems are <15% of the reported value.

[e]Not applicable (NA) for systems with a ΔE_a of >1 kcal/mol at 298 K.

[f]H/D KIEs.

[g]This model is not designed to fit inverse temperature dependence (ΔE_a<0).

[h]Errors unavailable because individual data points were not published; measurements were taken at >450 K, so the one population model was successful despite ΔE_a>1 kcal/mol.

nicotinamide cofactors (DHFR, bsADH, and FDH). One should interpret the precise results for the other three enzymes (MR, PETNR, and TSase) and the nonenzymatic reactions with caution, but we believe the overall trends among those reactions are fairly robust. To obtain more accurate results for those reactions, one could reparameterize the tunneling probability (eq. 2.9) to focus on H-transfers more relevant to those systems.

We display the KIEs of Figure 2.8 (and those in the Supporting Information) as Arrhenius plots (1/T vs. KIE on a log scale), following the tradition of phenomenological analysis of KIEs by the Arrhenius or Eyring equations[7,49]

$$KIE = \frac{k_L}{k_H} = \frac{A_L}{A_H} e^{\Delta E_a / kT} \qquad [2.12]$$

where A_i is the Arrhenius pre-exponential factor for isotope i, and ΔE_a is the difference in activation energy between the two isotopes. By this analysis, temperature-independent

KIEs give a ΔE_a close to 0, often associated with A_L/A_H greater than the semi-classical limits (i.e., greater than unity). Some temperature-dependent KIEs, however, show a very large ΔE_a that cannot be ascribed to mere isotopic differences in ZPE and, furthermore, show A_L/A_H much lower than the semiclassical limit. For other reactions, A_L/A_H is close to unity and ΔE_a also falls within the semiclassical limits. Despite this large variation in the behavior of KIEs, the method described here provides excellent fits to the entire range of results, using either a single population (where possible) or two distinct populations. Among the systems examined here, we find a cutoff at around ΔE_a=1.5 kcal/mol (at 298 K) for H/T KIEs, above which a single conformational population cannot fit the KIEs (see the Supporting Information). Thus, as seen in Table 2.1, all of the systems where the H/T KIE exhibits a ΔE_a of >1 kcal/mol at 298 K can be fit only with the model that uses two populations. Thus, in those systems, the parameters in the single population model are listed as not applicable (NA). Since the experimental data conform to a single-exponential function, two parameters are necessary and sufficient to describe the data. In the cases where ΔE_a=0 (within experimental error), the information content of the experimental data reduces to a single parameter (A_L/A_H), so only a lower bound is given for the second fitting parameter in each model in Table 2.1. Truly temperature-independent KIEs imply no DAD sampling ($f = \infty$, or $\Delta G = \infty$), so the lower bound indicates the certainty (based on experimental errors) that the KIEs are truly temperature-independent; a larger lower bound means more certainty. It is important to note that different values of this lower bound report on the quality of the data analyzed rather than the nature of the system under study. One of the mutant enzymes in ref 53 (V108A) apparently exhibited inverse temperature dependence ($\Delta E_a<0$), but the data and statistics are far from the quality of other data in the same work. Given the quality of these data and the fact that negative ΔE_a could not be appropriately modeled by either one population or two populations, and because much higher levels of theory have examined only a few such cases,[115] we do not address these data here.

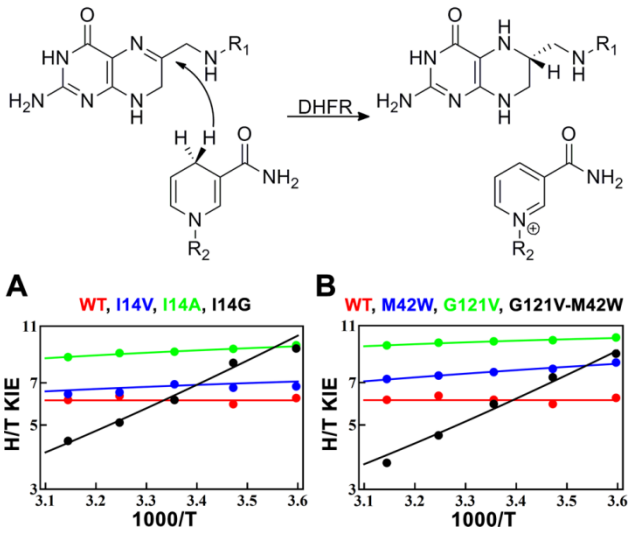

Figure 2.8 Reaction catalyzed by DHFR and the fits to KIEs from a series of active-site mutants (A), and a series of distal mutants (B). All fits correspond to the two-population model. Experimental data are from refs 66,67,88.

In general, the distributions we obtain using a single population for DHFR and its remote mutants agree qualitatively with QM/MM simulations that calculated the DAD PES for these enzymes,[44] suggesting that this kind of model truly captures the essential physics involved in H-transfer. Furthermore, in most cases our fits agree with the trends found using nonadiabatic tunneling models.[34,86] The fits to KIEs with little temperature dependence (ΔE_a<1 kcal/mol) show a correlation between ΔE_a and both the average DAD and the force constant of the corresponding harmonic potential (Table 2.1): a steep force constant and a short DAD gives a small ΔE_a, while a longer DAD and a smaller force constant gives a larger ΔE_a. Thus, in accordance with another recent analysis,[116] small force constants give smaller KIEs at higher temperatures because barrier compressions *decrease* rather than *increase* nuclear quantum effects. Barrier compression decreases the width and height of the barrier (Figure 2.4), allowing the isotopes to behave more similarly to one another. This behavior is consistent with the qualitative arguments that have emerged during recent years to describe these experimental results.[7,49]

The observation that changes, such as mutations, alternate substrates, and nonphysiological temperature ranges, can change temperature-independent KIEs into temperature-dependent KIEs motivates the hypothesis that the conformational distribution along the DAD coordinate is important for enzyme-catalyzed reactions.[34,44,53,88] In the context of small ΔE_a, the DAD potential has a lower force constant and longer average DAD.[34,53,86,100] We cannot, however, model the steeply temperature-dependent KIEs (ΔE_a > 1 kcal/mol at 298 K) with a single population and require at least two populations at the TRS. As with the one-population model, some clear trends emerge in how the interplay between the two populations affects the temperature dependence of the KIEs with ΔE_a > 1 kcal/mol (Table 2.1). If the DAD of the long population is especially long and much lower in energy, the system exhibits larger ΔE_a.

The molecular interpretation of the two conformational substates for reactions with large ΔE_a warrants further discussion. Perhaps the simplest interpretation comes in the context of the series of active-site mutants for *Escherichia coli* DHFR (Figure 2.8A). This set of experiments examined the effects of a hydrophobic residue in the active site (I14) that appears to hold the nicotinamide ring of the H-donor in place through steric effects.[66,67] As the size of the residue decreases from I to V to A to G, ΔE_a becomes larger and larger. The wild type has ΔE_a of ≈0, and thus, both fitting models converge to a single, narrowly defined conformation with a DAD of 3.06 Å. At the other end of the series, the I14G mutant has a ΔE_a of 3.31 kcal/mol, and only the model with two populations can fit the data. One can interpret this as an indication that the missing side chain leaves so much space in the active site that the substrates can adopt different conformations, as also suggested by molecular dynamics (MD) studies.[67] The I14V and I14A mutants (ΔE_a of 0.30 kcal/mol and 0.38 kcal/mol, respectively) can be modeled by either a single population or two populations. The results of a single population suggest that they have a smaller force constant and longer average DAD than the wild type; under

the two-population model they have a smaller ΔG and shorter DAD_{long} than I14G. Because both models give adequate fits to these systems, these methods cannot indicate a preference for one interpretation over the other, and higher-level simulations will be necessary to make a judgment.

A closer examination of the differences between wild-type DHFR and its I14G mutant reveals how two distinct populations may lead to the steep temperature dependence of KIEs exhibited by the mutant (Table 2.1 and Figure 2.8A). In the mutant, the vast majority of the TRS population has a DAD long enough (3.33 Å) that the probability of H-tunneling is much larger than the probability for T (or D). A small portion of the population (≈0.1 % at 298 K), however, is at a short enough DAD that all isotopes can cross the dividing surface between reactant and product equally well. At low temperatures, far greater overall population resides at the long DAD, where ^{1}H has a large advantage in tunneling, leading to a large KIE. Increasing temperature populates the short DAD (from which heavy isotopes can also be transferred), so the relative advantage of ^{1}H tunneling from the longer DAD decreases, resulting in strongly temperature-dependent KIEs. For the WT DHFR, on the other hand, a change in temperature will have the same effect on both isotopes: it will not cause a population shift, and the KIE change with temperature will be minimal.

The idea of a "steric hole" opening in the active site in the DHFR I14G mutant is a reasonable and intuitively satisfying explanation, but a similar interpretation of the conformational distributions of the G121V/M42W double mutant [residues distant from the active site (Figure 2.8B)], for example, seems less obvious. A limitation of this model is that it merely finds a one-dimensional distribution of DADs, without regard to other conformational fluctuations that may be important.[94] Thus, the distributions obtained represent ensembles of conformations, i.e., different states of "preorganization".[7,49]

The finding of distinct populations along the DAD coordinate is reminiscent of a recent suggestion that anomalously large Arrhenius pre-exponential factors in bsADH

(and its mutants) result from the sampling of distinct conformations, each of which has different kinetic properties.[117] Additionally, pre-steady state experiments on a mutant of MR also suggested multiple kinetically distinct, reactive conformations and indicated that steady-state rate measurements cannot probe the nature of such conformations.[118] Here we have shown that analysis of the temperature dependence of KIEs can uncover such reactive conformations, regardless of how the intrinsic KIEs were measured. Another recently published model of KIEs also suggested distinct reactive conformations.[12] Like the two-conformation model presented here, the model by Mulholland and coworkers[12] proposed one reactive conformation that proceeds by tunneling and one that surmounts the barrier. Like that model, our two-state model for temperature dependent KIEs does not depend on DAD fluctuations (only ΔG° between the states). This being said, nothing in the functional form of the model excludes the possibility of DAD fluctuations as we use for temperature independent KIEs. A difficulty with that model, however, is that it requires 9 parameters to describe data that fit to a single exponential (or two exponentials if the individual rates of the isotopes are considered). The model presented here, though, uniquely fits the temperature dependence of KIEs using just two fitting parameters.

Conclusions

We present a simple and user-friendly adiabatic model of H-tunneling in hydride- and proton-transfer reactions that can be used to generate a population distribution along the DAD coordinate by fitting to experimental KIEs and their temperature dependence. Practically, this new fit converts the isotope effect on entropy and enthalpy one gets from fitting to the Arrhenius or Eyring equations into two parameters indicative of the distribution of DADs. We suggest these two parameters provide a more molecular interpretation of the experimental data than ΔEa and A_H/A_D. We demonstrate the utility of this fit for several enzymatic and nonenzymatic systems, including a number of different types of C-H$\rightarrow$C and other H-transfers. This simple, quantitative fitting of the

experimental data, which is readily accessible to all experimentalists, gives a physically meaningful picture of how the temperature dependence of KIEs reflects the arrangement of H-donor and H-acceptor. In the case of enzymatic reactions, this model provides parameters that correlate with the effects of mutations, alternative substrates, or changes in conditions that alter the ensemble of reactive conformations. For the non-enzymatic reactions, the parameters correlate with the rigidity of the reacting system, e.g. an intramolecular reaction in a fused ring system versus reactants with more conformational flexibility (see the Supporting Information). Importantly, the results imply that reactions with steeply temperature-dependent KIEs must occur from at least two distinct conformational substates: one that involves inefficient tunneling from a long DAD and one in which heavy-atom rearrangement (isotopically insensitive enzyme or solvent motion) brings the system to a short DAD where the ZPE of the transferred particle is above the barrier. In contrast to earlier phenomenological models, the current procedure also reproduces small, steeply temperature-dependent KIEs (see the Supporting Information). Like previous phenomenological methods, the model presented here does not assume nonstatistical dynamic effects and uses the equilibrium distribution of DADs to calculate the tunneling probability. Because the model here that allows for multiple conformations can explain the full range of experimental data, while a single-population model cannot, this two-population model is more generally applicable. Of course, all the reactions studied here may occur from many different substates, and our model projects the full ensemble of substates onto two populations because the most one can extract from the given experimental data (KIEs and their temperature dependence) is two states, defined by two parameters. Additional experiments, as well as high-level calculations and simulations, will be necessary to determine more details of conformations that contribute to H-transfers for each specific system. This new tool is not meant to replace proper molecular calculations by QM/MM methods, but those techniques are expensive and highly specialized, whereas this program is very simple to use and is available, free of

charge at

http://chemmath.chem.uiowa.edu/webMathematica/kohen/marcuslikemodel.html

Supporting Information

Additional discussion of the limits of a single population

As mentioned in the main text, models with a single population along the DAD coordinate could not fit the data from the systems with the most steeply temperature-dependent KIEs. As an example of the failure of a single population, we show the resultant fits to the KIEs from I14G DHFR (ΔE_a=3.3 kcal/mol) using both the present model and a previous model for nonadiabatic tunneling (Figure 2.9).[48] At 298 K, the best fit using the present model has a ΔE_a=1.2 kcal/mol and the fit with the previous model has a ΔE_a=1.5 kcal/mol, which appear to be the upper limits for the temperature dependence that can be modeled with a single population. Note that these limits refer only to H/T KIEs: the limits for H/D KIEs will be different. Furthermore, the precise limit for ΔE_a will depend on the actual size of the KIEs in question. We have not provided an exhaustive list of the limits of various models of this type, but given that tunneling probability as a function of DAD is qualitatively very similar among these models,[34,48,86,119] we do not expect any of them to fit KIEs like those from I14G DHFR or the systems found to have even steeper temperature dependence.

Additional discussion of the overall behavior of the model

The overall behavior of the two models, that is, the KIE and its temperature dependence as a function of the two fitting parameters, is not, in general, simple to describe. Figures 2.10 and 2.11 show contour plots that demonstrate the complex behavior of the one- and two-population models, respectively, within relevant ranges of the fitting parameters. While trends exist within certain sectors of these figures, we hesitate to make any broad statements about the effects of any given fitting parameter.

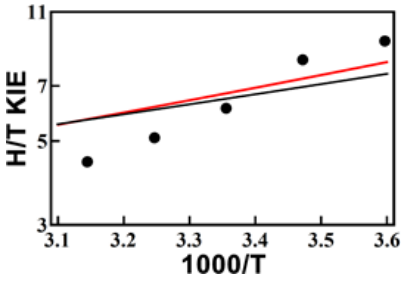

Figure 2.9 Best fits to the KIEs from I14G DHFR using a single population along the DAD coordinate in the model described in the main text (black) and a model for nonadiabatic H-transfer (red). Figure 2.8 in the main text presents the good fitting of the new model to the same set of data.

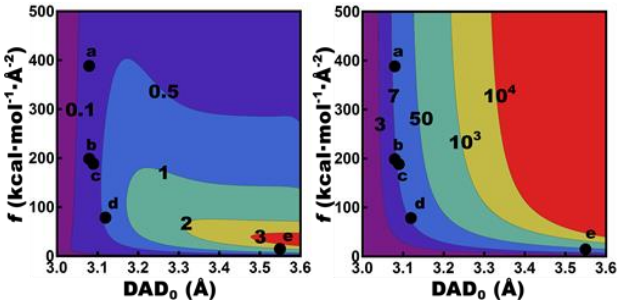

Figure 2.10 Contour plots of ΔE_a in kcal/mol (left) and H/T KIE (right) as a function of average DAD (DAD_0) and force constant (f), using the one population model for systems with little or no temperature dependence in their KIEs. The black dots represent the places where some of the systems re-analyzed in the present study fall on these surfaces and are labeled as follows: a, G121V DHFR; b, I14V DHFR; c, I14A DHFR; d, M42W DHFR; e, [1,5] sigmatropic rearrangement of pentadiene.

Details and discussion of examples addressing environmental and alternative-substrate effects

From all the examples presented in Table 2.1, only the active site and the remote mutations of dihydrofolate reductase (DHFR, Figure 2.8) and the studies of wild-type formate dehydrogenase (FDH, Figure 2.12) are discussed in the main text. Here we present a similar, though more concise, discussion of the other examples, for which reported KIEs' temperature dependence was fitted (Table 2.1).

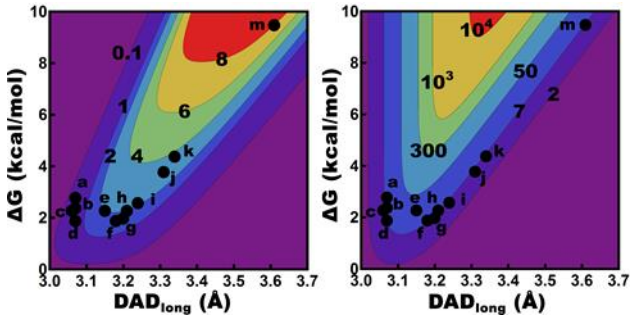

Figure 2.11 Contour plots of ΔE_a in kcal/mol (left) and H/T KIE (right) for the enzymes with steeply temperature dependent KIEs using two distinct populations along the DAD coordinate. This model is a function of the DAD of the long population (DAD_L) and the difference in free energy between the two populations (ΔG). The black dots represent the places where some of the systems examined in the present study fall on these surfaces and are labeled as follows: a, G121V DHFR; b, I14A DHFR; c, I14V DHFR; d, M42W DHFR; e, [1,5] sigmatropic rearrangement of pentadiene; f, PETNR/NADPH; g, bsADH < 30˚ C; h, wt MR; i, V108L MR; j, I14G DHFR; k, G121V-M42W DHFR; m, TSase H^+-transfer.

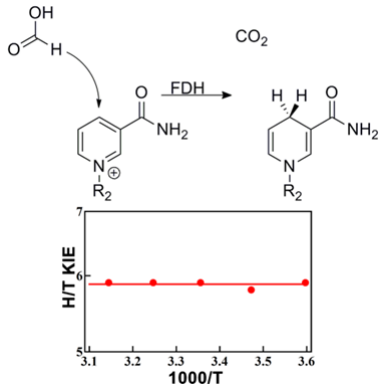

Figure 2.12 The reaction catalyzed by FDH and the fit to KIEs for the reaction. The fit corresponds to the two-population model. Experimental data are from ref. 92.

Morphinone reductase[53] In the main text, we primarily discussed differences resulting from specific mutations and their effects on conformational sampling along the DAD coordinate. The example of morphinone reductase (MR, Figure 2.13) is somewhat similar to that of the effect of mutations on DHFR (Figure 2.8).

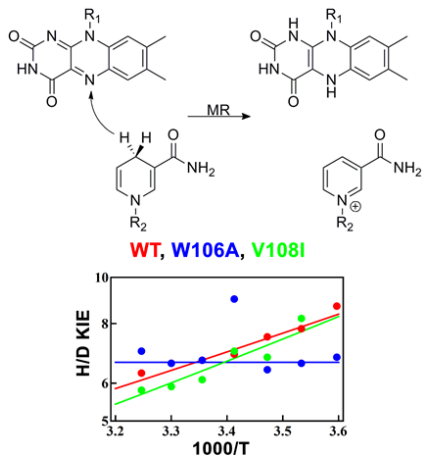

Figure 2.13 The reductive half-reaction catalyzed by MR and the fits to KIEs of the enzyme and a series of its mutants. All fits correspond to the two-population model. Experimental data are from ref 53.

ADH from *B. stearothermophilus*[33] In some cases it has been observed that a wild-type enzyme can exhibit temperature-independent KIEs under one set of conditions but give steeply temperature-dependent KIEs under a different set of conditions. The earliest example of this kind of behavior came from a study of a thermophilic ADH from *B. stearothermophilus* (bsADH) over a large temperature range (ref 33, Figure 2.14). The study found that above 30° C, the KIEs were temperature independent, but below that (outside the physiological range of the enzyme), the KIEs were temperature dependent. The authors posited that thermal motions dictating the DAD sampling at the TRS were "frozen" below 30° C, amounting to a sort of phase transition. Indeed, the present model could not achieve a good fit to the full range of KIEs, but we found that by fitting the KIEs above and below 30° C separately, the best-fit DAD distribution is substantially altered outside the physiological temperature range. From the new fitting (Table 2.1), the system appears to exhibit a single narrow distribution of DADs within the physiological range (above 30°C), but at temperatures below 30° C, rigidified portions of the protein seem to alter the available conformations, leaving most of the reactive ensemble in a state

with a longer DAD and only a small population in a state with a short DAD (ΔG of 1.1 kcal/mol between the two states, i.e., 15% at the short DAD). This result is consistent with the recent implication of multiple states to explain anomalous Arrhenius pre-exponential factors in the mutants of this enzyme.[117] We note that it is possible to fit the entire range of KIEs using a high-order polynomial as the PES dictating the DAD distribution, but the interpretability of the model declines with each additional fitting parameter so we prefer to fit the two ranges separately.

Recently, additional work on this enzyme showed that some of its mutants exhibit precisely the opposite effect of the wild type.[55] That is, some of the mutants show temperature dependent KIEs within the normal physiological range, but temperature independent KIEs at lower temperatures (Figure 2.14). Since many of the KIEs from that study were steeply temperature dependent and could not be fitted to a single population using our model, we cannot directly compare all of our fits to the qualitative interpretation described in ref 55, which assumed a single population along the DAD coordinate. We do note, however, that among the three systems that had temperature independent KIEs (wild type > 30 ˚C, L176Δ < 30 ˚C, and V260A < 40 ˚C) and could thus be fitted to a single population, the trend in DAD concurs with the conclusions of ref 55. That is, longer DADs in the mutants lead to larger KIEs. That said, since the best fit for the wild-type is slightly temperature dependent, its best fit force constant in the one population model is somewhat lower than those of the two mutants (despite the lower limit of error being the same), meaning that the same DAD gives smaller KIEs in the wild-type. A shorter DAD for the wild type >30 ˚C (leading to smaller KIE) is only observed for the two populations model (Figure 2.11 and Table 2.1). We note that as in ref 34, the size of temperature independent KIEs is very sensitive to the DAD (Figure 2.10). Thus, only very small changes in structure are needed to change the KIE from 3 (wild type > 30 ˚C) to 4 (L176Δ < 30 ˚C and V260A < 40 ˚C). The similarity of fitting parameters for these systems resembles the similarity of fitting parameters found in ref 34

for the wild type, L546A, and L754A mutants of soybean lipoxygenase, where within a reasonable level of precision, the fitting parameters were identical, despite some differences in the size of the KIEs. Thus, a general feature emerges: according to fits of KIEs to Marcus-like models, the KIE is so sensitive to small changes in DAD that small differences in the size of KIEs only reflect very subtle changes in average DAD. Nevertheless, observed differences in the temperature dependence of the KIEs (ΔE_a) do reflect significant differences in the distribution of DADs (*f* or ΔG).

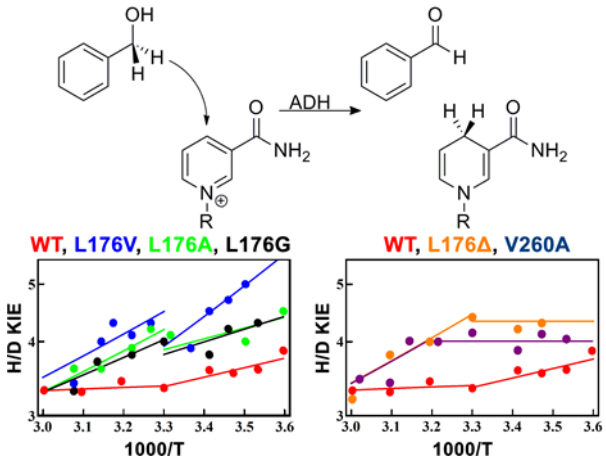

Figure 2.14 The reaction catalyzed by bsADH and fits to the KIEs of the wildtype and a series of mutants in the physiological temperature range (>30°) and below that range (<30°). The fits all belong to the same series of mutants and are only shown in two separate plots for clarity. All fits correspond to the two-population model. Note that the V260A has its break at 40° and above that temperature the best fit is nearly identical to the L176Δ. Experimental data are from refs 33,55.

Pentaerythritol tetranitrate reductase[77] Another intriguing case is the situation of PETNR, the KIEs of which were measured using both NADH and NADPH as substrates (ref 77, Figure 2.15). Despite being faster by a factor of 15 at 25° C, the reaction with NADPH exhibited temperature-dependent KIEs, giving two populations at the TRS instead of the single population for NADH. The large change in conformational

sampling for the alternate substrate is especially surprising given how far away the additional phosphate group is from the transferred H (15 Å in the crystal structure, PDB ID 3KFT). This finding, like the results for distal mutants of DHFR, supports the theory that motions involved in shaping the conformational distribution at the active site involve residues throughout the protein. The fact that the more reactive substrate shows a less optimal distribution may indicate that the enzyme can use both substrates under physiological conditions and experienced more evolutionary pressure to "fine tune" the slower reaction.

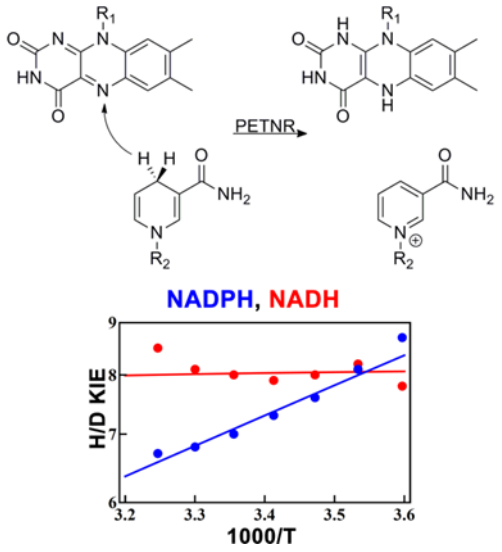

Figure 2.15 The reductive half-reaction catalyzed by PETNR and fits to KIEs measured with two different cofactors. Both fits correspond to the two-population model. Experimental data are from ref 77.

Thymidylate synthase[76,91] Finally, we address the interesting example of TSase, for which KIEs in both the H^+- and H^-- transfers were measured (refs 76,91, Figure 2.16). These studies found temperature-independent KIEs for the rate-limiting H^--transfer, which yield a single narrow population of DADs,[76] while the H^+-transfer showed very steeply temperature-dependent KIEs. These findings may again indicate that the enzyme

has experienced more evolutionary pressure to optimize the slower, rate-limiting step. Despite the fact that the fitting method was parameterized for C-H-C rather than C-H-O transfers, we suggest that the fit for the H^+-transfer, which gives two very distinctive populations, is at least qualitatively meaningful.

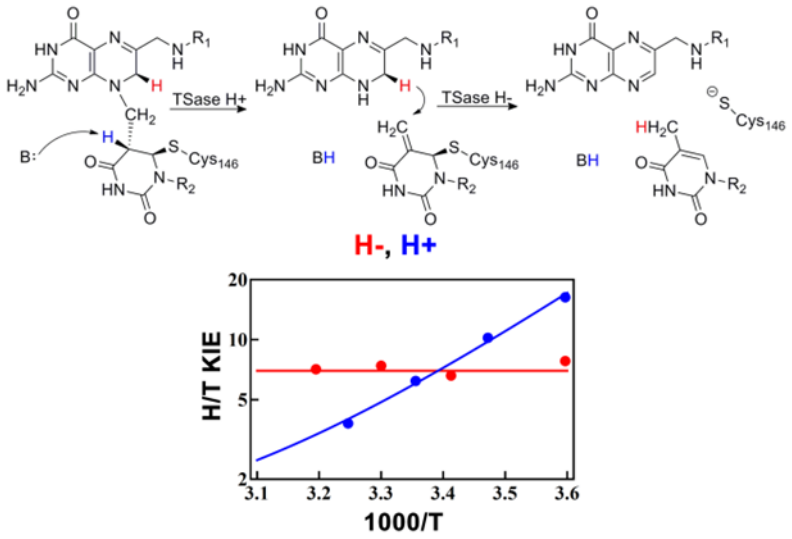

Figure 2.16 The H^+-transfer and H^--transfer catalyzed by TSase and fits to the KIEs for the two steps. Both fits correspond to the two-population model. Experimental data are from refs 76 and 91.

Non-enzymatic systems[79,93] We also analyzed the KIEs for two examples of non-enzymatic [1,5] sigmatropic rearrangements (refs 79,93, Figure 2.17). In these cases, the rearrangement of pentadiene yielded temperature-dependent KIEs suggesting two populations at the TRS, or alternatively, a single very loosely bound population. The KIEs measured for the reaction of quinolizine, on the other hand, were temperature independent, indicating a single narrow distribution of DADs. This corresponds well with the notion that the fused ring system of quinolizine severely hinders conformational flexibility, while the pentadiene has much more freedom at the TRS.

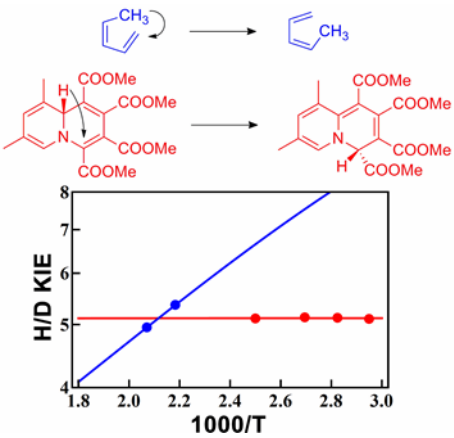

Figure 2.17 KIEs of the [1,5] sigmatropic rearrangements of quinolizine (red, ref 79) and pentadiene (blue, ref 93) and fits to the KIEs for the two reactions. Both fits correspond to the two-population model. Since the rates for H- and D-transfer in pentadiene were measured at different temperatures (though the same overall range of temperatures), the points shown represent the KIEs computed with the Arrhenius equation (eq. 2.12) from the difference in the Arrhenius parameters for the H- and D-transfer. The fitted line is then a fit to those two points using the computational model presented in the main text.

CHAPTER III

ELUSIVE TRANSITION STATE OF ALCOHOL DEHYDROGENASE UNVEILED

This chapter is reprinted from Roston, D; Kohen, A. *Proceedings of the National Academy of Sciences*. 2010, 107, 9572-9577.

Abstract

For several decades the hydride transfer catalyzed by alcohol dehydrogenase has been difficult to understand. Here we add to the large corpus of anomalous and paradoxical data collected for this reaction by measuring a normal (>1) 2° kinetic isotope effect (KIE) for the reduction of benzaldehyde. Because the relevant equilibrium effect is inverse (<1), this KIE eludes the traditional interpretation of 2° KIEs. It does, however, enable the development of a comprehensive model for the "tunneling ready state" (TRS) of the reaction that fits into the general scheme of Marcus-like models of hydrogen tunneling. The TRS is the ensemble of states along the intricate reorganization coordinate, where H tunneling between the donor and acceptor occurs (the crossing point in Marcus theory). It is comparable to the effective transition state implied by ensemble-averaged variational transition state theory. Properties of the TRS are approximated as an average of the individual properties of the donor and acceptor states. The model is consistent with experimental findings that previously appeared contradictory; specifically, it resolves the long-standing ambiguity regarding the location of the TRS (aldehyde-like vs. alcohol-like). The new picture of the TRS for this reaction identifies the principal components of the collective reaction coordinate and the average structure of the saddle point along that coordinate.

Introduction

Enzymes enhance the rates of chemical reactions by many orders of magnitude and extensive studies have uncovered many aspects of how they do so. The prevailing theory that enzymes stabilize the transition state (TS) relative to the reactants explains many phenomena and a great deal of contemporary research focuses on how enzymes stabilize the TS. An unfortunate hindrance to developing an understanding of how enzymes stabilize the TS lies in the enigmatic nature of the TS. Many enzymatic hydrogen (proton, hydrogen, or hydride) transfers, for example, occur by quantum mechanical tunneling, where a particle passes through an energy barrier due to its wave properties.[4,5,41,49,120,121]

Yeast alcohol dehydrogenase (yADH) serves as an excellent model system for enzyme catalyzed H-transfer because unlike many other enzymes, the chemical step, oxidation of a primary alcohol to an aldehyde by NAD^+, is rate limiting with aromatic substrates.[57] Furthermore, the thermodynamics of the reaction allow for examination of both the forward (alcohol to aldehyde) and reverse (aldehyde to alcohol) reactions under similar conditions.[58] This type of nicotinamide-dependent redox reaction appears ubiquitously in biology and a detailed picture of the TS of such reactions may facilitate many medical and industrial applications.

Intriguingly, decades of experiments on the reaction catalyzed by yADH have returned what appear to be contradictory results, some suggesting an early TS, while others point to a late TS.[57,58,122,123] In pioneering studies, Klinman measured linear free energy relationships (LFERs) using benzyl substrates in both forward and reverse directions, and found evidence to support an alcohol-like TS,[57,58] despite the fact that Hammond's postulate predicts a late TS for this slightly endothermic reaction (internal K_{eq}=0.15, i.e., ~1 kcal/mol).[122] Klinman also examined 2° kinetic isotope effects (KIEs) only to implicate an aldehyde-like TS.[58] 2° KIEs measure the ratio of reaction rates of substrates that differ only in isotopic substitution of a bond that is not cleaved during the

reaction. They serve as tools for determining TS structure because they reflect changes in hybridization along the reaction coordinate. The traditional formulation of 2° KIEs predicts that a very early TS will give a KIE of unity and a very late TS will give a KIE equal to the equilibrium isotope effect (EIE).[25] A few years later, though, experiments on the homologous horse liver ADH (hlADH) found that 2° KIEs on the nicotinamide exceeded the 2° EIEs. To explain these results, Cleland and co-workers suggested that the reaction involves quantum mechanical H-tunneling and coupled motion between the 1° and 2° hydrogens (Figure 3.1).[26] Subsequently, H tunneling appeared to be a common feature for H transfer in both enzymatic and nonenzymatic reactions.[2,124]

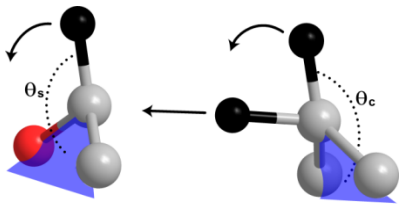

Figure 3.1 Schematic TRS of the reverse reaction (aldehyde to alcohol) showing 1°-2° coupling. The hydrogens are black, the carbons are grey, the oxygen red, and the three heavy atoms define the blue plane. Traditional models of "tunneling and coupled motion" proposed that the reaction coordinate involved motion of all three hydrogens (shown with arrows). The model presented here parameterized the out-of-plane bending angles of the benzyl substrate and nicotinamide cofactor, θ_s and θ_c, respectively, in order to obtain a symmetric double-well potential along the H-transfer coordinate.

Concurrent with these experimental findings, several theoreticians developed a simplified empirical underpinning to the concept of tunneling and coupled motion and predicted that deviations from the semi-classical Swain-Schaad exponents (SSEs)[30] could serve as strong evidence for such behavior.[61,63,125] Semi-classically, the SSE is

$$SSE = \ln(k_H/k_T)/\ln(k_D/k_T) = 3.3 \qquad [3.1]$$

where k_i is the reaction rate with isotope *i*. Confirmation of this prediction came quickly thereafter in a seminal paper by Klinman's group that found a glaringly elevated mixed-labeling SSE (mSSE) for 2° KIEs in yADH,[31] where

$$mSSE = \ln(k_H^H / k_T^H) / \ln(k_D^D / k_T^D) \quad [3.2]$$

where k_j^i is the rate when *i* is the hydrogen isotope at the 1° position and *j* is the hydrogen isotope at the 2° position. An elevated mSSE later appeared in other ADHs[32,33] as well as other types of enzymatic hydrogen transfers.[71]

Some empirical models[27,126] as well as QM/MM studies,[95,97,110,127] have achieved moderate success in replicating the observed 2° mSSEs. While not rigorously defined in those studies, the concept of "tunneling and coupled motion" complicated the traditional interpretation of 2° KIEs, so that the location of the TS needs not be proportional to the 2° KIEs. A new and more comprehensive empirical model is proposed below.

Here we report measurements of H/T and D/T 2° KIEs on benzaldehyde in the reverse reaction that fall outside the range of the EIE to unity, a finding that mirrors 2° KIEs on the nicotinamide cofactor.[26] The new KIE measurements completed the set of 2° KIEs for this reaction (both substrates in both directions). This set guided our development of a more complete empirical model that explains all the apparently contradictory findings regarding the ADH reaction. This model implies a "tunneling ready state" (TRS), which is a special case of the more general TS.[70] The TRS is the ensemble of states from which H tunneling occurs and like the general case of TS is a saddle point along a coordinate that represents the motions that bring the system from the ground state to the TRS. The present approach uses the framework of Marcus-like models of hydrogen tunneling[34,41,48-50,70,74] and identifies some of the principle components of the collective reaction coordinate. This empirically parameterized model quantitatively replicates all of the 2° KIEs in the forward and reverse directions, as well as their mSSEs, and the LFER findings. The model also indicates an asynchronized hybridization for the

donor and acceptor carbons, which was first identified for dihydrofolate reductase (DHFR) by QM/MM calculations.[128] Finally, in accordance with the EA-VTST results from Truhlar, Gao, and coworkers,[95,110] the model supports the recently articulated hypothesis that the inflated mSSEs reported for many ADHs since 1989 result from deflated 2° D/T KIEs due to the shorter donor-acceptor distance (DAD) required for D-transfer.[41,54] The new model mirrors some of the previous empirical calculations on ADH and other systems,[27,61,125,126,129] but provides a more comprehensive molecular and electronic interpretation. The interpretation of experiment by this method agrees well with the results from QM/MM simulations[95,110] that also led to deviations from semiclassical 2˚ mSSEs in the forward direction.

Results and Discussion

Measuring 2° H/T and D/T KIEs on Benzaldehyde Reduction

Traditionally, models expected the magnitude of 2° KIEs to vary between unity for a reactant-like TS and the EIE for a product-like TS (see ref. 128 for a thorough discussion), but quantum mechanical tunneling and 1°-2° coupled motion have given experimental results that elude such simplistic interpretations. The 2° H/T KIE measured here for the reduction of benzaldehyde by NADH clearly escapes interpretation by semi-classical models. The value we measured (as described under Materials and Methods) was 1.05 ± .01, which is obviously outside the range of unity to the inverse EIE (0.75, ref. 59). An early attempt to measure this KIE produced results within error of unity, which did not surprise the authors because the KIE in the forward direction (alcohol to aldehyde) was equal to the EIE, suggesting a TRS close to the aldehyde.[59] Our measurements differ from unity and appear to be quite precise as a result of using only the aromatic-active isozyme of yADH,[123] and a broad range of time points.

The term “tunneling and coupled motion” has been applied to ADHs and other systems that exhibit 2° KIEs outside the semiclassical range,[26,69,70,130] as well as reactions that violate the Rule of the Geometric Mean, as evidenced by inflated mSSEs.[31,41,71] The term “tunneling and coupled motion” appears to be used for both abnormalities in 2° KIEs. Below, we describe the development of a model that interprets these abnormalities without any explicit inclusion of “coupled motion” and show that the two types of observations differ in their physical origins.

Modeling the TRS

The model developed here fits into the framework of Marcus-like models of H-tunneling in enzymes.[34,41,48-50] A generalized functional form of these phenomenological models gives a rate constant (k) as

$$k = Ce^{-\frac{(\Delta G+\lambda)^2}{4\lambda RT}} \int_{DAD_1}^{DAD_0} e^{F(m,DAD)} e^{-E(DAD)/kT} dDAD \qquad [3.3]$$

where the first exponential is the traditional “Marcus term” for a reaction with driving force ΔG and reorganization energy λ at temperature T. The integral includes terms that adapt Marcus theory to the situation of H-tunneling. The first exponential inside the integral, the “Franck-Condon term”, is a nuclear overlap integral, which describes the efficiency of tunneling through a given barrier and is a function of the tunneling particle’s mass (m) and the DAD. The second integrated exponential, the “Gating term”, measures the relative contributions of the ensemble of DADs, which are in dynamic equilibrium. This phenomenological model was developed to describe the temperature dependency of 1° KIEs, where most of the isotopic sensitivity is in the nuclear overlap term. The mass of the 2° hydrogens, however, does not significantly affect the integrated terms. 2° KIEs are mostly embedded in the Marcus term of this equation.

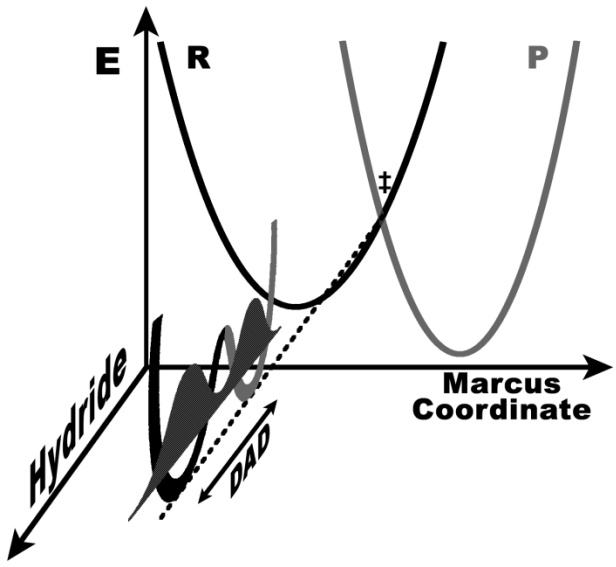

Figure 3.2 Marcus-like model of a reaction with H-tunneling. At the TRS (‡), the reactant (black) and product (gray) surfaces are degenerate, which allows the probability density of the hydrogen (shaded) to spread from the donor well to the acceptor well (i.e., quantum mechanical tunneling) at a rate dependent on the DAD and the particle's mass. Once degeneracy is broken, the hydride wavefunction can collapse into the acceptor well, giving a net transfer (i.e., dissipative tunneling). The Marcus coordinate is a complex amalgamation of many modes, some of the most important of which are discussed in the text.

The physical interpretation of eq (3.3) mirrors the VTST treatment[131] which has been quite successful in modeling enzymatic reactions that involve H-tunneling.[95,110,128] In these models, the enzyme facilitates tunneling of the transferred particle by creating energetic degeneracy between a donor and acceptor state. When the two states are degenerate, the probability density of the transferred particle (depending on its mass and the DAD) passes from the donor well to the acceptor well (Figure 3.2). Thus, the TRS is not a saddle point in the H-transfer coordinate; it is the state(s) along the more intricate heavy-atom coordinate, in which H-transfer from donor to acceptor can occur, namely, the Marcus crossing point. In eq 3.3 this corresponds to the structure where the integrand is at its maximum. We approximated the TRS as a linear combination of two states that

are degenerate distortions of the heavy atom framework and differ only as to whether the transferred hydride is in the donor or acceptor well.

To find the structure of the heavy atom skeleton at the TRS, we adapted Redington's method to model the TRS of the proton transfer in tropolone.[132] The substrates were optimized to a geometry with the transferred H at the midpoint on a straight line between the donor and acceptor carbons using a range of DADs. Since these structures did not yield the degenerate double-well potential necessary for tunneling, the hybridizations of the donor and acceptor carbons were parameterized (see Supporting Information) to give a symmetric potential energy surface (PES) for the motion of the H between the donor and acceptor (Figure 3.3). The TRS was then approximated as a linear combination of the two states where the transferred H is in the donor well or the acceptor well. The geometric mean of the KIEs calculated for the donor and acceptor states of the TRS at each DAD was compared with experiment to determine the best fit.

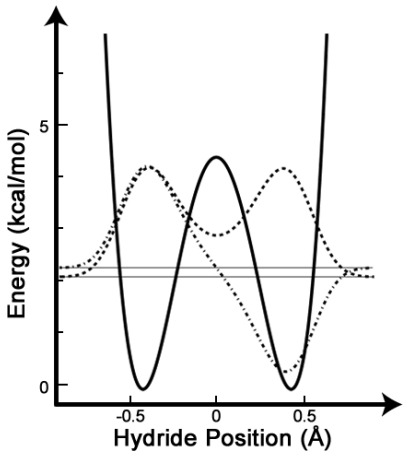

Figure 3.3 Least-squares quartic fit to 25 single point calculations at the B3LYP/6-31+G* level along the H-transfer coordinate at the TRS. The vibrational wavefunctions of the ground state (---) and first excited state (-•-) of the tunneling hydride were calculated as described in the supporting information. This surface is equivalent to the 1-D slice of the "hydride coordinate" at the TRS in Figure 3.2.

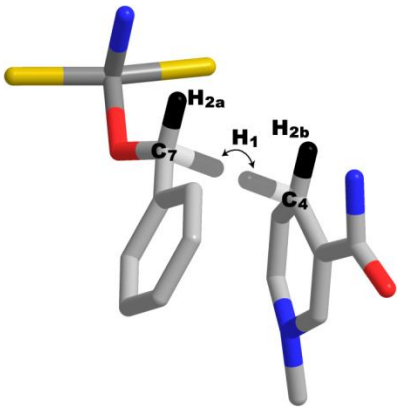

Figure 3.4 TRS structure for H-transfer found by the present methods, showing all heavy atoms used in the model along with hydrogen atoms of particular interest. The dividing surface of conformations that yield a TRS with two degenerate wells ($\Delta E_{D-A}=0$) is quite broad, so this structure represents the weighted average (via Boltzmann distribution) of the full conformational ensemble for which $\Delta E_{D-A}=0$. The 1° hydrogen is shown in both the donor and acceptor positions, but faded, as it has just half of its probability density in each position. Important geometric values are listed in Table 3.2.

Parameterization of the Zn-O bond length at the TRS also enhanced the fit to experimental KIEs and is discussed in the supporting information. Figure 3.4 shows the structure that best matched experimental KIEs, Table 3.1 shows the values of the KIEs, and Table 3.2 lists important geometrical values in the TRS and their corresponding values in the ground state structures. While there might be other structural solutions that fit the data, these are outside the conformational space we scanned and might not be physically relevant. The solution we report may not be the only one that reproduces some of the KIEs, but it is physically meaningful and it meets a large number of experimental restrictions that are quite sensitive to the geometric parameters surveyed.

As one would expect, the DAD at the TRS in this model has a somewhat longer DAD (3.2 Å) than the distance of 2.6 Å cited in some previous ADH models.[95,97] That shorter distance referred to the saddle-point for the over-the-barrier process and the authors of those studies stressed that corrections for tunneling played a vital role in replicating experimental KIEs. The DAD in our calculations, though, refers to that of the

Table 3.1 Computed and Experimental 2° KIEs and EIEs

	Forward[a]		Reverse[a]		Equilibrium[b]	
	Comp	Exp	Comp	Exp	Comp	Exp
H_{2a} (H/T)[c]	1.33[e]	1.33[g]	1.05[e]	1.05[e]	1.26[e]	1.33[g]
H_{2b} (H/D)[c]	1.06[e]	1.08[f]	1.22[e]	1.24[f]	0.87[e]	0.89[f]
H_{2a} (D/T)[d]	1.03[e]	1.03[h]	0.97[e]	1.01[e]		

Note: Experimental errors are omitted here for clarity but are available in the supporting information. The 2° hydrogens H_{2a} and H_{2b} are indicated in Figure 3.4.

[a]The forward direction is the oxidation of benzyl alcohol and the reverse is the reduction of benzaldehyde.

[b]Equilibria refer to the forward direction.

[c]H-transfer.

[d]D-transfer.

[e]This work.

[f]Ref. 26.

[g]Ref. 59.

[h]Ref. 31.

Table 3.2 Properties of the TRS and ground states

	Reactants[a]	Products[a]	TRS
C_7-C_4[b]	3.8 Å	3.8 Å	3.2 Å
C_7-C_4[c]	3.8 Å	3.8 Å	3.0 Å
Zn-O	1.8 Å	2.3 Å	2.25 Å
C_7 hybridization	sp^3	sp^2	$sp^{2.76}$
C_4 hybridization	sp^2	sp^3	$sp^{2.34}$

[a]Reactants and products refer to those of the forward reaction.

[b]H-transfer.

[c]D-transfer

TRS, from which tunneling occurs. In our model no barrier is present for DADs shorter than 2.8 Å and the zero point energy of the hydride is above the barrier even beyond that. This echoes a model by Hammes-Schiffer and co-workers that found no barrier to this reaction at such short DADs, but demonstrated how tunneling can contribute to rates with a DAD in excess of 3.1 Å.[127] Furthermore, a model of the H-transfer in soybean lipoxygenase found that the "distance of most probable transfer" (the DAD at the TRS) could be as long as 3.25 Å.[86] To clarify, the DAD refers to the distance between the two carbon atoms, but the actual distance between the two minima of the double-well potential at the TRS described here is just 0.8 Å, which is within the deBroglie wavelength of H at room temperature (1.0 Å at an energy of k_BT). Nonetheless, to ensure the feasibility of tunneling at 3.2 Å, we calculated the tunneling splitting for the double well potential in Figure 3.3 and found a value of 0.19 kcal/mol, which is similar to previous estimates of this value using other levels of theory.[127] The tunneling splitting is inversely proportional to the rate of H-tunneling at the TRS, and the value we found indicates that once the system reaches the TRS, all of the probability density of the hydride will pass from donor to acceptor in 250 fs.[103]

Hybridization at the TRS

Parameterization of the donor and acceptor hybridization gave a particularly transparent view of the role of rehybridization in the reaction. Using the parameterized out-of-plane bending angle of the 2° hydrogens (Figure 3.1), we calculated hybridization (sp^H) at the TRS ranging from sp^2 to sp^3 where

$$H = 2 + \frac{180 - \theta}{180 - \theta_0} \qquad [3.4]$$

Here θ is the out-of-plane bend at the TRS and θ_0 is that angle in the relevant reduced form of each substrate. The calculated hybridizations at the TRS are $sp^{2.76}$ for the donor (C7 of the substrate) and $sp^{2.34}$ for the acceptor (C4 of the cofactor - Figure 3.5).The

hybridizations of the donor and acceptor carbons, therefore, are unsynchronized, as found for DHFR.[128] Other models have described anomalous rehybridization like this as 1°-2° coupled motion,[27,61,125,126] but gave little insight into the physical source of the coupling. The present picture provides a more concrete description of the motion of the 2° hydrogens and how it is necessary to give a symmetric double-well potential at the TRS. The unsynchronized rehybridization reported here and for DHFR[128] may be a general phenomenon in nicotinamide-dependent redox reactions and even in other types of reactions involving H-tunneling. We are currently examining this question in other enzymes that involve both hydride and proton transfers.

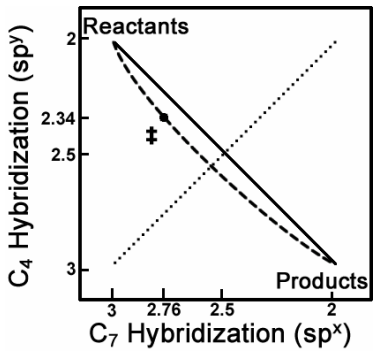

Figure 3.5 Rehybridization during the course of the reaction. The location of the TRS is marked (‡) and the dashed line indicates a reasonable reaction pathway from reactants to products that passes through the TRS. The solid line indicates a reaction pathway with perfectly synchronized rehybridization. The dotted line indicates the surface with perfectly symmetric rehybridization.

According to the current model, the physical origin of the inflated 2° H/T (relative to semiclassical predictions), is the effect of tunneling of the 1° hydrogen (delocalized at the TRS) on the 2° vibrational modes, as has been suspected since the earliest observations of 2° KIEs outside the semiclassical range,[26,31] and was first demonstrated for another ADH by QM/MM calculations.[95]

The Situation with D-Transfer

Up to this point, we have only addressed the (physiological) H-transfer scenario. Some of the most inexplicable behavior of this reaction, however, particularly inflated mSSEs, occurs when D is the transferred nucleus.[41] Importantly, the TRS structure we present for H-transfer does not replicate the observed 2° KIEs for D-transfer nor does it give inflated mSSEs or the 1° KIEs. However, prompted by the recent proposition of Klinman,[41,54] we tested whether a structure with a shorter DAD would reproduce the observed behavior for D-transfer. Shortening the DAD by 0.2 Å did, in fact, give the diminished value of 1.03 for the D/T 2° KIE with D-transfer in the forward direction, leading to an inflated mSSE in excellent agreement with the experimental data.[31] At the shorter DAD, the effects of hybridization on energy (both total energy and degeneracy between donor and acceptor) are nearly identical to those at the longer DAD so the hybridization at the TRS is the same with the transfer of the heavier nucleus. Nonetheless, non-covalent interactions between the substrates diminish the 2° D/T KIEs, and are the main source of the inflated mSSEs that were long used to indicate tunneling and coupled motion in the ADH reaction.

Notably, the current model suggests that w*hen a different nucleus is transferred, the system goes through a different TRS.* Eq. 3.3 above predicts this type of behavior, since the contribution of the integral to the rate constant is greater for a heavier nucleus at shorter DADs and similar findings resulted from EA-VTST calculations of ADH.[95] A recent VTST study of another system also showed that an H-transfer from NADH proceeds via large-curvature tunneling, but the corresponding D-transfer is dominated by small-curvature tunneling.[133] To further explore this property, we calculated the H/D 1° KIE based on the vibrational zero point energy of H and D for the double-well potential at a TRS of 3.2 and 3.0 Å, respectively, along with the difference in energy between the two TRSs (see supporting information). This simple approximation gave the value of 3.0 for the H/D 1° KIE in both directions, which agrees well with experimental

measurements of this value.[57,58] This supporting evidence for Klinman's recent suggestion of the source of the inflated 2° mSSE[41,54] is likely to assist the development of more general and less empirical models that account for the effect of a shorter DAD on reactions with D- or T-transfer in both enzymatic and non-enzymatic reactions.

A Unified Picture of the Reaction Coordinate

In addition to replicating all of the KIEs measured for yADH, the model presented here rationalizes the apparent paradox regarding the traditional interpretations of 2° KIEs, LFERs, and the Hammond Postulate. The LFER experiments showed that substituents at the para-position of the substrate have little effect on the oxidation of alcohols, but substantially alter the rate of aldehyde reduction, which typically indicates a TS that more closely resembles the alcohol.[57,58,123] For many years, this finding was seen as contradictory to the data on 2° KIEs, which, when interpreted semi-classically, suggest an aldehyde-like TS. To examine the present model's consistency with the studies on substituent effects, we explored how two representative electron donating and electron withdrawing para substituents (-OCH_3 and –Br) affected the charge density on the benzylic carbon in both directions. A recent analysis of substituent effects on a similar system showed that Mulliken charge (Q_M) on the benzylic carbon, as calculated by the theory used in this model, scales linearly with Hammett substituent constants,[134] suggesting that Q_M at the TRS versus reactants (ΔQ_M) could serve as a probe for reactivity. In accordance with experimental rates, para substituents do not change ΔQ_M significantly in the forward direction, but they give drastic changes in the reverse reaction (Figure 3.6). That is not to say that Q_M on the benzylic carbon does not change between the alkoxide and the TRS—only that substituents do not affect that change. In the case of aldehyde reduction, though, substituents strongly modulate how charge accumulates on the benzylic carbon during the reaction.

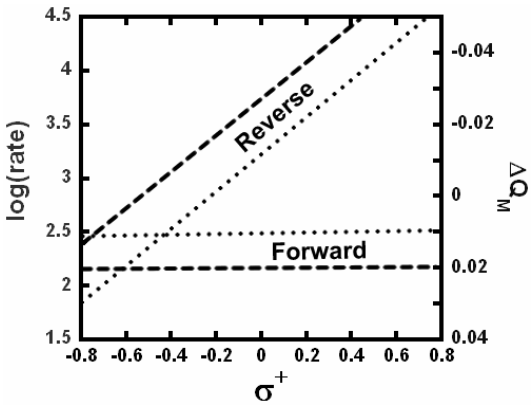

Figure 3.6 The effect of para-substituents on the forward and reverse reactions catalyzed by yADH. In accordance with previous studies[57,58] the experimental rates (•••)[123] showed that the forward reaction is unaffected by electronic changes (substituents with different values of σ^+), but that electron-withdrawing substituents greatly accelerate the reverse reaction. Calculations (---) of the reaction with a representative range of para substituents (-OCH_3,-H,-Br) showed similar trends in the change of Mulliken charge (ΔQ_M) on the benzylic carbon between reactants and the TRS. Substituents on benzyl alcohol (forward) do not affect the electronic changes along the reaction coordinate, but substituents on benzaldehyde (reverse) severely alter the electronic changes that accompany the TRS.

In terms of the Marcus-like model used as a framework for these calculations, ΔQ_M appears to be a good probe for the reorganization along the Marcus coordinate (the first exponential term of equation 3.3). Reorganization energy indicates the extent to which the electrostatic environment of the tunneling particle must change in order to reach the TRS.[83] The fact that electronic changes have little effect in the forward direction suggests that the system is well pre-organized for the forward reaction. That is, by binding the substrates, and forming the Zn-alkoxide intermediate, the enzyme accomplishes much of the necessary changes to reach the TRS. In the reverse direction, however, reorganization after binding plays a crucial role and electronic changes affect the extent to which the system must reorganize to reach the TRS.

How can one reconcile an early TRS (for the forward reaction) with the overall endothermicity of the reaction? The Hammond postulate predicts a late TRS for an

endothermic reaction. The equilibrium in solution favors the alcohol-NAD^+ side of the reaction (at catalytically relevant pH),[57] but the solution equilibrium is not directly relevant to the rate-limiting hydride transfer step under study. Measurements of internal (on the enzyme) equilibrium gave a value of K_{eq}=0.15 in favor of the alcohol-NAD^+ side, predicting a late TRS,[122] but the internal equilibrium is close to unity and very likely a combination of at least two steps: the deprotonation of the alcohol and the hydride transfer that follows.[135] Indeed, QM/MM calculations for this reaction found that the hydride transfer step is exothermic, despite the fact that the overall reaction was endothermic.[95,97] Our results indicating an alkoxide-like TRS for the hydride transfer bolster the argument that this step truly is exothermic.

The overall course of the reaction appears to be the following: after the Zn-alkoxide forms, the Zn-O bond lengthens, accompanied by changes in the hybridization of the donor and acceptor carbons to reach a symmetric double well potential along the H-transfer coordinate (Figure 3.3). Once the system achieves this TRS, rate-promoting vibrations of the enzyme[136] allow the substrates to sample a range of DADs. When the DAD reaches 3.2 Å (weighted average), the probability density of the hydride can spread from the donor well to the acceptor well on a timescale similar to the lifetime of the TRS. Once the degeneracy of the TRS dissolves, the wavefunction of the tunneling hydride collapses and it is trapped in the product state.

Conclusions

For nearly four decades, data addressing the yADH catalyzed reaction appeared contradictory and could not be rationalized within a single model. New measurements of H/T and D/T 2° KIEs for the yADH catalyzed reduction of benzaldehyde by NADH deviated from the range predicted by semiclassical theories. These data completed the set of 2° KIEs available for this enzyme, and allowed us to develop an empirical model that

is consistent with all the data. This model shed light on the nature of the phenomenon described in the past as H-tunneling and 1°-2° coupled motion.[26,31,61,63,125]

The new picture of the reaction emphasizes the dual importance of a short DAD as well as degenerate donor and acceptor wells at the TRS. Such a picture opens the doorway to a better understanding of how enzymes stabilize the TRS. The current findings are likely to spur both experimental and theoretical work to better understand the TRS of yADH and other enzymatic and non-enzymatic reactions. To test and consolidate this picture, its predictions will be assessed experimentally. The present model predicts, for example, that H/T 2° KIEs in the forward direction will be greater with H-transfer than with D-transfer, and that the 2° SSE will conform to the semi-classical value so long as both the H/T and D/T KIEs are measured with the same nucleus at the 1° position. Additionally, the findings presented here are likely to inspire high level theoretical studies of yADH, for which a crystal structure is now available (PDB: 2HCY), to illuminate the question of how the substrates reach the TRS, and what role the enzyme plays in that process.

Materials and Methods

Detailed experimental and computational methods are available in the supporting information. A brief description is provided below.

Kinetic Experiments

The H/T and D/T 2° KIEs for the reduction of benzaldehyde were measured competitively in reaction conditions designed to mimic those used in previous studies of this enzyme.[31] [7-^{3}H]-benzaldehyde was synthesized by reduction of benzoyl chloride by [^{3}H]-$NaBH_4$.[137] [ring-^{14}C]-benzaldehyde (as a trace for ^{1}H or ^{2}H) was commercially available (American Radiolabeled Chemicals). [7-^{2}H; ring-^{14}C]-benzaldehyde was produced by CN-catalyzed exchange of the aldehydic proton with D_2O.[138] *R*-[4-^{2}H]-NADH (NADD) was produced by ADH-catalyzed reduction of NAD^+ by EtOH-d_6.[139] To

measure the H/T KIE, [ring-^{14}C]-benzaldehyde was copurified with [7-^{3}H]-benzaldehyde and the substrate was consumed by an excess of NADH in the presence of yADH. The D/T KIE used [7-^{2}H; ring-^{14}C]-benzaldehyde and NADD. The reactions were quenched at a range of time points, and samples were analyzed as described in the supporting information to measure the depletion of tritium in the product as a function of fractional conversion, to yield the KIE.

Computational Modeling

KIEs and EIEs were calculated based on isotopic differences in vibrational frequencies between reactants and the TRS according to the Bigeleisen equation[22] using the program *ISOEFF 07*.[140] Vibrational frequencies were calculated by *Gaussian 03*[98] at the B3LYP level. To model the effects of hydrogen tunneling on KIEs, the TRS was treated as a simple linear combination of degenerate donor and acceptor states:

$$\Psi_{TRS} \approx \frac{1}{\sqrt{2}}\Psi_d + \frac{1}{\sqrt{2}}\Psi_a \qquad [3.5]$$

Vibrational frequencies at the TRS were approximated as the average between the frequencies calculated for the individual donor and acceptor states (see supporting information for details). To obtain fits to experimentally determined KIEs, geometrical properties of the TRS were parameterized as described in the text.

Supporting Information

Materials and Methods

Kinetic Experiments

Materials. All chemicals were from Sigma unless otherwise specified. 2° KIEs on the yADH-catalyzed reduction of benzaldehyde by NADH were measured competitively in conditions meant to mimic those used in other studies of this system.[31] Competitive

measurements use two different isotopically labeled substrates in the same reaction vessel and measure the enrichment of one of the isotopologues in the products at various time points. In the case of the H/T KIE for benzaldehyde reduction, [7-^{3}H]-benzaldehyde and [ring-^{14}C]-benzaldehyde (as a trace for ^{1}H) served as the labeled substrates. [ring-^{14}C]-benzaldehyde was commercially available (American Radiolabeled Chemicals) and [^{3}H]-benzaldehyde was produced by reduction of benzoyl chloride by [^{3}H]-$NaBH_4$ (American Radiolabeled Chemicals) in the presence of Cd^{2+} according to an adaptation of a published procedure.[137] D/T experiments used [ring-^{14}C-7-^{2}H]-benzaldehyde (as a trace for D), which was produced by CN^- catalyzed exchange of the aldehydic proton with D_2O by an adaptation of a published procedure.[138] *R*-[4-^{2}H]-nicotinamide adenine dinucleotide (NADD) was used for experiments with D-transfer and it was synthesized by reduction of NAD^+ with EtOH-d_6 by yADH.[139]

Enzyme preparation. While most previous studies[31,57-59,141] used commercially available yADH, a recent report found that commercially available materials are mixtures of isozymes, only one of which is active toward aromatic substrates.[123] The aromatic-active isozyme, yADH 2, was expressed and purified as described previously[142] in a strain of yeast deficient in genes for the other isozymes (a generous gift from Bryce V. Plapp).

Kinetic measurements. Prior to each reaction, synthesized [^{3}H]-benzaldehyde was copurified with the [^{14}C]-benzaldehyde (either H or D at the aldehydic position) by HPLC over a C-18 column (4.6 x 250 mm) at 1 ml/min in 25:75 MeCN:H_2O. The final 1 ml reaction mixtures, meant to mimic the conditions of ref. 31, contained 2 mM benzaldehyde (300,000 dpm ^{14}C and 1,500,000 dpm ^{3}H), 80 mM glycine (pH 8.5), 20 mM NADH (or NADD), and sufficient enzyme to reach complete conversion to products within a few hours. Reactions were initiated by addition of the enzyme and maintained at 25° until quenching with 10 mM $HgCl_2$ at a range of time points. Samples were frozen at –80° C until ready for HPLC analysis.

Reactants and products were separated by C-18 HPLC using the method above and collected in 1 min fractions. In these conditions, benzyl alcohol elutes at 8-9 minutes and benzaldehyde at 15-16 min. The ^{14}C and ^{3}H contents of the fractions were measured by liquid scintillation counting with a Packard Tri-Carb 2900TR liquid scintillation analyzer. KIEs were calculated according to

$$KIE = \frac{\log(1-f)}{\log(1-fR_p/R_0)} \qquad [3.6]$$

where f is the fractional conversion to products, R_p is the isotopic ratio in the products, and R_0 is the initial isotopic ratio in the reactants.[143]

Computational Modeling

All geometry optimizations, calculations of vibrational frequencies, and potential energy surface (PES) scans were done with density functional theory using *GAUSSIAN 03* at the B3LYP level.[98] Although no solvent model was used, the calculations are not "gas-phase" calculations, as geometric restrictions were imposed to fit the kinetic data and represent the enzymatic/solvent environment. Following the footsteps of other empirical models of this type,[27,61,63,125,126] the geometrical parameterization bypasses the need to explicitly include solvent, active site, or other environmental effects in the calculations. The chosen level of theory gave good initial results for the EIEs, suggesting that it was suitable to model vibrational changes over the course of the reaction. The model incorporated a total of 43 atoms, which were the same atoms used in another model of the ADH-catalyzed reaction,[127] and included the entire benzyl substrate, the catalytic zinc and its ligands, and the nicotinamide moiety of the cofactor. The ground state structures for both forms of both substrates (benzyl alkoxide, benzaldehyde, NAD^+ and NADH) were treated separately and completely optimized to their equilibrium geometries (Figure 3.7), aside from some dihedral angles around the catalytic zinc and the Zn-O bond distance, which were constrained to match the newly available crystal

structure of yADH (PDB: 2HCY) and a structure of hlADH with an aldehyde analogue (PDB: 1LDY).

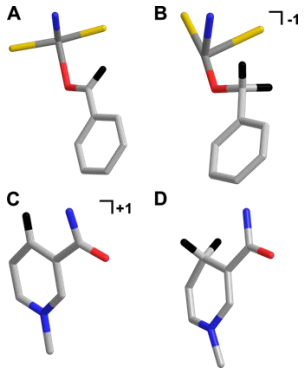

Figure 3.7 Optimized reactant and product ground states of the substrate and cofactor showing all heavy atoms and hydrogens of particular interest. A) benzaldehyde. B) benzyl alkoxide. C) NAD^+. D) NADH.

To assess the TRS for this system, we assumed that the 1° hydride cannot be modeled classically and is delocalized between the reactant and product wells in accordance with Marcus-like models of hydrogen tunneling (Figure 3.2).[41,48-50] We adapted the method used by Redington to calculate the TRS for the proton transfer in tropolone.[132] The 1° hydrogen was frozen directly midway between the donor and acceptor carbons with an angle of 180°. This angle was chosen for computational simplicity, but QM/MM models demonstrate that the angle indeed does not substantially deviate from linearity[95,127] The positions of the other 42 atoms in the system were then optimized at a range of DADs and Zn-O bond lengths. The optimized geometries for the heavy atom skeleton were then frozen and the hybridizations of the donor and acceptor carbons were parameterized by altering the out-of-plane bend (θ) of the 2° hydrogens (Figure 3.1). This parameterization was necessary to give a degenerate double-well potential ($\Delta E_{D\text{-}A}=0$) in accordance with Marcus-like models of hydrogen tunneling. Each

combination of DAD and Zn-O bond length has an ensemble of structures with $\Delta E_{D\text{-}A}$ =0, so the minimum energy point along the $\Delta E_{D\text{-}A}$ =0 surface was taken as the weighted average of the full ensemble of TRS structures. KIEs were calculated at that point for each combination of DAD and Zn-O bond length and compared with experiment to find the best fit.

Calculations of 2˚ KIEs

To calculate 2° KIEs, we approximated the position of the delocalized hydrogen as a simple linear combination of donor and acceptor positions (Figure 3.4).

$$\Psi_{TRS} \approx \frac{1}{\sqrt{2}}\Psi_d + \frac{1}{\sqrt{2}}\Psi_a \qquad [3.7]$$

where Ψ_{TRS} represents the overall wavefunction of the TRS, and Ψ_d and Ψ_a represent the wavefunctions when the hydride is localized in the donor well and acceptor well, respectively. Thus, KIEs were calculated for both the donor (k_{Hd}/k_{Td}) and acceptor (k_{Ha}/k_{Ta}) states according to the Bigeleisen equation,[22]

$$\frac{k_{Hd}}{k_{Td}} = \kappa_d \cdot MMI_d \cdot EXC_d \cdot \frac{e^{-\beta h(\nu^{\circ}_{Hd} - \nu_H)}}{e^{-\beta h(\nu^{\circ}_{Td} - \nu_T)}} \qquad [3.8]$$

$$\frac{k_{Ha}}{k_{Ta}} = \kappa_a \cdot MMI_a \cdot EXC_a \cdot \frac{e^{-\beta h(\nu^{\circ}_{Ha} - \nu_H)}}{e^{-\beta h(\nu^{\circ}_{Ta} - \nu_T)}} \qquad [3.9]$$

Here β is $1/k_BT$, h is Planck's constant, and ν represents the vibrational frequencies of the isotopically labeled molecules at the ground state (ν_H andν_T) and the donor (ν°_{Hd} and ν°_{Td}) and acceptor (ν°_{Ha} and ν°_{Ta}) states that compose the TRS. The leading terms of these equations (κ, MMI, and EXC) represent isotopic differences in transmission coefficient, mass moment of inertia, and vibrationally excited populations, respectively. These terms do not make significant contributions to 2° KIE, so the overall KIE reduces to:

$$\left(\frac{k_{Hd}}{k_{Td}}\cdot\frac{k_{Ha}}{k_{Ta}}\right)^{1/2}\approx\frac{e^{-\beta h\left(\frac{\nu^{\circ}_{Hd}+\nu^{\circ}_{Ha}}{2}-\nu_H\right)}}{e^{-\beta h\left(\frac{\nu^{\circ}_{Td}+\nu^{\circ}_{Ta}}{2}-\nu_T\right)}}\approx\frac{k_H}{k_T} \qquad [3.10]$$

The program *ISOEFF07*[140] was used to calculate KIEs based on vibrational frequencies from *Gaussian* (uniformly scaled by 0.95 following the correction suggested by Rucker and Klinman[126]).

Calculations of 1˚ KIEs

1° KIEs were estimated assuming that the reaction is vibrationally adiabatic and that the principal sources of the KIE are the change in the C-H(D) stretch vibrational energy (E_v) as the system evolves from the ground state to the TRS, and the difference in electronic energy (E_e) between the TRS for H- and for D-transfer. The 1-D PES for the C-H stretch was calculated at the ground state and the TRS for both forward and reverse reactions using a larger basis set (B3LYP/6-31+G*) to obtain more realistic results near the barrier of the double well potential at the TRS. 20-25 single point energies for different positions of the hydrogen were fit (least-squares) to a quartic function at the TRS. For the ground states, initial fits to a Morse-type potential gave noticeable deviations from the calculated points, but an 8th order polynomial approximation gave a very good fit for the region near the minimum of the PES.

The vibrational zero point energy for each PES was determined numerically by finding upper and lower limits on the energy for which solutions to the Schrödinger equation were convergent. By iteratively narrowing those limits, the eigenvalues of the Hamiltonian could be determined to any precision desired. Using these vibrational energies and their associated electronic energies, KIEs were estimated as

$$\frac{k_H}{k_D}=\frac{Exp[-\beta(^{H}\Delta E^{\circ}_{e}+^{H}\Delta E^{\circ}_{v})]}{Exp[-\beta(^{D}\Delta E^{\circ}_{e}+^{D}\Delta E^{\circ}_{v})]} \qquad [3.11]$$

where ${}^{i}\Delta E_{e}^{\ddagger}$ is the electronic activation energy for isotope *i* and ${}^{i}\Delta E_{v}^{\ddagger}$ is the vibrational activation energy for isotope *i*.

The time (t) required for all of the probability density of the hydride to pass through the barrier at the TRS was calculated according to[103]

$$t = \frac{\hbar}{2\Delta E_{split}} \qquad [3.12]$$

where ΔE_{split} is the tunneling splitting (the energy difference between the ground- and first-excited vibrational states of the tunneling particle). ΔE_{split} was calculated by the method described above for determining eigenvalues of the Hamiltonian at the TRS.

Experimental Results

Competitive H/T and D/T 2° KIE measurements for the reduction of benzaldehyde by NADH and NADD, respectively, are displayed in Figure 3.8. The fact that the measured KIEs are invariant over a large range of fractional conversions indicates that the results are reliable. Importantly, the value measured for the H/T KIE (1.05 ± .01) is within the error reported in a previous measurement of this KIE,[59] but is more precise and shows definitively that the KIE is normal (>1), despite the inverse (<1) EIE measured for this reaction. The D/T KIE with D-transfer (1.01 ± .02) is within error of unity, though, and the mSSE measured for this reaction (4.9 ± 2.0) is within error of the semiclassical value of 3.3. Deviations from the semi-classical mSSE in the forward reaction have served as strong evidence for tunneling in yADH,[31] but the large errors associated with the small KIEs in the reverse direction prevent such a conclusion from these data.

Nonetheless, the mere fact that the H/T KIE is normal, despite the inverse EIE, provides strong evidence that tunneling and coupled motion play an important role in the reaction. 2° KIEs outside the range of the 2° EIE to unity are rare, but not unprecedented,

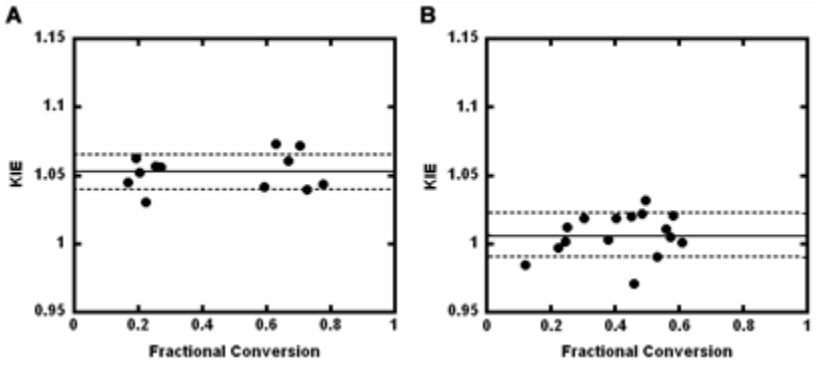

Figure 3.8 Measured 2° KIEs for the reduction of benzaldehyde as a function of fractional conversion to products. A) H/T with H-transfer. B) D/T with D-transfer. Each data point indicates a single time point during one of two independent reactions (per labeling scheme). The solid line indicates the average value and the dashed lines are (1σ) above and below the average.

especially in enzymatic reactions, and are generally interpreted as evidence for tunneling and coupled motion, without giving significantly deeper analysis.[26,29,69,70] Other anomalies in 2° KIE measurements in ADH, especially inflated mSSEs, have received a great deal of theoretical treatment,[27,95,97,126,144] but these models have typically failed to address the abnormal KIEs on the nicotinamide cofactor or predicted the previously unavailable KIE reported here. The implications of such KIEs for TRS structure are described in the main text.

Additional discussion regarding ligation to the catalytic Zinc

Some of the most striking features apparent from the optimized ground states (Figure 3.7) are the changes around the catalytic Zn between reactants and products. The Zn-O bond lengths were constrained during the optimizations to reflect the crystal structure of yADH with trifluoroethanol (PDB: 2HCY) and a structure of hlADH with cyclohexyl formamide (PDB: 1LDY). The latter structure, which is meant to serve as an analog for the aldehyde, has a Zn-O bond length of 2.3 Å and reflects the trigonal

pyramidal geometry around the Zn observed in our optimized aldehyde ground state. The situation in the yADH/trifluoroethanol structure is somewhat more complicated. Although the enzyme is a homotetramer, two of the subunits did not crystallize with a cofactor and exhibit alternative ligation to the catalytic Zn. The two subunits that bound both substrates have a Zn-O bond length of 1.8 Å, which is the value used to constrain the alkoxide ground state in our calculations.

Notably, the changes in ligation around the Zn at the TRS were vital to replicating the KIEs in our model. We explored the whole range of values for the Zn-O bond length between 1.8-2.3 Å and found the best fit to experimental KIEs near the upper limit, at 2.25 Å. In contrast to our findings of an early TRS in terms of H-donor and H-acceptor hybridizations, this value represents a late TRS for the chemistry around the Zn. We hope to experimentally test this aspect of the model using freeze-quench x-ray absorption spectroscopy, which can measure changes in ligation around the Zn during the reaction with incredible spatial and temporal resolution.[145]

CHAPTER IV

STEREOSPECIFIC MULTIPLE ISOTOPIC LABELING OF BENZYL ALCOHOL

This chapter has been submitted by Daniel Roston and Amnon Kohen for publication in *Journal of Labeled Compounds and Radiopharmaceuticals*.

Abstract

Isotopically labeled enzymatic substrates and biological metabolites are useful for many mechanistic analyses, particularly the study of kinetic and equilibrium isotope effects, determining the stereospecificity of enzymes, and resolving metabolic pathways. Here we present the 1-pot synthesis, purification, and kinetic analysis of 7*R*-[^{2}H]-phenyl-[^{14}C]-benzyl alcohol. The procedure involves a chemoenzymatic synthesis that couples formate dehydrogenase to alcohol dehydrogenase with a catalytic amount of nicotinamide cofactor. The reaction goes to completion overnight, and the measurement of a competitive kinetic isotope effect on the enzymatic oxidation of the purified product identified no ^{1}H contamination. This measurement is very sensitive to such isotopic contamination and verified the high level of isotopic and enantiomeric purity yielded by the new synthetic procedure.

Research Report

Isotopically labeled compounds can be profoundly useful in determining the stereospecificity of enzymes and resolving metabolic pathways, where the isotope is followed in downstream products and secreted metabolites. Additionally, such compounds can help to elucidate the chemical mechanism of enzymes and other organic reactions, as well as to decipher the physical processes involved in the activation of specific bonds. A very common technique in enzymology, for example, is the

measurement of kinetic isotope effects (KIEs), which assess the ratio of rates for reactions that differ only in isotopic composition (i.e., isotopologues):

$$KIE = \frac{k_L}{k_H} \quad [4.1]$$

where k_L and k_H are the rates with the light and heavy isotopes, respectively. KIEs can report on the extent to which a particular step in a reaction mechanism is rate limiting, the structures of transition states, the role of nuclear quantum mechanical effects on a reactive trajectory, and even the effects of enzyme dynamics on the catalyzed chemistry.[1,7,36,146]

Applications of specific relevance to the currently reported compound are studies of the enzyme alcohol dehydrogenase (ADH) using KIEs.[7,146,147] The reaction of ADH entails the oxidation of an alcohol using nicotinamide adenine dinucleotide (NAD^+) as a cofactor. Study of this system has led to tremendous advances in the understanding of hydrogen transfer processes by enzymes, but has been slowed since 1999 by the unavailability of stereospecifically-labeled benzyl alcohols, which are necessary to test certain theoretical predictions.[54,68,126]

Measuring hydrogen KIEs with tritium (i.e., $k_{\text{hydrogen}}/k_{\text{tritium}}$) leads to the largest– and thus least ambiguous—values of all KIEs. To use manageable levels of radioactivity, such measurements require a competitive method, where the two isotopologues are mixed together with only a trace amount of tritium, and they compete for the enzyme's active site.[56] The most common way to analyze the results of a competitive experiment is to track the fractionation of the two isotopologues using different radioactive labels. For hydrogen KIEs, the heavy istopologue is often the ^{3}H-labeled substrate so only the light substrate, which has either ^{1}H or ^{2}H at the position of interest, requires a remote ^{14}C label. Most competitive KIE experiments, therefore, require doubly labeled (^{14}C and ^{2}H) substrates. Many KIE experiments in ADH, for example, have taken advantage of this kind of complex labeling scheme.[31-33,68,141] Those experiments, however, were limited by

the lack of stereospecific labeling, which prohibited directly testing primary (1°) or secondary (2°) isotope effects without the interference of the hydrogen isotope at the geminal position. Recently, for example, it became apparent that two theoretical explanations for 1˚-2˚ coupled motion[54] could be resolved by measuring the effect of isotopic substitution at the 1˚ position on the 2˚ KIE in yeast ADH (yADH); that is, measurement of the 2˚ H/T KIE with either H or D as the transferred isotope.[148] The D-transfer reaction requires that the ^{14}C-labeled material be stereospecifically labeled with ^{2}H at the 1˚ position (pro-*R*) and ^{1}H at the 2˚ position (pro-*S*). In particular, the measurement requires 7*R*-[^{2}H]-phenyl-[^{14}C]-benzyl alcohol with an isotopic- and enantio-purity greater than 99.5%.

Figure 4.1A shows the overall synthetic approach we report here. The synthesis coupled two enzymatic reactions in the same reaction mixture. The first reaction, catalyzed by formate dehydrogenase (FDH) was the transfer of $^{2}H^{-}$ from formate-d to NAD^{+}, producing 4*R*-NADD. The second reaction, catalyzed by horse ADH (hADH), was the transfer of the *R*-$^{2}H^{-}$ from NADD to the *re*-face of phenyl[^{14}C]-benzaldehyde, yielding the desired 7*R*-[^{2}H]-phenyl-[^{14}C]-benzyl alcohol. The NAD^{+} cofactor was only present in catalytic amounts as it was recycled by the two enzymes, and the only source of reducing hydride equivalents was the formate-d (99.8 %D). The 500 µl reaction contained 100 mM phosphate (pH 7.5), 140 mM DCO_2Na, 10 mM phenyl[^{14}C]-Benzaldehyde (2 mCi/mmol), and 0.1 mM NAD^{+}. All materials were from Sigma, except the phenyl[^{14}C]-Benzaldehyde, which was from ViTrax. The reaction was initiated by the simultaneous addition of pre-mixed FDH from *Candida boidinii* and hADH such that the final concentration of both enzymes was approximately 1 U/ml. The reaction was incubated at room temperature and reached complete conversion to products (i.e. quantitative conversion of benzaldehyde to benzyl alcohol) overnight, as evidenced by HPLC analysis (Figure 4.1, B and C).

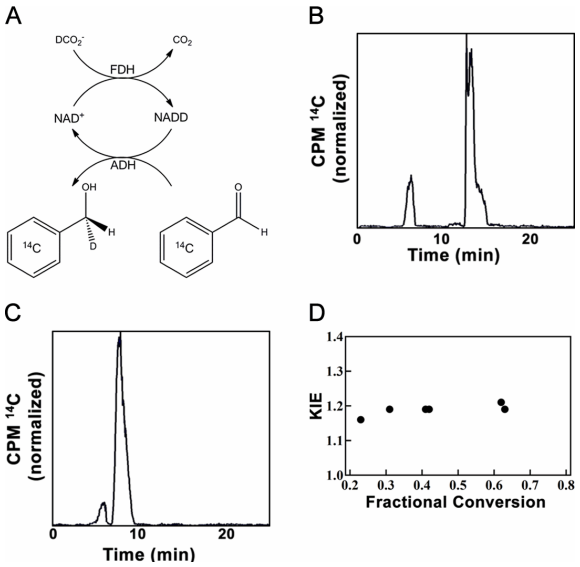

Figure 4.1 Synthesis and use of 7*R*-[^{2}H]-phenyl-[^{14}C]-benzyl alcohol. (A) Synthetic scheme. (B) HPLC chromatogram of the starting material for the synthesis, measured in radioactivity counts per minutes (CPM). (C) HPLC chromatogram of the synthetic reaction mixture after overnight incubation. The HPLC method was 75:25 H_2O:MeCN at 1 ml/min on a C-18 column. Commercially available standards showed that the larger peak in panel B is benzaldehyde and the larger peak in panel C is benzyl alcohol. The smaller peak in both chromatograms, which does not change during the course of the reaction, is likely to be benzoic acid that formed from the oxidation of the benzaldehyde starting material prior to using it in this synthesis. The starting material, purchased from ViTrax, normally comes packaged in toluene, which apparently provides stability against oxidation. In order to use the material in this enzymatic synthesis, we requested that it be packaged in water, which the manufacturer had not tested for stability. Regardless, this contaminant did not affect the synthesis and was easily removed from the product by HPLC purification. (D) KIE as a function of fractional conversion (f) for 0.2<f<0.8, where the reactants and products both have sufficient quantities of ^{3}H and ^{14}C to accurately assess the KIE. The lack of a declining trend provides strong evidence of the isotopic and enantiomeric purity of the synthesized materials.

The ^{2}H-content of the only source of reducing hydrides (formate-d) was 99.8% (actual lot analysis) and the enzymatic reactions are expected to be highly stereospecific. To be sure, though, we tested the isotopic and enantiomeric purity of the synthesized material by using it in a competitive KIE experiment, which is very sensitive to isotopic contamination (even 0.5% of ^{1}H-contamination at the pro-*R* position would lead to a decreasing trend in KIE as a function of fractional conversion to products).[56] We co-

purified the material with the other isotopologue in our experiment (racemic 7[^{2}H,^{3}H]-benzyl alcohol) by HPLC on a C-18 column (5 x 250 mm) using 88:12 H_2O:MeCN at 1 ml/min. We then added this copurified material to a final concentration of 1 mM in a reaction containing 80 mM glycine (pH 8.5), 300 mM semicarbazide, 10 mM NAD^+, and 1 mg/ml yADH isozyme 2 at 25˚ C. These conditions reflect the conditions used by previous competitive KIE experiments on yADH.[31,68,141] At a range of fractional conversions, we quenched 100 µl aliquots of the reaction by the addition of 10 µl saturated $HgCl_2$. We then separated the reactants from products by HPLC using 76:12:12 H_2O:MeOH:MeCN at 1 ml/min and analyzed the ^{3}H and ^{14}C contents of the fractions by liquid scintillation counting. From this, we calculated the KIE as a function of fractional conversion to products as[143]

$$KIE = \frac{\log(1-f)}{\log(1-f*\frac{R_p}{R_\infty})} \quad [4.2]$$

where R_p and R_∞ are the ratio of ^{3}H:^{14}C (heavy to light isotope) in products at a fractional conversion, *f*, and when the reaction reaches completion, respectively.

If the ^{14}C-labeled material had more than 0.5 % isotopic contamination, a trend in the observed KIE as a function of fractional conversion would have been detectable within experimental error.[56] For example, if instead of pure ^{2}H at the 7 pro-*R* position, the material contained more than 0.5 % ^{1}H, that contaminant would react much faster than the ^{2}H-labeled material due to a 1˚ KIE of around 3.5.[58] Thus, the observed KIE at low fractional conversion would be significantly inflated, but would approach the "real" KIE at high fractional conversion, after the light contaminant has been consumed. Our reaction shows no decreasing trend (within experimental error) in the KIE as a function of fractional conversion and the magnitude of the KIE is within the expected range for this reaction[68,126] (Figure 4.1D), providing strong evidence that the synthesized material is isotopically and enantiomerically pure. We note as a word of caution that initial attempts to synthesize the material using the same procedure, but with yADH instead of

hADH, led to significant ^{1}H-contamination at the 7 pro-*R* position. While the reason for this ^{1}H-contamination is not clear, as the only reducing equivalent in the system is the ^{2}H from DCO_2Na, the analysis of the contaminated product confirmed the usefulness of the above analysis.

In summary, we present here a synthetic route to 7*R*-[^{2}H]-phenyl-[^{14}C]-benzyl alcohol, which may have a number of applications in studying the mechanism of ADH, and could find use in synthetic routes to other materials that are useful for a variety of biochemical applications. Additionally, the coupled synthetic system, which uses a NAD^+ cofactor in catalytic amounts, could easily be adapted to other synthetic procedures.

CHAPTER V

A CRITICAL TEST OF THE "TUNNELING AND COUPLED MOTION" CONCEPT IN ENZYMATIC ALCOHOL OXIDATION

This chapter has been submitted by Daniel Roston and Amnon Kohen for publication in *Journal of the American Chemical Society*.

Abstract

The physical mechanism of C-H bond activation by enzymes is the subject of intense study and we have tested the predictions of two competing models for C-H activation in the context of alcohol dehydrogenase. The kinetic isotope effects (KIEs) in this enzyme have previously suggested a model of quantum mechanical tunneling and coupled motion of primary (1˚) and secondary (2˚) hydrogens. Here we measure the 2˚ H/T KIEs with both and H and D at the 1˚ position and find that the 2˚ KIE is significantly deflated with D-transfer, consistent with the predictions of recent Marcus-like models of H-transfer. The results suggest that the fast dynamics of H-tunneling result in a 1˚ isotope effect on the structure of the tunneling ready state: the trajectory of D-transfer goes through a shorter donor-acceptor distance than that of H-transfer.

Research Report

Alcohol dehydrogenase (ADH) is an important model system for studying the physical processes involved in enzyme-catalyzed hydrogen transfers. ADH catalyzes the oxidation of alcohol using a nicotinamide cofactor (Scheme 5.1), and this reaction has provided many surprising experimental results that have caused the enzymology community to rethink many facets of enzymology.[7,8]

One of the most significant concepts to come out of work on ADH is the notion of "quantum mechanical tunneling and coupled motion" between primary (1˚) and secondary (2˚) hydrogens. The theory of tunneling and coupled motion (Figure 5.1) posits

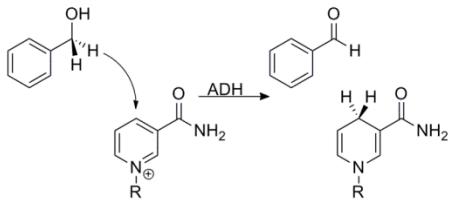

Scheme 5.1 The reaction catalyzed by ADH (using benzyl alcohol as an alternative substrate). R= adenine diphosphate ribosyl-.

that the reaction coordinate for hydride transfer involves motion of both the 1˚ and 2˚ hydrogens, and that together, the hydrogens tunnel through the reaction barrier.[26,61,63,125,149] This concept seems to explain some surprising KIE data, and additional KIE experiments[31] apparently confirmed one of the model's most significant predictions, that Swain-Schaad Exponents (SSEs) would be inflated. The SSE is the relationship between KIEs using different combinations of isotopes of hydrogen.[30] A simple derivation making the assumptions of semiclassical transition state theory, no tunneling, and harmonic vibrational frequencies, showed that the SSE should be a constant, regardless of what reaction is studied or which atom is isotopically labeled:[30]

$$SSE = \frac{\ln(\frac{k_H}{k_T})}{\ln(\frac{k_D}{k_T})} = 3.3 \qquad [5.1]$$

where k_i is the rate with isotope i. Since Klinman and co-workers found that the relationship was extraordinarily inflated for 2˚ KIEs in yeast ADH (yADH),[31] inflated SSEs have been cited prolifically as evidence for tunneling and coupled motion.[7,146]

Perhaps due to the relative ease of synthesizing the necessary isotopically labeled materials, the particular experiments that showed the inflated 2˚ SSEs (in yeast,[31] as well as other ADHs[32,33]) were mixed-labeling experiments,[27] where the 2˚ H/T KIE was measured with H at the 1˚ position, but the 2˚ D/T KIE was measured with D at the 1˚ position. Thus, the experiments measured the mixed-labeling 2˚ SSE (mSSE):

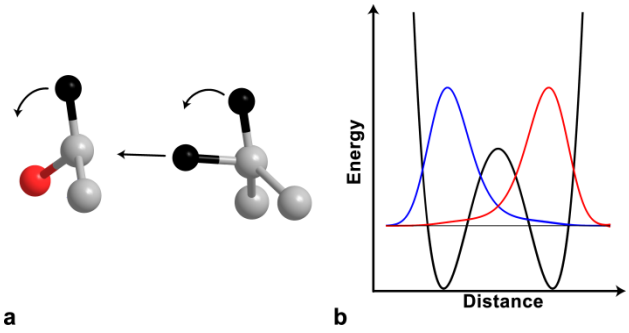

Figure 5.1 The model of tunneling and coupled motion. A) The reaction coordinate mode consists of motion of the 1˚ hydrogen, as well as the 2˚ hydrogens that allow the donor and acceptor carbons to rehybridize. B) Tunneling of this coupled mode through the reaction barrier depends on the overlap between the reactant (blue) and product (red) wavefunctions. Reproduced with permission from ref. 8.

$$mSSE = \frac{\ln(\frac{k_{HH}}{k_{HT}})}{\ln(\frac{k_{DD}}{k_{DT}})} \quad [5.2]$$

where k_{ij} is the rate with isotope *i* at the 1˚ position and isotope *j* at the 2˚ position. According to semi-classical transition state theory and the Bigeleisen equation,[22] the mSSE should equal the SSE, since the rule of the geometric mean (RGM) states that there are no isotope effects on isotope effects.[62,150] Nonetheless, one of the great mysteries has been why inflated SSEs have appeared in so few other systems,[71] despite evidence that tunneling is important to most or all H-transfers.

An analysis of the inflated mSSEs from many different ADHs showed that the source of the inflation was not that the 2˚ H/T KIE was inflated, as expected from the traditional model of tunneling and coupled motion, but the D/T KIEs were *deflated*.[54] The data suggested that the shorter donor-acceptor distance (DAD) necessary for D-tunneling caused steric hindrance between the substrates to inhibit rehybridization of the donor carbon, thus deflating the 2˚ KIEs. A recent experimental study of the yADH reverse reaction led to QM calculations that explained all 2˚ KIEs and most other data on the C-H activation for this enzyme.[68] A critical component in these calculations was a shorter

DAD for D-transfer than for H-transfer. These calculations were based on Marcus-like models of hydrogen tunneling (Figure 5.2), which have found great use in rationalizing both 2˚ and 1˚ KIEs and their temperature dependence.[5,34,48,50,51,53,85] Marcus-like models explain C-H activation in terms of a separation between heavy atom motion and hydrogen tunneling and give a rate constant (k) of the form

$$k = \frac{|V|^2}{\hbar}\sqrt{\frac{\pi}{\lambda k_B T}}\, e^{-\frac{(\Delta G^\circ + \lambda)^2}{4 k_B T \lambda}} \int_0^\infty F(m, DAD)\, e^{-E(DAD)/k_B T}\, dDAD \qquad [5.3]$$

The factors in front of the integral give the rate of reaching a tunneling ready state (TRS) based on the electronic coupling between reactants and products (V), the reaction driving force (ΔG°), and the reorganization energy (λ). A TRS is a point of transient degeneracy between reactants and products, where the H can tunnel while still conserving energy. The process of reaching a TRS is depicted in Figure 5.2a. The integral computes the probability of transmission to products once the system reaches a TRS (Figure 5.2b). This probability is based on the probability of tunneling as a function of mass and DAD, F(m,DAD), and a Boltzmann factor giving the probability of being at any given DAD. Integrating over all DADs gives the overall probability of transmission to products. This kind of model proposes that all isotopes of H react by tunneling, but expects that the trajectory of heavier isotopes will pass through a shorter DAD (Figure 5.2b).

So far, all the experimental evidence supporting this explanation was quite complex and thus indirect.[26,31-33,59,68,141] Here we have conducted one of the simplest possible tests of the predictions of that model: we have measured the 2˚ H/T KIEs on the oxidation of benzyl alcohol with both H- and D-transfer (Table 5.1). This experiment directly tests the effect of the 1˚ (transferred) isotope on the 2˚ KIEs (the RGM) without the many possible effects of assessing it from mixed labeling measurements (eqs 5.2 and 5.4). The usefulness of directly measuring k_{DH}/k_{DT} was initially suggested by simple calculations of coupling between the 1˚ and 2˚ C-H bonds,[126] but has not yet been attempted experimentally due to the required stereospecific labeling pattern. The new

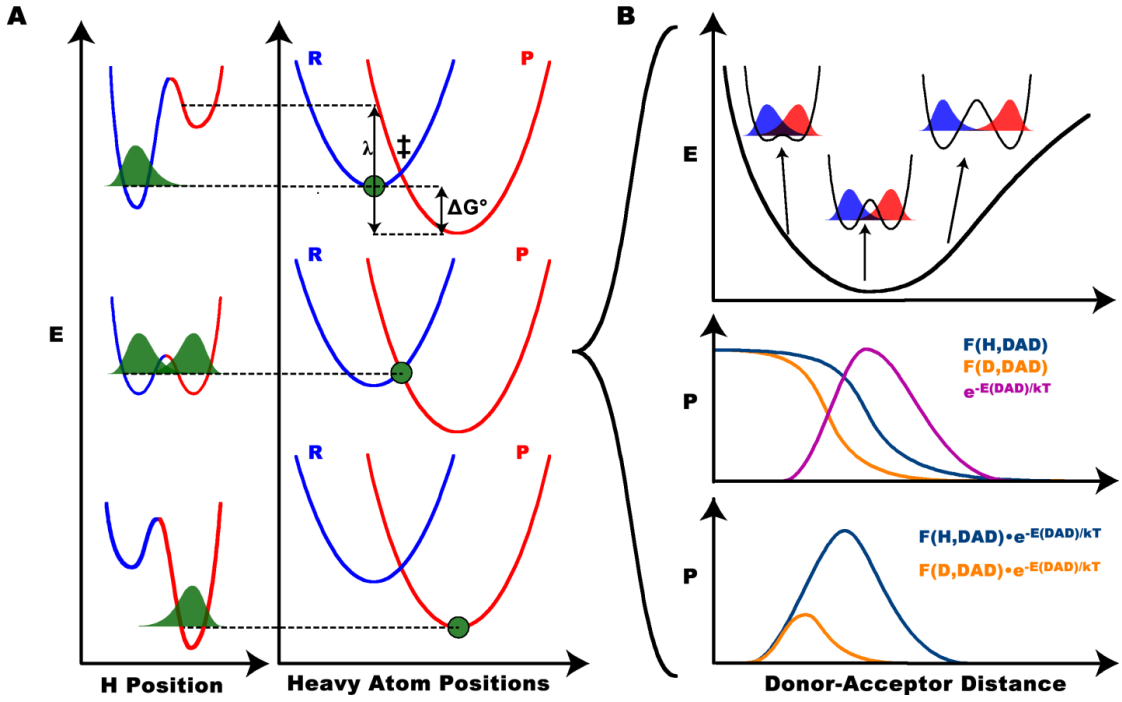

Figure 5.2 Marcus-like model of H-tunneling. A) The top, middle, and bottom panels show three stages of the reaction in two designated coordinates: the H position, and the positions of the heavy atoms that modulate the potential surfaces (reactant surface is blue and product surface is red) for the transferred H. In the top panel, the heavy atoms are in a position such that the zero point energy (ZPE) of the H is lower in the reactant well, so the H-wavefunction (green) is localized there. In the middle panel, the heavy atoms have rearranged to a tunneling ready state (TRS, ‡), where the ZPE for the transferred H is equal in the reactant and product wells and the H-wavefunction can tunnel through the barrier. The rate of reaching this tunneling ready state depends on the reaction driving force (ΔG˚) and the reorganization energy (λ). In the bottom panel, the heavy atoms have rearranged further, making the ZPE of the product lower than the reactant, and thus trapping the transferred H in the product well. B) At the TRS (middle panel of A) fluctuations of the DAD affect the tunneling probability. The top panel shows a free energy surface for the designated DAD coordinate, indicating the different levels of reactant-product wavefunction overlap at different DADs. The middle panel shows the Boltzmann probability distribution of the system being at any given DAD (magenta), along with the tunneling probabilities of H and D as a function of DAD (orange and purple, respectively). The bottom panel shows the product of the Boltzmann factor and the tunneling probability for each particle, yielding the probability of a reactive trajectory as a function of DAD. Panel B illustrates that the reactive trajectories for H and D go through different average DADs, constituting an isotope effect on TRS structure. In ADH, the difference in average DAD for hydride transfer vs. deuteride transfer leads to differences in 2˚ KIEs when the transferred isotope is different.[68]

Table 5.1: 2° KIEs and SSEs on oxidation of benzyl alcohol by yADH

	Measured	Predicted[d]	Predicted[e]
k_{DH}/k_{DT}	**1.18 ± 0.03[a]**	**1.11**	**1.12**
k_{HH}/k_{HT}	1.33 ± 0.05[b]	1.32	1.33
k_{DD}/k_{DT}	1.03 ± 0.01[c]	1.03	1.04
mSSE	8.9 ± 3.0	9.4	7.7
SSE_D	5.6 ± 2.0	3.4	2.9

[a]This work.

[b]Ref 59. This value was also measured in ref 31 and in the present work, and all measurements are within error of one another.

[c]Ref 31.

[d]Ref 68.

[e]Ref 126.

measurement was made possible by the chemoenzymatic synthesis of 7*R*-[^{2}H]-phenyl-[^{14}C]-benzyl alcohol, which had previously been attempted for over 10 years (see Supplementary Information and ref 151). We measured the KIEs competitively using the same conditions as in previous studies on yADH (25˚ C, pH 8.5),[31,141] and the results (Table 5.1) are qualitatively consistent with the predictions based on both 1˚-2˚ coupled motion[126] and Marcus-like models.[54,68] Specifically, the 2˚ KIE is significantly deflated with D-transfer versus H-transfer (1.30 ± 0.02 and 1.18 ± 0.03 with H- and D-transfer, respectively). Together with the value of the 2˚ D/T KIE with D-transfer (1.03 ± 0.01),[31] our measurements yield the SSE_D:

$$SSE_D = \frac{\ln(\frac{k_{DH}}{k_{DT}})}{\ln(\frac{k_{DD}}{k_{DT}})} \quad [5.4]$$

where, as in Eq 5.2, k_{ij} is the rate with isotope *i* at the 1˚ position and isotope *j* at the 2˚ position. The value we obtain for SSE_D (5.6 ± 2.0) is slightly higher than values

calculated for the SSE_D,[68,126] but it is within the (larger) range calculated by models that have dispensed with some simplifying assumptions.[27,64,152]

This measurement directly confirms that the inflated mSSE comes from a deflation of 2˚ KIEs when D is at the 1˚ position, as originally suggested in ref 54. Furthermore, this measurement reveals that the deflation of the 2˚ KIEs with D-transfer is not unique to D/T KIEs, as observed before, but is a general phenomenon reflecting the suppression of donor rehybridization at the TRS due to the close proximity of the H-acceptor. Both refs 126 (using a truncated Bell correction[40]) and 68 (using a Marcus-like model) suggested a critical role for H-tunneling in predicting this breakdown of the RGM and the two studies made similar predictions for the value of the 2˚ H/T KIE with D-transfer, which we have measured here for the first time (Table 5.1). Nonetheless, the Marcus-like model has several advantages. First, the Bell-type corrections used in early models of tunneling and coupled motion[61,63,125,126] cannot account for temperature independent KIEs when reaction rates are temperature dependent.[33,39,146] This, however, is precisely the observed behavior of many enzyme reactions,[7,8,36] including that of a thermophilic ADH, which also showed inflated mSSEs.[33] In fact, ref 126 stated explicitly that the temperature dependence of KIEs in that model was steeper than the observed data.[31] Additionally, the nature of the coupling between vibrational modes in that study was vague and difficult to interpret. Thus, the more recent Marcus-like model that can account for all of the behavior of these reactions within an intuitively satisfying model is more compelling.

Marcus-like models originally arose out of the need to explain the temperature dependence of 1˚ KIEs,[34,48,50,51,53] but they describe a mechanism for C-H bond activation which, if right, should also account for 2˚ KIEs. Thus far, though, very little work has attempted to test the predictions of Marcus-like models in the context of 2˚ KIEs.[54,68,70] The experiments here directly demonstrate the deflation of 2˚ KIEs for D-transfer relative to H-transfer. Since the current experiment does not involve mixed labeling, it directly

reveals the source of one of the most puzzling results for 2˚ KIEs (inflated mSSEs), and contributes strong support for the mechanism of C-H activation described by Marcus-like models. In this mechanism, H-tunneling is modulated by the "heavy atoms" coordinate that tunes the transient degeneracy necessary for tunneling. Once degeneracy is achieved, the transferred atom can tunnel to products with efficiency dependent on its mass and the DAD. Since the DAD must be shorter for D to tunnel than for H to tunnel, the average DAD of transfer is shorter with D than with H (Figure 5.2b).

In summary, the ADH reaction with H-transfer effectively goes through a different TRS than the reaction with D-transfer. The electronic potential surface is the same for the two reactions, consistent with the Born-Oppenheimer approximation, but the dynamics of nuclear tunneling contribute to the reaction's bottleneck (i.e., the point along the reaction coordinate with the lowest flux of forward trajectories, analogous to the variational transition state).[2,153] One can describe this result as an isotope effect on the structure of the TRS. In a general sense, it is perhaps not surprising that the dynamics of H-tunneling contribute to the rate limitation of the H-transfer step, but here we have demonstrated clearly that this dynamic bottleneck[154] has important implications for the structure of the TRS. Furthermore, we have shown that 2˚ KIEs provide important information to determine the structure of a TRS. In contrast to 1˚ KIEs, though, 2˚ KIEs are only indirectly affected by tunneling: they are a manifestation of isotopic differences in the structural rearrangement necessary to reach the TRS (differences in ZPE contributions to ΔG° and λ of eq. 5.3). The structural information provided by 2˚ KIEs has been very useful in developing powerful transition state analog inhibitors for enzymes that catalyze heavy atom bond cleavages,[1] and now the door is open to use analogous methods for enzymes that catalyze H-transfers.

Supporting Information

Experimental Details

Materials

All chemicals were from Sigma unless otherwise noted. [^{3}H]-$NaBH_4$ (350 mCi/mmol) was from American Radiolabeled Chemicals. Phenyl-[^{14}C]-benzaldehyde (55 mCi/mmol) was from ViTrax. [^{2}H]-$NaBH_4$ was from Cambridge Isotope Labs. 7-[^{3}H]-benzyl alcohol (racemic) was prepared by reduction of benzaldehyde by [^{3}H]-$NaBH_4$. 7-[^{3}H],[^{2}H]-benzyl alcohol (racemic) was prepared by reduction of benzoyl chloride by a mixture of [^{3}H]-$NaBH_4$ and [^{2}H]-$NaBH_4$. Phenyl-[^{14}C]-benzyl alcohol was prepared by reduction of phenyl-[^{14}C]-benzaldehyde by $NaBH_4$. 7*R*-[^{2}H]-phenyl-[^{14}C]-benzyl alcohol was prepared by a coupled synthesis depicted in scheme 5.2. The synthesis of this material has been of interest to various groups for over 10 years, and is relevant to broader application than the current paper, thus the details of the synthesis will be published elsewhere.[151] Briefly, the reduced form of 4*R*-[^{2}H]-nicotinamide adenine dinucleotide (NADD) was produced *in situ* by reduction with formate-d, catalyzed by formate dehydrogenase (FDH). The resultant NADD was used to reduce phenyl-[^{14}C]-benzaldehyde, catalyzed by horse liver ADH, yielding the desired 7*R*-[^{2}H]-phenyl-[^{14}C]-benzyl alcohol. Yeast alcohol dehydrogenase (yADH) isozyme 2 was expressed and purified according to a published procedure[142] using a strain of yeast deficient for other isozymes of ADH (a generous gift from Bryce V. Plapp, Dept. of Biochemistry, University of Iowa).

Kinetic Measurements

We measured 2˚ H/T KIEs with both H-transfer and D-transfer using competitive methods and conditions as described before.[31,68,141] Briefly, in such measurements both the light and heavy substrate react in the same container, competing for the enzyme's

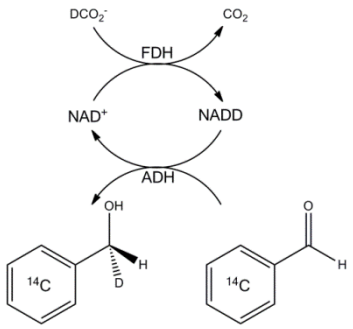

Scheme 5.2 Synthesis of 7*R*-[^{2}H]-phenyl-[^{14}C]-benzyl alcohol

active site.[56,143] Competitive methods give very precise measurements, but generally require radiotracers for both substrates. Our methods used ^{3}H in the heavy substrates and the light substrates (which had either ^{1}H or ^{2}H) always had a remote ^{14}C label. To conduct these experiments, the heavy and light substrates must be co-purified and subsequently added to the reaction mixture. For the measurement of the 2˚ H/T KIE with H-transfer, 7-[^{3}H]-benzyl alcohol (racemic) was copurified with phenyl-[^{14}C]-benzyl alcohol. For 2˚ H/T KIE with D-transfer, 7-[^{3}H],[^{2}H]-benzyl alcohol (racemic) was copurified with 7*R*-[^{2}H]-phenyl-[^{14}C]-benzyl alcohol. The copurified alcohol was added to 1 ml reaction mixtures that contained 10 mM NAD^{+}, 300 mM semicarbazide, 80 mM glycine (pH 8.5), and 1 mM benzyl alcohol (300,000 dpm ^{14}C and 3,000,000 dpm ^{3}H). These conditions are based on those used in previous studies of yADH.[31,68,141] Reactions began after the addition of approximately 1 mg yADH and were incubated at 25˚ C. At a range of timepoints, we removed 100 µl aliquots and quenched them by the addition of 10 µl saturated $HgCl_2$. We stored the quenched aliquots at room temperature until ready for analysis by HPLC. The addition of $HgCl_2$ generated a precipitate, which we removed by centrifugation prior to HPLC analysis.

The semicarbazide in the reaction mixture traps the product benzaldehyde as benzaldehyde semicarbazone, which ensures that the reaction is irreversible. We separated the reactants and products at a range of time points by HPLC and analyzed the

reactant and product fractions for ^{3}H and ^{14}C contents by LSC. We then calculated KIEs according to[143]

$$KIE = \frac{\log(1-f)}{\log(1-f*\frac{R_p}{R_\infty})} \quad [5.5]$$

where R_p is the ratio of ^{3}H:^{14}C (heavy to light isotope) in products at a fractional conversion, *f*, and R_∞ is the ratio of ^{3}H:^{14}C in products when the reaction reaches completion.

Additional Results

Like previous studies,[31-33,141] our ^{3}H-labeled substrates were all racemic mixtures, which is synthetically more convenient, and has the added advantage that the same reaction yields both a 2˚ KIE and a 1˚ KIE (as we only analyze products and these lead to tritium in different products). For example, in the 2˚ H/T with H-transfer experiments, half of the ^{3}H from the substrate ends up in the product semicarbazone, contributing to the measurement of the 2˚ KIE, but the other half ends up in the product NADH, allowing for the measurement of the 1˚ H/T KIE. Note that since we determine *f* from the ^{14}C contents of reactants and products, the fact that ^{3}H is split between two products does not affect the calculation of *f*. Our results for the 1˚ H/T KIE (7.0 ± 0.2) and 2˚ H/T KIE with H-transfer (1.30 ± 0.02) are within error of those previously measured for this enzyme,[31] which gives us confidence about the validity of both their and our experimental methods. The labeling scheme we used to measure the 2˚ H/T KIE with D-transfer does not yield the 1˚ D/T KIE, but a more complicated KIE that involves differences in both the 1˚ and 2˚ isotopes. Specifically, the 7*R*-[^{2}H]-phenyl-[^{14}C]-benzyl alcohol has D at the 1˚ position and H at the 2˚ position, while the other substrate (one of the enantiomers of the racemic material) has T at the 1˚ position, but D at the 2˚ position. Thus, the measured KIE (1.57 ± 0.08) involves mixed 1˚ and 2˚ effects and we do not speculate on how best to interpret the value; we only point out that the measured value is significantly deflated from the

naïve prediction of semiclassical theory that this mixed KIE will be the product of the 1˚ D/T KIE (1.73 ± 0.03)[31] and the 2˚ H/D KIE (1.21 ± 0.01 , from 2˚ H/T KIE and SSE), which is 2.09 ± 0.04.

CHAPTER VI

COMPUTATIONAL ANALYSIS OF THE TUNNELING READY STATE IN AN UNCATALYZED ANALOGUE OF ALCOHOL DEHYDROGENASE

Abstract

Kinetic isotope effects (KIEs) have traditionally yielded vital information on the structure of transition states in both solution and enzyme active sites. In hydrogen transfers, though, where nuclear quantum tunneling is important, secondary (2°) KIEs can be either inflated or deflated relative to the predictions of semiclassical transition state theory (TST). With no quantum mechanical considerations, TST analysis of the 2˚ KIEs contradicts Hammett substituent effects and the Hammond postulate, hindering the understanding of the reaction coordinate. Here we use Marcus-like models to quantitatively model the structure of the tunneling ready state (TRS) in the non-enzymatic oxidation of benzyl alcohol. We then compare the results to those found for the oxidation catalyzed by alcohol dehydrogenase (ADH). We find that the hydrogen donor-acceptor distance (DAD) is similar in both reactions, but whereas the enzymatic TRS is early and associative, the uncatalyzed TRS is late and dissociative. This outcome accords well with the reaction's thermodynamics, as the enzymatic reaction is exothermic while the uncatalyzed one is endothermic. We discuss how these similarities and differences reflect on the catalytic power of the enzyme.

Research Report

One of the biggest difficulties facing the study of enzyme catalysis is that in general, one cannot directly compare the catalyzed reaction to the uncatalyzed reaction because the uncatalyzed reaction does not occur on a timescale amenable to measurement. Most studies, therefore, can probe the mechanism of enzymes, but have no real access to information on the catalytic effects of the enzyme.[155] We recently made

progress in overcoming this barrier by developing a reaction to compare with the model enzyme alcohol dehydrogenase (ADH). ADH catalyzes the oxidation of alcohol by nicotinamide adenine dinucleotide (NAD^+). The ADH reaction does not occur in the absence of a catalyst, but we have studied the analogous oxidation of alcohol by 9-phenylxanthyllium (PhX^+) (Scheme 6.1).[156-160]

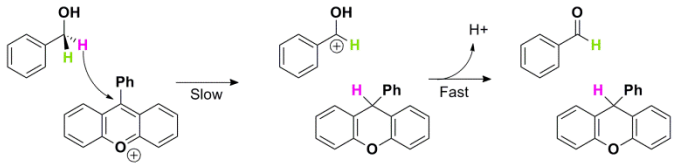

Scheme 6.1: Mechanism of alcohol oxidation by PhX^+.

While both the catalyzed and uncatalyzed reactions involve the oxidation of benzyl alcohol, and both reactions are rate-limited by their hydride transfers, there are some notable differences between the two. In the catalyzed reaction, for example, a Zn^{2+} at the active site serves as a Lewis acid, allowing the deprotonation of the alcohol to precede the hydride transfer, which occurs from the activated Zn-alkoxide. This initial deprotonation is somewhat endothermic, but the subsequent hydride transfer is exothermic, so Hammond's Postulate predicts an early (reactant-like) transition state (TS) for the hydride transfer in ADH.[97] In the uncatalyzed reaction, however, the hydride transfer occurs first, creating an unstable α-hydroxy carbocation.[159] Thus, the uncatalyzed hydride transfer is endothermic and expected to have a late (product-like) TS.

We recently probed the TS of the uncatalyzed reaction using both kinetic isotope effects (KIEs) and Hammett substituent effects (HSEs) to understand the physical nature of the C-H bond activation of this reaction.[157] Interpreting the experimental results by a traditional semi-classical model presented difficulties because by that interpretation the

KIEs and the HSEs contradicted each other. The HSEs indicated a large value of ρ (substituents substantially affected the reaction rate), consistent with a late TS, which is consistent with the Hammond's postulate. The 2˚ KIEs, however, were smaller than semi-classical models[25] would predict for a product-like TS. Intriguingly, this is precisely the opposite contradiction that the ADH-catalyzed reaction exhibits. Namely, in ADH, the HSEs indicated an early TS,[57,58,123] but the KIEs indicated a late TS.[57-59] While the experimental 2˚ KIEs do not conform to semi-classical (no tunneling) models of reactivity, we recently found success in quantitatively explaining both the KIEs and HSEs in ADH using a Marcus-like Model of H-tunneling.[68]

Marcus-like models are an adaptation of Marcus Theory of electron tunneling[47] to the situation of hydrogen tunneling and have been referred to by a variety of other names, such as full tunneling models, environmentally-coupled tunneling, vibrationally-assisted tunneling, and others.[5,7,48,50,36,85,146] This kind of model assumes that H-transfer occurs by tunneling once heavy-atom reorganization brings the system to a tunneling-ready state (TRS) where the reactants and products are degenerate and tunneling can occur efficiently (Figure 6.1). The rate constant (k) in this kind of theory has the functional form[34,48,51,53]

$$k = \frac{|V|^2}{\hbar}\sqrt{\frac{\pi}{\lambda k_B T}}\, e^{-\frac{(\Delta G^\circ+\lambda)^2}{4k_B T\lambda}} \int_0^\infty F(m, DAD)\, e^{-E(DAD)/k_B T}\, dDA \qquad [6.1]$$

In this equation, the factors in front of the integral determine the rate of reorganization to reach a TRS, which depends on the adiabaticity of the reaction (electronic coupling between reactants and products, *V*), the reorganization energy (λ), and the reaction driving force (ΔG°). The integral, then, determines the overall probability of transmission to products once the system reaches a TRS. This depends on the probability of tunneling, F(m,DAD), which is a function of mass (m) and donor-acceptor distance (DAD), as well as a Boltzmann factor giving the probability of being at any given DAD. The integral over all DADs gives the total probability of tunneling to products. This model arose

primarily out of a need to explain the temperature dependence of 1° KIEs, but it has also successfully explained[68] and predicted[148] 2° KIEs.

Here we sought to use a Marcus-like model to gain a deeper understanding of the TRS of the hydride transfer in scheme 6.1. We employed the method initially developed for the ADH-catalyzed reaction[68] and that we recently used for a similar non-enzymatic oxidation of alcohol.[160] The overall procedure involves parameterizing the structure of the reacting species in the gas phase in order to fit the requirements of a TRS (degenerate reactants and products, relatively short DAD, etc.), and then adjusting additional geometric parameters in order to computationally reproduce the experimental KIEs. Details of the method are available in the supporting information. The experimentally determined KIEs had relatively large error bars (1.11 ± 0.06 for 2° H/D with H-transfer and 1.12 ± 0.09 for 2° H/D with D-transfer),[157] which made the comparison with calculated values somewhat difficult. Nonetheless, at a DAD of 3.2 Å the calculated 2° H/D KIE (1.10) agreed well with the experimental values. As indicated in Table 6.2, the calculated KIE is not particularly sensitive to DAD for DAD>3.2 Å. 3.2 Å seems like the most likely DAD, though, because the 1° KIE is expected to increase drastically at longer DADs,[51] but the observed 1° KIE for this reaction is just 3.3.[157] Additionally, this DAD is very similar to the DADs found for other alcohol oxidations.[68,160]

Within experimental error, this reaction shows no difference in 2° KIE with H-transfer vs. D-transfer,[157] an observation that has been very important in studies of ADH.[31,54,68,148] Marcus-like models predict that reactions with D-transfer will go through a shorter DAD than those with H-transfer (Figure 6.1B). This can be observed by measuring isotope effects on isotope effects, which violates the semiclassical rule of the geometric mean.[161] Unfortunately, the error bars on the KIEs of the uncatalyzed reaction are fairly large and likely obscure any differences in 2° KIE with H-transfer vs. D-transfer, so we cannot make any judgments in this regard.

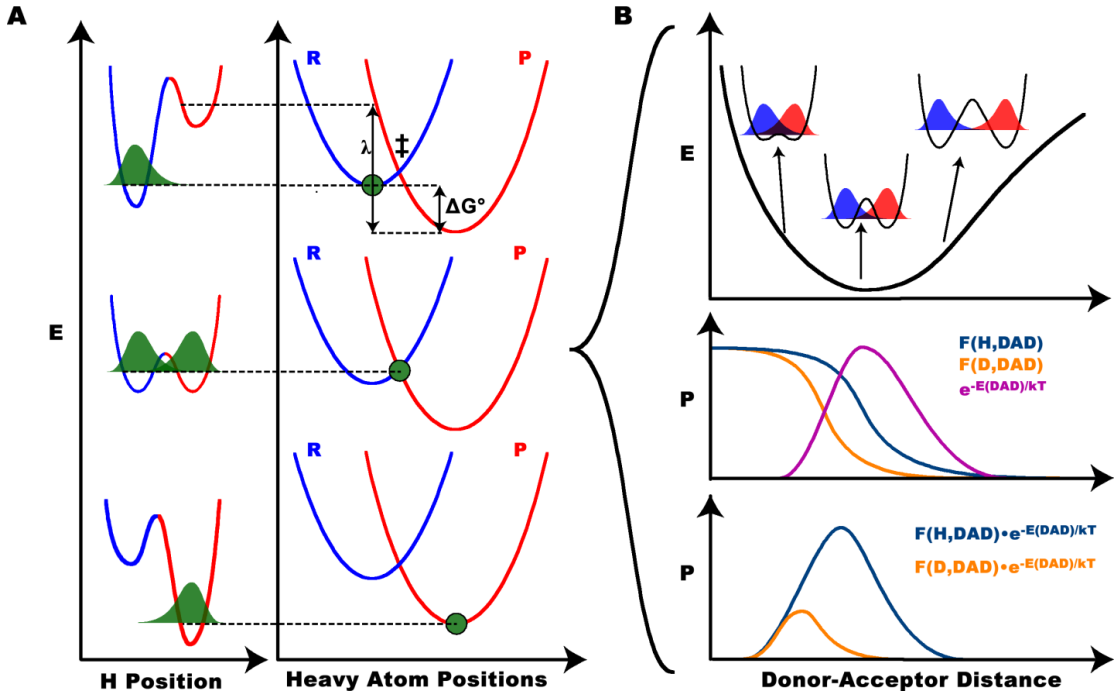

Figure 6.1: Marcus-like Model of hydrogen tunneling. A) Three stages of reaction progress (top to bottom) in two coordinates: 1) the hydrogen position, with its probability density in green, moving between a donor and acceptor well and 2) the progress of the heavy atom reorganization that determines the relative ZPEs of the reactant (blue) and product (red) wells. In the top panel, the reactant well is more stable, so the hydrogen is localized in that well. In the middle panel, the heavy atoms have rearranged to a TRS, where the reactant and product are degenerate and the H wavefunction is delocalized between the two wells. Upon further reorganization, in the bottom panel, the system traps the hydrogen in the product well. B) The probability of tunneling at the TRS depends on the mass and DAD. The top panel shows the free energy surface determining the distribution of DADs, emphasizing the extent of reactant-product wavefunction overlap as a function of DAD. The middle panel shows the Boltzmann distribution of DADs (magenta), along with the tunneling probability as a function of DAD for H (purple) and D (orange). The product of the distribution of DADs and the tunneling probability gives the overall probability of a reactive trajectory as a function of DAD (bottom panel). This model predicts that D-transfer will require a shorter DAD than H-transfer, and this has had significant effects on 2° KIEs in ADH,[31,54,68,148] but appears not to be as important in the uncatalyzed reaction.[157] Reproduced with permission from ref. 148.

The hybridizations of the donor and acceptor carbons at the TRS, calculated as previously,[68] were $sp^{2.29}$ and $sp^{2.54}$, respectively (Figure 6.3). These hybridizations are asynchronous, which has been observed in enzymatic H-transfers[68,128] and may be a

general phenomenon among hydride transfers. The hybridization of the acceptor carbon is nearly perfectly balanced between reactant- and product-like, but the donor carbon is very product-like at the TRS, which is consistent with the predictions of Hammond's postulate for an endothermic reaction, as well as the experimental HSEs.[157] Thus, the TRS based on Marcus-like Models can explain both the 2° KIEs and the HSEs, which blatantly contradict each other if interpreted by semiclassical theories.

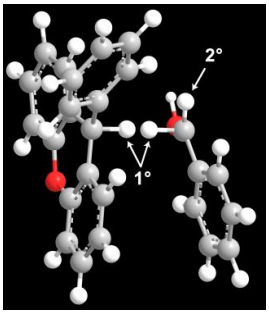

Figure 6.2: Computed TRS structure showing benzyl alcohol on the right and PhX^+ on the left. The 1° (transferred) hydride is shown in both the donor and acceptor wells, as it is actually delocalized between the two positions. The 2° hydrogen relevant to the KIEs used to parameterize the model is also labeled.

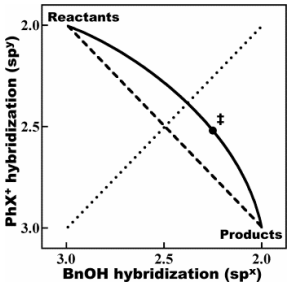

Figure 6.3: Two-dimensional reaction coordinate as a function of the donor (BnOH) and acceptor (PhX^+) carbon hybridizations. The black dot, labeled with (‡), indicates the TRS and the solid line represents a reasonable reaction trajectory that passes through the TRS. The dashed line indicates the reaction path for completely synchronized rehybridization and the dotted line indicates the dividing surface for a symmetric (i.e., equally reactant- and product-like) TRS.

Table 6.1: Geometry of uncatalyzed and catalyzed TRS

	Uncatalyzed	Catalyzed[a]
DAD	3.2 Å	3.2 Å
C_{Donor} hybridization	$sp^{2.29}$	$sp^{2.76}$
$C_{Acceptor}$ hybridization	$sp^{2.54}$	$sp^{2.34}$

[a]Ref. 68.

Now that we have computed the TRS for this reaction and shown that it is consistent with all experimental data, we can make a thorough comparison between the TRS of this reaction and the TRS computed for the ADH-catalyzed reaction (Table 6.1).[68] The enzymatic TRS is reactant-like, but the uncatalyzed TRS is product like, consistent with the differing thermodynamics of the reactions. The fact that the enzyme can deprotonate the alcohol prior to the hydride transfer apparently lowers the barrier of the hydride transfer by making that step exothermic. One might also ask if the enzyme directly affects the rate by forcing the substrates to a short DAD, as has been debated recently.[9,10,17] One can easily imagine, for example, that the active site compresses the substrates toward one another to enhance the rate of transfer (by both narrowing and lowering the barrier). We find no evidence of this, as the uncatalyzed reaction appears to have the same DAD as the catalyzed reaction (3.2 Å). In some sense, this fits with intuition: at short DADs, the primary force affecting the DAD is the van der Waals repulsion between the reactants, and this repulsion does not depend on the solvent/enzyme environment. QM/MM simulations of the dihydrofolate reductase catalyzed reaction, for example, examined the PES along the DAD coordinate and showed that the primary differences between a wild-type enzyme, its mutants, and the reaction in solution, appeared at long DADs, while the short DAD side was relatively invariant.[44,155] We find no evidence, therefore, that "compressive motions" that enhance enzymatic rates by lowering and narrowing the barrier serve a significant role in

catalysis. The enzyme does its work through electrostatic stabilization of a TRS with a similar DAD to that found in solution. This said, the DAD from our fit is an average DAD, while ref 44 suggested a broader DAD distribution for the water and mutants relative to the WT. That effect appears to be consistent with the "compression" proposed in refs 17 and 162. However, our current calculations and experiments cannot assess the DAD distribution.

In summary, we have computed the structure of the TRS for the oxidation of benzyl alcohol by PhX^+ within the framework of a Marcus-like model, and shown that this kind of model can reconcile the observed contradiction between the semiclassical interpretation of 2˚ KIEs vs. HSEs and Hammond's postulate. Previous work had shown that Marcus-like Models can reconcile the exact opposite contradiction,[68] thus demonstrating the versatility of this kind of model. Based on these results, experimental HSEs and the reaction thrmodynamics appear to be a reliable qualitative (reactant-like vs. product-like) indication of TRS structure, but 2° KIEs are nonetheless reliable for quantitative modeling. By comparing the uncatalyzed reaction with the analogous ADH-catalyzed oxidation of benzyl alcohol, we have elucidated some catalytic effects of the enzyme. We find no evidence that a shorter average DAD plays a role in catalysis, but cannot exclude possible contributions to catalysis from narrowing of the distribution of DAD. The data and analysis are consistent with enzyme achieving its catalytic power not by forcing the substrates below their van der Waals radii, but by forming favorable electrostatic interactions with the TRS.

Supporting Information

Computational Methods

The methods used here closely follow those described previously.[68,160] Briefly, the reacting species were optimized using Gaussian 09[163] at the B3LYP/6-31+G* level with the transferred hydride at the midpoint of a straight line between the donor and acceptor

carbons. The calculations included both reactants in their entirety, so the system involved 49 atoms and an overall charge of +1 (Figure 6.2). This optimization was carried out at a range of DADs. These optimized structures do not have degenerate donor and acceptor wells of a TRS, though, so in order to achieve degeneracy, the hybridization of the benzylic (donor) carbon was adjusted by altering the out-of-plane bend of the 2° hydrogen. Since the acceptor carbon is surrounded by static heavy atoms, their positions were not adjusted to find a point of degeneracy. Using the resultant skeletal structure, we calculated vibrational frequencies for the system when the transferred H is localized in either the donor or acceptor well and used the average of these frequencies as the overall frequencies of the TRS when calculating KIEs. The KIEs were then calculated according to the Bigeleisen equation[22] using the program ISOEFF.[140] The computed TRS is the structure that yields the best fit to experimental KIEs. Table 6.2 shows the computed KIE across the range of DADs examined here.

Table 6.2: 2° KIE as a function of DAD.

DAD (Å)	3.1	3.2	3.3	3.4
KIE	1.07	1.10	1.10	1.11

CHAPTER VII

CONCLUSIONS

We have examined the physical mechanisms of hydride transfers through a combination of experiments and theoretical analysis. The results provide in depth information about the tunneling ready states (TRSs) of enzymatic and uncatalyzed H-transfers, ranging from the detailed structures of the TRS to how enzyme dynamics affect the ensemble of reactive trajectories. In some cases the quantitative analyses provided here have simply afforded a level of quantitative precision that had previously been lacking in this field. The method for using secondary kinetic isotope effects (2° KIEs) to determine the structure of the TRS, which was developed in ch. II and then experimentally confirmed in chs. III-IV, constitutes an important advance in understanding the reaction coordinates of H-transfers. The level of detail given by this method provides rational drug designers with a means to determine the detailed structure of potential transition state analog inhibitors (or, perhaps more appropriately, TRS-analog inhibitors). The method also provides designers of biomimetic catalysts with an understanding of the detailed structure of the species that must be stabilized in order to achieve catalysis in H-transfers. Additionally, the results of the modeling based on the temperature dependence of KIEs described in ch. II illuminate how enzyme dynamics contribute to the reaction, potentially offering additional information to those who wish to exploit the many unique features of enzymes. Finally, the comparison of an enzymatic H-transfer with a non-enzymatic analogue in ch. VI highlights some similarities and differences between catalyzed and uncatalyzed reactions, thus elucidating some physical aspects of the *catalytic* power of the enzyme. In particular, we find that the electrostatic nature of the active site stabilizes a TRS with a similar DAD to the uncatalyzed reaction.

In addition to providing necessary detail on these topics, some of the conclusions from the work have sketched a somewhat different picture of reactivity than related

qualitative explanations had previously yielded. Perhaps most striking is our conclusion that steeply temperature dependent KIEs indicate that a reaction must occur by at least two trajectories: one trajectory that involves tunneling from a longer donor-acceptor distance (DAD), which has a very large KIE, and another trajectory that involves the DAD shortening to a point where there is no longer a barrier to H-transfer. In this case, conducting a thorough quantitative analysis of the data indicated that our intuition was missing an essential component in cases of steeply temperature dependent KIEs, namely, it was missing the second population that appears vital in accounting for these KIEs. Not surprisingly, this component of our analysis has generated some controversy,[164,165] even among those who had previously attempted to rationalize their findings with qualitative arguments based on similar models. Clearly, additional tests of this aspect of Marcus-like models will be important for this field.

As it stands, Marcus-like models are not alone in vying for enzymologists' acceptance. Many researchers conducting high-level simulations prefer some form of transition state theory (TST),[2,43,46,166] while others advocate for a contribution from non-statistical dynamics along the reaction coordinate.[11,165,167] TST, of course, has the advantage that it is a quite established theory[168] and many details and corrections have been added that can accommodate a wide variety of problems.[2] The other options are much younger and researchers have not yet tested their applicability in as many problems. The work here, though, constitutes a significant step forward toward the goal of showing the broad applicability of Marcus-like models. The model already shows much promise in explaining a set of problems that prove especially difficult for classical TST without substantial corrections (e.g., quantum mechanical effects, recrossing, etc.). In addition to explaining these problems, Marcus-like models have begun to yield unique predictions that can distinguish it from classical TST in the coming years and testing those predictions is now of critical importance.

REFERENCES

1. Schramm, V. L. *Ann. Rev. Biochem.* 2011, 80, 703.

2. Truhlar, D. G. *J. Phys. Org. Chem.* 2010, 23, 660.

3. Sen, A.; Kohen, A. *J. Phys. Org. Chem.* 2010, 23, 613.

4. Warshel, A.; Sharma, P. K.; Kato, M.; Xiang, Y.; Liu, H. B.; Olsson, M. H. M. *Chem. Rev.* 2006, 106, 3210.

5. Hammes-Schiffer, S. *Acc. Chem. Res.* 2006, 39, 93.

6. Schwartz, S. D. In Isotope effects in chemistry and biology; Kohen, A., Limbach, H. H., Eds.; Taylor & Francis, CRC Press: Boca Raton, FL, 2006; Vol. Ch. 18, p 475.

7. Nagel, Z. D.; Klinman, J. P. *Chem. Rev.* 2010, 110, PR41.

8. Wang, Z.; Roston, D.; Kohen, A. *Adv. Protein Chem. Struct. Biol.* 2012, 87, 155.

9. Nagel, Z. D.; Klinman, J. P. *Nat. Chem. Biol.* 2009, 5, 543.

10. Kamerlin, S. C. L.; Warshel, A. *Proteins.* 2010, 78, 1339.

11. Hay, S.; Scrutton, N. S. *Nat. Chem.* 2012, 4, 161.

12. Glowacki, D. R.; Harvey, J. N.; Mulholland, A. J. *Nat. Chem.* 2012, 4, 169.

13. Editorial. *Nat. Chem.* 2012, 4, 141.

14. Boekelheide, N.; Salomon-Ferrer, R.; Miller, T. F. *Proc. Natl. Acad. Sci.* 2011, 108, 16159.

15. Bhabha, G.; Lee, J.; Ekiert, D. C.; Gam, J.; Wilson, I. A.; Dyson, H. J.; Benkovic, S. J.; Wright, P. E. *Science.* 2011, 332, 234.

16. Adamczyk, A. J.; Cao, J.; Kamerlin, S. C. L.; Warshel, A. *Proc. Natl. Acad. Sci.* 2011, 108, 14115.

17. Dametto, M.; Antoniou, D.; Schwartz, S. D. *Mol. Phys.* 2012, 110, 531.

18. Kelly, K. K.; Hirschi, J. S.; Singleton, D. A. *J. Am. Chem. Soc.* 2009, 131, 8382.

19. Kramers, H. A. *Physica.* 1940, 7, 284.

20. Pu, J.; Gao, J.; Truhlar, D. G. *Chem. Rev.* 2006, 106, 3140.

21. Bigeleisen, J.; Mayer, M. G. *J. Chem. Phys.* 1947, 15, 261.

22. Bigeleisen, J. *J. Chem. Phys.* 1949, 17, 675.

23. Melander, L.; Saunders, W. H. Reaction rates of isotopic molecules; 4th ed.; Krieger, R. E: Malabar, FL, 1987.

24. Westheimer, F. H. *Chem. Rev.* 1961, 61, 265.

25. Streitwieser, A.; Jagow, R. H.; Fahey, R. C.; Suzuki, S. *J. Am. Chem. Soc.* 1958, 80, 2326.

26. Cook, P. F.; Oppenheimer, N. J.; Cleland, W. W. *Biochemistry.* 1981, 20, 1817.

27. Kohen, A.; Jensen, J. H. *J. Am. Chem. Soc.* 2002, 124, 3858.

28. Kurz, L. C.; Frieden, C. *J. Am. Chem. Soc.* 1980, 102, 4198.

29. Hermes, J. D.; Morrical, S. W.; O'Leary, M. H.; Cleland, W. W. *Biochemistry.* 1984, 23, 5479.

30. Swain, C. G.; Stivers, E. C.; Reuwer, J. F.; Schaad, L. J. *J. Am. Chem. Soc.* 1958, 80, 5885.

31. Cha, Y.; Murray, C. J.; Klinman, J. P. *Science.* 1989, 243, 1325.

32. Bahnson, B. J.; Park, D. H.; Kim, K.; Plapp, B. V.; Klinman, J. P. *Biochemistry.* 1993, 32, 5503.

33. Kohen, A.; Cannio, R.; Bartolucci, S.; Klinman, J. P. *Nature.* 1999, 399, 496.

34. Knapp, M. J.; Rickert, K.; Klinman, J. P. *J. Am. Chem. Soc.* 2002, 124, 3865.

35. Sikorski, R. S.; Wang, L.; Markham, K. A.; Rajagopalan, P. T.; Benkovic, S. J.; Kohen, A. *J. Am. Chem. Soc.* 2004, 126, 4778.

36. Hay, S.; Sutcliffe, M. J.; Scrutton, N. S. In Quantum Tunnelling in Enzyme-Catalysed Reactions; Allemann, R. K., Scrutton, N. S., Eds.; Royal Society of Chemistry: Cambridge, 2009, p 199.

37. Stern, M. J.; Weston, R. E. *J. Chem. Phys.* 1974, 60, 2808.

38. Bell, R. P. *Trans. Faraday Soc.* 1959, 55, 1.

39. Kohen, A.; Klinman, J. P. *Chem. Biol.* 1999, 6, R191.

40. Bell, R. P. The tunnel effect in chemistry.; NY: Chapman & Hall.: London, UK and New York,, 1980.

41. Nagel, Z. D.; Klinman, J. P. *Chem. Rev.* 2006, 106, 3095.

42. Pu, J.; Ma, S.; Gao, J.; Truhlar, D. G. *J. Phys. Chem. B.* 2005, 109, 8551.

43. Kanaan, N.; Ferrer, S.; Martin, S.; Garcia-Viloca, M.; Kohen, A.; Moliner, V. *J. Am. Chem. Soc.* 2011, 133, 6692.

44. Liu, H.; Warshel, A. *J. Phys. Chem. B.* 2007, 111, 7852.

45. Major, D. T.; Heroux, A.; Orville, A. M.; Valley, M. P.; Fitzpatrick, P. F.; Gao, J. *Proc. Natl. Acad. Sci.* 2009, 106, 20734.

46. Fan, Y.; Cembran, A.; Ma, S.; Gao, J. *Biochemistry.* 2013, 52, 2036.

47. Marcus, R. A.; Sutin, N. *Biochim. Biophys. Acta.* 1985, 811, 265.

48. Kuznetsov, A. M.; Ulstrup, J. *Can. J. Chem.* 1999, 77, 1085.

49. Kohen, A. In Isotope effects in chemistry and biology; Kohen, A., Limbach, H.-H., Eds.; Taylor & Francis: Boca Raton, 2006, p 743.

50. Marcus, R. A. *J. Phys. Chem. B.* 2007, 111, 6643.

51. Roston, D.; Cheatum, C. M.; Kohen, A. *Biochemistry.* 2012, 51, 6860.

52. Knapp, M. J.; Klinman, J. P. *Eur. J. Biochem.* 2002, 269, 3113.

53. Pudney, C. R.; Johannissen, L. O.; Sutcliffe, M. J.; Hay, S.; Scrutton, N. S. *J. Am. Chem. Soc.* 2010, 132, 11329.

54. Klinman, J. P. *Phil. Trans. Roy. Soc. B.* 2006, 361, 1323.

55. Nagel, Z. D.; Meadows, C. W.; Dong, M.; Bahnson, B. J.; Klinman, J. P. *Biochemistry.* 2012, 51, 4147.

56. Kohen, A.; Roston, D.; Stojković, V.; Wang, Z. In Encyclopedia of Analytical Chemistry; Meyers, R. A., Ed.; John Wiley & Sons, Ltd: Chichester, UK, 2011; Vol. S1-S3, p 77.

57. Klinman, J. P. *J. Biol. Chem.* 1972, 247, 7977.

58. Klinman, J. P. *Biochemistry.* 1976, 15, 2018.

59. Welsh, K. M.; Creighton, D. J.; Klinman, J. P. *Biochemistry.* 1980, 19, 2005.

60. Cook, P. F.; Blanchard, J. S.; Cleland, W. W. *Biochemistry.* 1980, 19, 4853.

61. Huskey, W. P.; Schowen, R. L. *J. Am. Chem. Soc.* 1983, 105, 5704.

62. Bigeleisen, J. *J. Chem. Phys.* 1958, 28, 694.

63. Saunders, W. H., Jr. J. Am. Chem. Soc. 1985, 107, 164.

64. Hirschi, J.; Singleton, D. A. *J. Am. Chem. Soc.* 2005, 127, 3294.

65. Bahnson, B. J.; Colby, T. D.; Chin, J. K.; Goldstein, B. M.; Klinman, J. P. *Proc. Natl. Acad. Sci.* 1997, 94, 12797.

66. Stojkovic, V.; Perissinotti, L. L.; Lee, J.; Benkovic, S. J.; Kohen, A. *Chem. Comm.* 2010, 46, 8974.

67. Stojkovic, V.; Perissinotti, L. L.; Willmer, D.; Benkovic, S. J.; Kohen, A. *J. Am. Chem. Soc.*2012, 134, 1738.

68. Roston, D.; Kohen, A. *Proc. Natl. Acad. Sci.*2010, 107, 9572.

69. Karsten, W. E.; Hwang, C. C.; Cook, P. F. *Biochemistry.* 1999, 38, 4398.

70. Pudney, C. R.; Hay, S.; Sutcliffe, M. J.; Scrutton, N. S. *J. Am. Chem. Soc.* 2006, 128, 14053.

71. Alston, W. C.; Kanska, M.; Murray, C. J. *Biochemistry.* 1996, 35, 12873.

72. Siegel, J. B.; Zanghellini, A.; Lovick, H. M.; Kiss, G.; Lambert, A. R.; Clair, J. L. S.; Gallaher, J. L.; Hilvert, D.; Gelb, M. H.; Stoddard, B. L.; Houk, K. N.; Michael, F. E.; Baker, D. *Science.* 2010, 329, 309.

73. Baker, D. Protein *Science.* 2010, 19, 1817.

74. Kiefer, P. M.; Hynes, J. T. In Isotope effects in chemistry and biology; Kohen, A., Limbach, H. H., Eds.; Taylor & Francis, CRC Press: Boca Raton, FL, 2006; Vol. Ch. 21, p 549.

75. Bell, R. P. *The Proton In Chemistry*; 2d ed.; Cornell University Press: Ithaca, N.Y., 1973.

76. Agrawal, N.; Hong, B.; Mihai, C.; Kohen, A. *Biochemistry.* 2004, 43, 1998.

77. Pudney, C. R.; Hay, S.; Levy, C.; Pang, J. Y.; Sutcliffe, M. J.; Leys, D.; Scrutton, N. S. *J. Am. Chem. Soc.* 2009, 131, 17072.

78. Fan, F.; Gadda, G. *J. Am. Chem. Soc.* 2005, 127, 17954.

79. Kwart, H.; Brechbiel, M. W.; Acheson, R. M.; Ward, D. C. *J. Am. Chem. Soc.* 1982, 104, 4671.

80. Braun, J.; Schwesinger, R.; Williams, P. G.; Morimoto, H.; Wemmer, D. E.; Limbach, H. H. *J. Am. Chem. Soc.* 1996, 118, 11101.

81. Langer, U.; Hoelger, C.; Wehrle, B.; Latanowicz, L.; Vogel, E.; Limbach, H. H. *J. Phys. Org. Chem.* 2000, 13, 23.

82. Hay, S.; Sutcliffe, M. J.; Scrutton, N. S.; Royal Society of Chemistry: 2009, p 199.

83. Villa, J.; Warshel, A. *J. Phys. Chem. B.* 2001, 105, 7887.

84. Kiefer, P. M.; Hynes, J. T. *J. Phys. Chem. A.* 2004, 108, 11793.

85. Borgis, D.; Hynes, J. T. *J. Phys. Chem.* 1996, 100, 1118.

86. Meyer, M. P.; Klinman, J. P. *Chem. Phys.* 2005, 319, 283.

87. Hatcher, E.; Soudackov, A. V.; Hammes-Schiffer, S. *J. Am. Chem. Soc.* 2007, 129, 187.

88. Wang, L.; Goodey, N. M.; Benkovic, S. J.; Kohen, A. *Proc. Natl. Acad. Sci.* 2006, 103, 15753.

89. Wang, L.; Goodey, N. M.; Benkovic, S. J.; Kohen, A. *Phil. Trans. R. Soc. B.* 2006, 361, 1307.

90. Wang, L.; Tharp, S.; Selzer, T.; Benkovic, S. J.; Kohen, A. *Biochemistry*. 2006, 45, 1383.

91. Wang, Z.; Kohen, A. *J. Am. Chem. Soc.* 2010, 132, 9820.

92. Bandaria, J. N.; Cheatum, C. M.; Kohen, A. *J. Am. Chem. Soc.* 2009, 131, 10151.

93. Roth, W. R.; Konig, J. *Annal. Chem.* 1966, 699, 24.

94. Brooks, C. L.; Thorpe, I. F. *J. Am. Chem. Soc.* 2005, 127, 12997.

95. Alhambra, C.; Corchado, J. C.; Sanchez, M. L.; Gao, J. L.; Truhlar, D. G. *J. Am. Chem. Soc.* 2000, 122, 8197.

96. Agarwal, P. K.; Webb, S. P.; Hammes-Schiffer, S. *J. Am. Chem. Soc.* 2000, 122, 4803.

97. Cui, Q.; Elstner, M.; Karplus, M. *J. Phys. Chem. B.* 2002, 106, 2721.

98. Frisch, M. J.; Trucks, G. W.; Schlegel, H. B.; Scuseria, G. E.; Robb, M. A.; Cheeseman, J. R.; Montgomery, J., J. A.; Vreven, T.; Kudin, K. N.; Burant, J. C.; Millam, J. M.; Iyengar, S. S.; Tomasi, J.; Barone, V.; Mennucci, B.; Cossi, M.; Scalmani, G.; Rega, N.; Petersson, G. A.; Nakatsuji, H.; Hada, M.; Ehara, M.; Toyota, K.; Fukuda, R.; Hasegawa, J.; Ishida, M.; Nakajima, T.; Honda, Y.; Kitao, O.; Nakai, H.; Klene, M.; Li, X.; Knox, J. E.; Hratchian, H. P.; Cross, J. B.; Bakken, V.; Adamo, C.; Jaramillo, J.; Gomperts, R.; Stratmann, R. E.; Yazyev, O.; Austin, A. J.; Cammi, R.; Pomelli, C.; Ochterski, J. W.; Ayala, P. Y.; Morokuma, K.; Voth, G. A.; Salvador, P.; Dannenberg, J. J.; Zakrzewski, V. G.; Dapprich, S.; Daniels, A. D.; Strain, M. C.; Farkas, O.; Malick, D. K.; Rabuck, A. D.; Raghavachari, K.; Foresman, J. B.; Ortiz, J. V.; Cui, Q.; Baboul, A. G.; Clifford, S.; Cioslowski, J.; Stefanov, B. B.; Liu, G.; Liashenko, A.; Piskorz, P.; Komaromi, I.; Martin, R. L.; Fox, D. J.; Keith, T.; Al-Laham, M. A.; Peng, C. Y.; Nanayakkara, A.; Challacombe, M.; Gill, P. M. W.; Johnson, B.; Chen, W.; Wong, M. W.; Gonzalez, C.; Pople, J. A.; *Gaussian 03*; Revision C.02 ed.; Gaussian, Inc.: Wallingford, CT., 2004.

99. Wolfram Research, I.; 7.0 Student. ed.; Wolfram Research, Inc.: Champaign, Illinois, 2008.

100. Hay, S.; Sutcliffe, M. J.; Scrutton, N. S. *Proc. Natl. Acad. Sci.* 2007, 104, 507.

101. Warshel, A.; Chu, Z. T. *J. Chem. Phys.* 1990, 93, 4003.

102. Kim, Y.; Truhlar, D. G.; Kreevoy, M. M. *J. Am. Chem. Soc.* 1991, 113, 7837.

103. Cohen-Tannoudji, C.; Diu, B.; Laloë, F. *Quantum Mechanics*; Wiley: New York, 1977.

104. Kiefer, P. M.; Hynes, J. T. *J. Phys. Chem. A.* 2003, 107, 9022.

105. de la Lande, A.; Rezac, J.; Levy, B.; Sanders, B. C.; Salahub, D. R. *J. Am. Chem. Soc.* 2011, 133, 3883.

106. Borgis, D. C.; Lee, S. Y.; Hynes, J. T. *Chem. Phys. Lett*. 1989, 162, 19.

107. Ohta, Y.; Soudackov, A. V.; Hammes-Schiffer, S. *J. Chem. Phys.* 2006, 125, 144522.

108. Hwang, J. K.; King, G.; Creighton, S.; Warshel, A. *J. Am. Chem. Soc.* 1988, 110, 5297.

109. Olsson, M. H. M.; Parson, W. W.; Warshel, A. *Chem. Rev.* 2006, 106, 1737.

110. Alhambra, C.; Corchado, J.; Sanchez, M. L.; Garcia-Viloca, M.; Gao, J.; Truhlar, D. G. *J. Phys. Chem. B.* 2001, 105, 11326.

111. Agarwal, P. K.; Billeter, S. R.; Hammes-Schiffer, S. *J. Phys. Chem. B.* 2002, 106, 3283.

112. Olsson, M. H. M.; Mavri, J.; Warshel, A. *Phil. Trans. Roy. Soc. B.* 2006, 361, 1417.

113. Warshel, A. *J. Phys. Chem.* 1982, 86, 2218.

114. Warshel, A. *Proc. Natl. Acad. Sci.* 1984, 81, 444.

115. Ludlow, M. K.; Soudackov, A. V.; Hammes-Schiffer, S. *J. Am. Chem. Soc.* 2009, 131, 7094.

116. Kamerlin, S. C. L.; Mavri, J.; Warshel, A. *FEBS Lett*. 2010, 584, 2759.

117. Nagel, Z. D.; Dong, M.; Bahnson, B. J.; Klinman, J. P. *Proc. Natl. Acad. Sci.* 2011, 108, 10520.

118. Pudney, C. R.; Hay, S.; Pang, J. Y.; Costello, C.; Leys, D.; Sutcliffe, M. J.; Scrutton, N. S. *J. Am. Chem. Soc.* 2007, 129, 13949.

119. Hay, S.; Johannissen, L. O.; Sutcliffe, M. J.; Scrutton, N. S. *Biophys. J.* 2010, 98, 121.

120. Pu, J. Z.; Gao, J. L.; Truhlar, D. G. *Chem. Rev.* 2006, 106, 3140.

121. Masgrau, L.; Roujeinikova, A.; Johannissen, L. O.; Hothi, P.; Basran, J.; Ranaghan, K. E.; Mulholland, A. J.; Sutcliffe, M. J.; Scrutton, N. S.; Leys, D. *Science.* 2006, 312, 237.

122. Dickinson, F. M.; Dickenson, C. J. *Biochem. J.* 1978, 171, 629.

123. Pal, S.; Park, D.-H.; Plapp, B. V. *Chem. Biol. Interact.* 2009, 178, 16.

124. Meyer, M. P.; Tomchick, D. R.; Klinman, J. P. *Proc. Natl. Acad. Sci.* 2008, 105, 1146.

125. Huskey, W. P. *J. Phys. Org. Chem.* 1991, 4, 361.

126. Rucker, J.; Klinman, J. P. *J. Am. Chem. Soc.* 1999, 121, 1997.

127. Webb, S. P.; Agarwal, P. K.; Hammes-Schiffer, S. *J. Phys. Chem. B.* 2000, 104, 8884.

128. Pu, J. Z.; Ma, S. H.; Garcia-Viloca, M.; Gao, J. L.; Truhlar, D. G.; Kohen, A. *J. Am. Chem. Soc.* 2005, 127, 14879.

129. Lin, S.; Saunders, W. H. *J. Am. Chem. Soc.* 1994, 116, 6107.

130. Wilde, T. C.; Blotny, G.; Pollack, R. M. *J. Am. Chem. Soc.* 2008, 130, 6577.

131. Truhlar, D. G.; Garrett, B. C. *Ann. Rev. Phys. Chem*. 1984, 35, 159.

132. Redington, R. L. *J. Chem. Phys.* 2000, 113, 2319.

133. Pang, J. Y.; Hay, S.; Scrutton, N. S.; Sutcliffe, M. J. *J. Am. Chem. Soc.* 2008, 130, 7092.

134. Essa, A. H. *Int. J. Quant. Chem.* 2007, 107, 1574.

135. Shearer, G. L.; Kim, K. Y.; Lee, K. M.; Wang, C. K.; Plapp, B. V. *Biochemistry.* 1993, 32, 11186.

136. Antoniou, D.; Schwartz, S. D. The *J. Phys. Chem. B.* 2001, 105, 5553.

137. Entwistle, I. D.; Boehm, P.; Johnstone, R. A. W.; Telford, R. P. *J. Chem. Soc*. 1980, 27.

138. Chancellor, T.; Quill, M.; Bergbreiter, D. E.; Newcomb, M. *J. Org. Chem.* 1978, 43, 1245.

139. Rafter, G. W.; Colowick, S. P. *Method Enzymol.* 1957, 3, 887.

140. Anisinov, V.; Paneth, P. *ISOEFF*. Lodz, Poland, 2007.

141. Rucker, J.; Cha, Y.; Jonsson, T.; Grant, K. L.; Klinman, J. P. *Biochemistry.* 1992, 31, 11489.

142. Ganzhorn, A. J.; Green, D. W.; Hershey, A. D.; Gould, R. M.; Plapp, B. V. *J. Biol. Chem.* 1987, 262, 3754.

143. Cook, P. F.; Cleland, W. W. *Enzyme Kinetics and Mechanism*; Taylor & Francis Group: New York, 2007.

144. Billeter, S. R.; Webb, S. P.; Agarwal, P. K.; Iordanov, T.; Hammes-Schiffer, S. *J. Am. Chem. Soc.* 2001, 123, 11262.

145. Kleifeld, O.; Frenkel, A.; Martin, J. M. L.; Sagi, I. *Nat. Struct. Biol.* 2003, 10, 98.

146. Roston, D.; Islam, Z.; Kohen, A. *Molecules.* 2013, 18, 5543.

147. Rubach, J. K.; Ramaswamy, S.; Plapp, B. V. *Biochemistry*. 2001, 40, 12686.

148. Roston, D.; Kohen, A. *J. Am. Chem. Soc.* Submitted.

149. Hermes, J. D.; Cleland, W. W. *J. Am. Chem. Soc.*1984, 106, 7263.

150. Bigeleisen, J. *Angew. Chem. Int. Edit.* 1957, 69, 565.

151. Roston, D.; Kohen, A. *J. Label. Comp. Radiopharma.* Submitted.

152. Stern, M. J.; Vogel, P. C. *J. Am. Chem. Soc.* 1971, 93, 4664.

153. Truhlar, D. G.; Garrett, B. C. *Acc. Chem. Res.* 1980, 13, 440.

154. Truhlar, D. G.; Garrett, B. C. *J. Chim. Phys. Pcb.* 1987, 84, 365.

155. Liu, H. B.; Warshel, A. *Biochemistry.* 2007, 46, 6011.

156. Hammann, B.; Razzaghi, M.; Kashefolgheta, S.; Lu, Y. *Chem. Comm.* 2012, 48, 11337.

157. Liu, Q.; Zhao, Y.; Hammann, B.; Eilers, J.; Lu, Y.; Kohen, A. *J. Org. Chem.* 2012, 77, 6825.

158. Lu, Y.; Qu, F. R.; Zhao, Y.; Small, A. M. J.; Bradshaw, J.; Moore, B. *J. Org. Chem.* 2009, 74, 6503.

159. Lu, Y.; Qu, F. R.; Moore, B.; Endicott, D.; Kuester, W. *J. Org. Chem.* 2008, 73, 4763.

160. Kashefolgheta, S.; Hammann, B.; Razzaghi, M.; Eilers, J.; Roston, D.; Lu, Y. *J. Org. Chem.* Submitted.

161. Bigeleisen, J. *J. Chem. Phys.* 1958, 28, 694.

162. Klinman, J. P.; Kohen, A. *Ann. Rev. Biochem.* 2013, 82, 471.

163. Frisch, M. J.; Trucks, G. W.; Schlegel, H. B.; Scuseria, G. E.; Robb, M. A.; Cheeseman, J. R.; Scalmani, G.; Barone, V.; Mennucci, B.; Petersson, G. A.; Nakatsuji, H.; Caricato, M.; Li, X.; Hratchian, H. P.; Izmaylov, A. F.; Bloino, J.; Zheng, G.; Sonnenberg, J. L.; Hada, M.; Ehara, M.; Toyota, K.; Fukuda, R.; Hasegawa, J.; Ishida, M.; Nakajima, T.; Honda, Y.; Kitao, O.; Nakai, H.; Vreven, T.; Montgomery, J., J. A.; Peralta, J. E.; Ogliaro, F.; Bearpark, M.; Heyd, J. J.; Brothers, E.; Kudin, K. N.; Staroverov, V. N.; Kobayashi, R.; Normand, J.; Raghavachari, K.; Rendell, A.; Burant, J. C.; Iyengar, S. S.; Tomasi, J.; Cossi, M.; Rega, N.; Millam, J. M.; Klene, M.; Knox, J. E.; Cross, J. B.; Bakken, V.; Adamo, C.; Jaramillo, J.; Gomperts, R.; Stratmann, R. E.; Yazyev, O.; Austin, A. J.; Cammi, R.; Pomelli, C.; Ochterski, J. W.; Martin, R. L.; Morokuma, K.; Zakrzewski, V. G.; Voth, G. A.; Salvador, P.; Dannenberg, J. J.; Dapprich, S.; Daniels, A. D.; Farkas, Ö.; Foresman, J. B.; Ortiz, J. V.; Cioslowski, J.; Fox, D. J.; Gaussian 09; Revision A.1 ed.; Gaussian, Inc.: Wallingford, CT., 2009.

164. Klinman, J. P. *Biochemistry* 2013, 52, 2068.

165. Pudney, C. R.; Guerriero, A.; Baxter, N. J.; Johannissen, L. O.; Waltho, J. P.; Hay, S.; Scrutton, N. S. *J. Am. Chem. Soc.* 2013, 135, 2512.

166. Doron, D.; Major, D. T.; Kohen, A.; Thiel, W.; Wu, X. *J. Chem. Theory Comp*. 2011, 7, 3420.

167. Schwartz, S. D.; Schramm, V. L. *Nat. Chem. Biol.* 2009, 5, 551.

168. Eyring, H. *J. Chem. Phys.* 1935, 3, 107.